INTERIM REPORT

7-12-79

Accession No. _____

Contract Program or Project Title:

Subject of this Document: "RELAP4/MOD6 Predictions Comparisons with LOFT LOCE L2-2 Data"

Type of Document:

Author(s): E. J. Kee, J. R. White

Date of Document: May 1979

Responsible NRC Individual and NRC Office or Division: D. McPherson

Kay Rose

H. P. Pearson, Supervisor
Information Processing
EG&G Idaho

Prepared for
U.S. Nuclear Regulatory Commission
Washington, D.C. 20555

NRC Fin #A6048

INTERIM REPORT

EG&G Idaho

FORM EG&G 954
(Rev. 9-76)

INTEROFFICE CORRESPONDENCE NO. R-4628

date

to DISTRIBUTION

from LOFT CDCS, TAN 602, Ext. 6177 S K Hathaway

subject DOCUMENT TRANSMITTAL

The following documents released by LOFT CDCS, are hereby transmitted for your use and information:

DOCUMENT NO.	REV.	CHG.	DATE
LTR 20-100	Ø		5-3-79
"RELAP4/MOD6 PREDICTIONS COMPARISONS WHITH LOFT LOCE L2-2 DATA"			
E. J. Kee, J. R. White			

REMARKS: This LTR documents conditions pertinent to computer codes for LOCA analysis. There are no recommendations specific to LOFT Plant Configuration.

DISTRIBUTION

W. Amidei
B. O. Anderson
E. C. Anderson w/o Att.
J. G. Arendts
G. A. Dinneen
D. B. Engelman
B. L. Freed-Orig.+7
R. C. Gottula
R. C. Guenzler
J. C. Haire
K. Hofmann
G. L. Hunt w/o Att.
F. K. Hyer w/o Att.
N. C. Kaufman w/o Att.
J. L. Liebenthal
A. S. Lockhart
D. W. Marshall
S. Matovich
M. I. McKnight
G. D. McPherson
O. R. Meyer w/o Att.
N. E. Pace w/o Att.
T. F. Pointer
L. O. Saukkoriipi
G. Sonneck
W. A. Spencer
J. C. Stachew w/o Att.
K. C. Sumpter
K. Tasaka-2
R. E. Tiller
L. Winters
J. R. White-5
L. P. Leach
E. J. Kee-5
T. K. Samuels
S. A. Naff SAN/per telecon 5-16-79
R. M. Gill-4

755 063

700253

LOFT TECHNICAL REPORT LTR 20-100

MAY 3, 1979

P 394

RELAP4/MOD6 PREDICTIONS COMPARISONS WITH LOFT LOCE L2-2 DATA

E. J. Kee, J. R. White

EG&G Idaho, Inc.

IDAHO NATIONAL ENGINEERING LABORATORY

DEPARTMENT OF ENERGY

IDAHO OPERATIONS OFFICE UNDER CONTRACT DE-AC07-76IDO1570

EG&G Idaho, Inc.

LOFT TECHNICAL REPORT
LOFT PROGRAM

FORM EG&G-229
(Rev. 12-76)

TITLE	REPORT NO.
RELAP4/MOD6 Predictions Comparisons With LOFT LOCE L2-2 Data	LTR 20-100
AUTHOR: E. J. Kee; J. R. White	GWA NO.
PERFORMING ORGANIZATION: J. R. White for S. A. Naff	DATE: May 3, 1979
LOFT APPROVAL: LEPD Mgr.	

DISPOSITION OF RECOMMENDATIONS: This LTR documents conditions pertinent to computer codes for LOCA analysis. There are no recommendations specific to LOFT Plant Configuration.

SUMMARY

This document contains comparisons between RELAP4/MOD6 predicted and experimental measured quantities for Loss-of-Fluid Test Loss-of-Coolant Experiment L2-2. These data comparisons provide a detailed record for subsequent analysis.

Comparisons indicate that the trends in the system hydraulic response were generally predicted well. However, the broken cold leg break flow was probably overpredicted in subcooled and saturated critical flow which led to an incorrect core flow which resulted in overpredicting the fuel rod cladding surface temperature response.

CONTENTS

FIGURES

TABLE

RELAP4/MOD6 PREDICTIONS COMPARISONS WITH LOFT LOCE L2-2 DATA

1. INTRODUCTION

An extensive comparison has been made with RELAP4/MOD6 predictions and Loss-of-Fluid Tests (LOFT) Loss-of-Coolant Experiment (LOCE) L2-2 data. This LTR primarily makes these comparisons generally available. Qualitative observations are included that represent the authors' understanding of how the physical processes which occurred during the LOCE L2-2 relate to the approximation made in RELAP4/MOD6 calculations.

In the context of this report, the experimental data are most easily compared as presented in the report figures; however, the reader is asked to keep in mind the error associated with the instrument response listed in Appendix A. Additionally, individual plots are classified with respect to the experimental data in five categories as discussed in the following sections.

1.1 Qualified Engineering Unit Data (QEUD)

Qualified Engineering Unit Data (QEUD) must meet the following criteria:

(1) Have had all calibration corrections applied

(2) Have been compared with independent data and found to agree during the period of interest within specified uncertainty limits

(3) Have been verified to represent the parameter being measured.

Analytical use of the data is unrestricted for the specified time periods and within the defined uncertainty bands.

1.2 Restrained Data

Restrained data (REST) appear reasonable but cannot be classified QEUD because they meet either one of the following criteria:

(1) They are outside uncertainty bands established by reference measurements or derived from redundant measurements when such are available

(2) There are no independent data available for applying required calibration corrections during particular time intervals, and there are either no redundant measurements with which to compare the data, or the data are outside uncertainty bands derived by such comparison when redundant measurements are available.

The data have restrictive statements applied. Examples are:

(1) Not corrected for density changes after TZERO:

(2) Unexplained offset after T + X s

(3) Uncorrected for temperature sensitivity after T + X s

(4) Valid only while sensor is immersed in liquid at T + X, Y, and Z s

(5) Uncertainty band of + D.D E/U applies between T + X and T + Y s.

Restricted data used in numerical analyses are constrained by their restrictive statements.

1.3 Trend Data

Trend data (TREN) meet the following criteria:

(1) The basic data are thought to be good

(2) The calibration and performance of the data acquisition system are not suspect

(3) There are no reference measurements and there may be or may not be redundant measurements of the parameter available for comparison

(4) The form of, and/or coefficient values for, calibration correction equations are not well enough known to provide QEUD data.

The data are suitable for illustrative purposes. The data are to be used in numerical analysis only with caution.

1.4 Not Reviewed Data

Not reviewed data (NORE) have not been reviewed by the DIRC (this definition is for internal record-keeping only).

1.5 Computed Data

Computed data (COPE) have been calculated from measured data using an Idaho National Engineering Laboratory (INEL) subroutine. In the figures, the four letter acronym appears on the plot; the test data trace is indicated by open squares while the calculated trace is indicated by solid circles.

2. DATA COMPARISONS

Appendix B contains figures of the LOFT experimental facility with transducer locations that can be viewed with the data by folding the pages with the figures out.

In consideration of the large amount of data presented, some comments that generally apply to all the comparisons are made here.

Many plots show that the initial value boundary condition was improperly stated. This difference is probably the result of one of two errors or a combination of them. The first is that the initial test conditions were not exactly known prior to the experiment and the second is that the physical system was not accurately described via input data to the RELAP4/MOD6 solution scheme.

2.1 Density

Figures 1 and 2 show that the calculated broken loop density values follow the general trend in the experimental data. Some important differences are shown in the 4- to 5-s range. In this interval, the experimental data show a rapid increase with a subsequent decrease in the broken cold leg and in the broken hot leg, a much slower decrease than the calculation.

The intact cold leg density (Figure 3) again shows a favorable trend comparison; however, the knee in the experimental data at about 6 s is calculated to occur at about 4 s. Furthermore, the actual system density appears to decrease more rapidly than the calculations indicate once flashing begins. After about 20 s, density spikes shown in the data, are probably the result of subcooled ECC water entering the cold leg piping at right angles and splashing in two directions. Because RELAP4/MOD6 assumes one-dimensional behavior, these spikes are not calculated. Similar discrepancies are shown in Figure 4, a density comparison in the intact loop hot leg. Here, the calculated

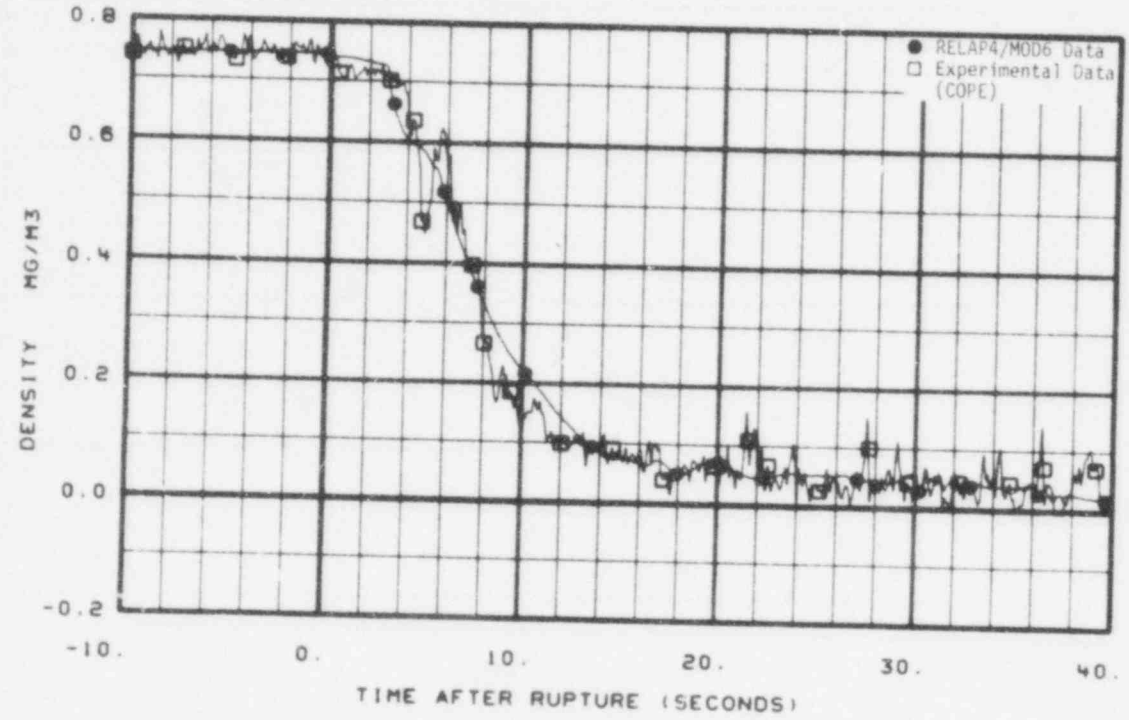

Fig. 1 Comparison of predicted and measured average density in broken loop cold leg (DE-BL-1).

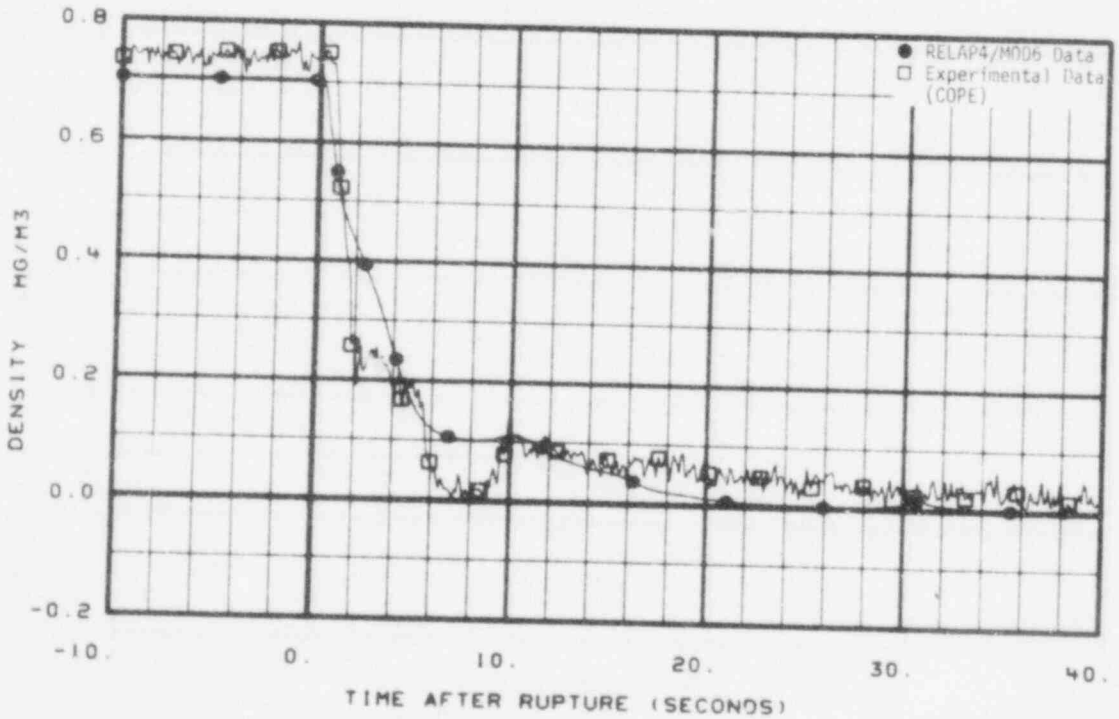

Fig. 2 Comparison of predicted and measured average density in broken loop hot leg (DE-BL-2).

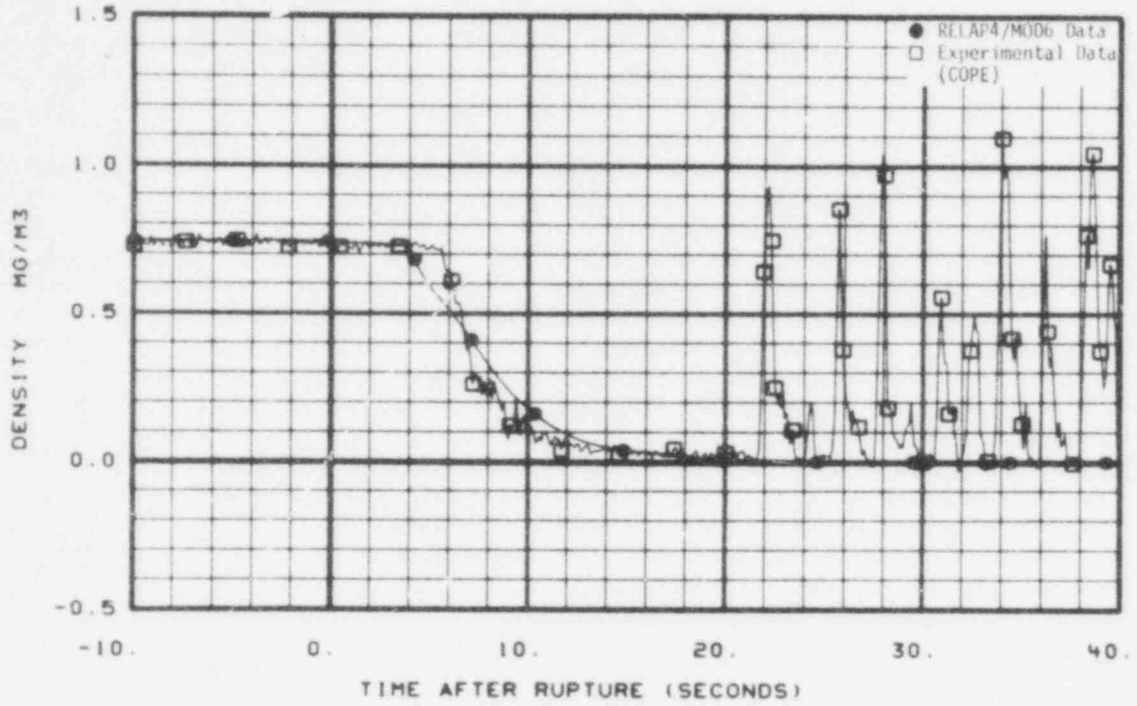

Fig. 3 Comparison of predicted and measured average density in intact loop cold leg (DE-PC-1).

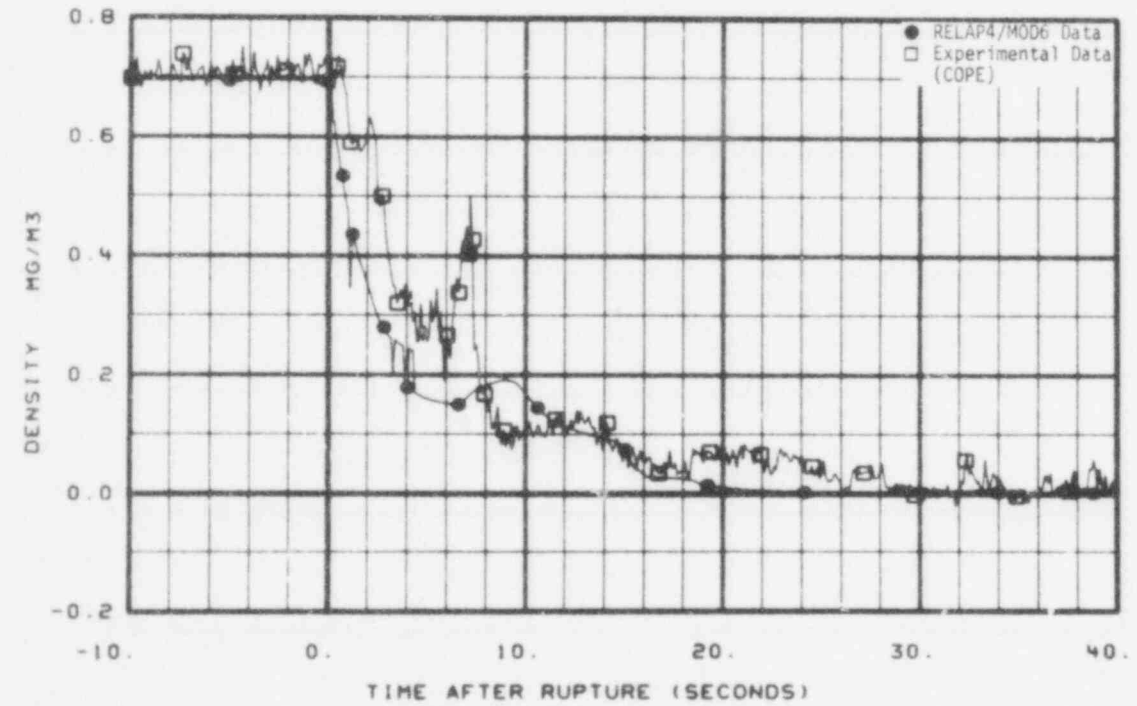

Fig. 4 Comparison of predicted and measured average density in intact loop hot leg (DE-PC-2).

trace starts to decrease earlier and remains below the experimental data until 8 s. The increasing trend in the experimental data after 6 s is not followed by the calculations. Generally, the calculated data indicate an early flashing and low mass inventory in the intact loop.

2.2 Differential Pressure

Figure 5 shows the calculated hot leg 14- to 5-in. contraction differential pressure trace exhibits similar characteristics to the experimental data. The higher calculated values in the 2- to 16-s interval indicate a higher mass flow to the break than the experimental data. The measured differential pressure trend across the pump simulator, Figure 6, is not reflected in the calculations. Furthermore, the calculated data are greater than or equal to the experimental data for time less than 15 s, indicating a high mass flow calculation. The differential pressure traces shown in Figure 7 have similar characteristics; however, the times at which the different curves reach their minima and maxima are shifted. Particularly in the 1- to 4-s range, the calculated minimum occurs about 2 s earlier than the measured one, indicating an early flow reduction was calculated in the hot leg.

The intact loop pump differential pressure comparison, shown in Figure 8, shows the pump head degrades more rapidly in the calculations than in the actual system. The intact loop steam generator, Figure 9, shows a differential pressure degradation comparison similar to the pumps. The calculated intact loop flow is considered low compared to the experimental data for time less than 10 s. The early differential pressure degradation in the intact loop is most likely a result of low calculated density in this loop.

2.3 Flow Rate

Figures 10 and 11 show the accumulator and low-pressure injection system (LPIS) flow rates, respectively. Both of these flows are a

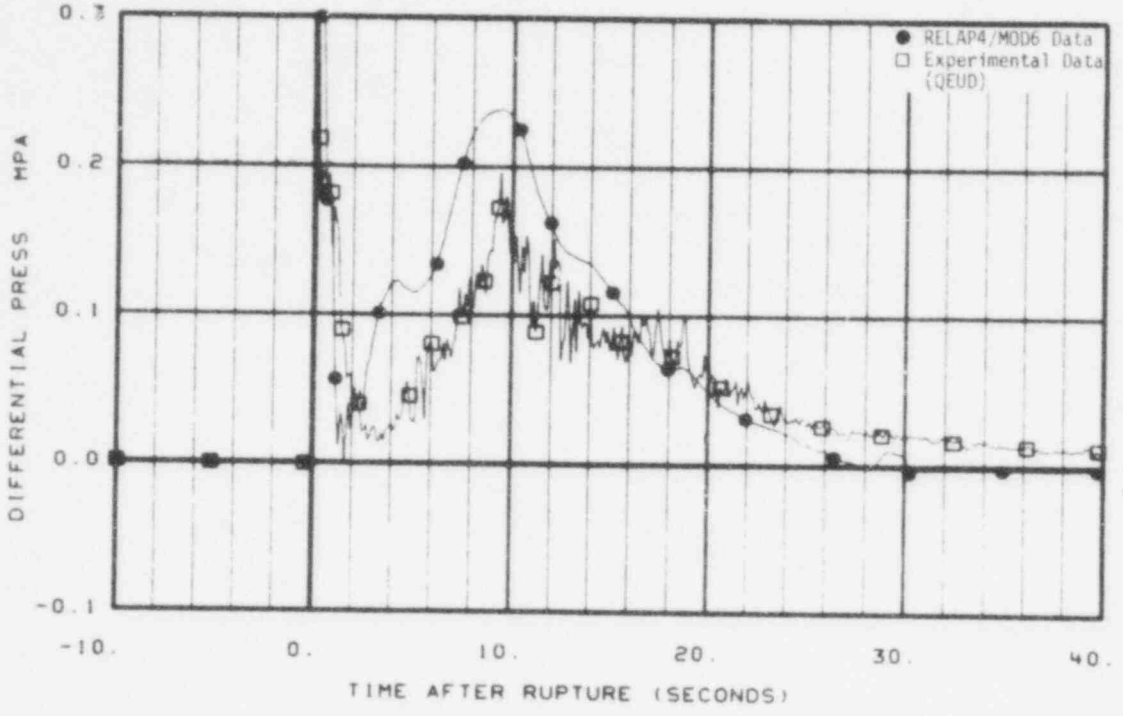

Fig. 5 Comparison of predicted and measured differential pressure across 14- to 5-in. reducer (PDE-BL-1).

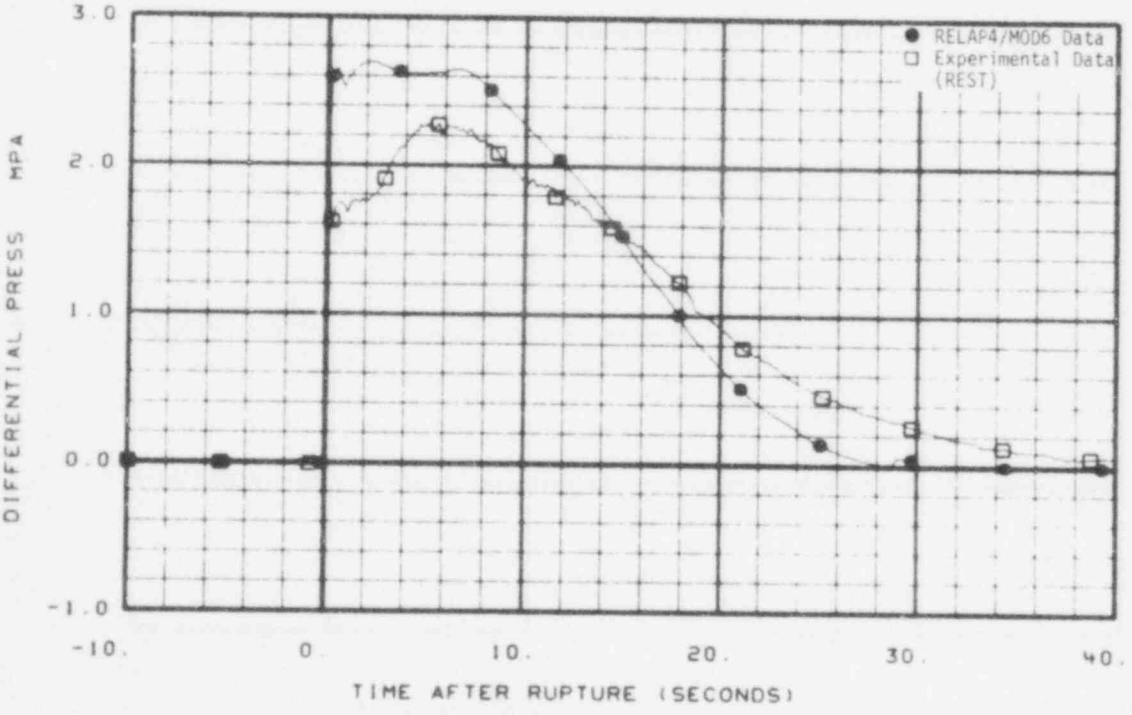

Fig. 6 Comparison of predicted and measured differential pressure across pump simulator (PDE-BL-5).

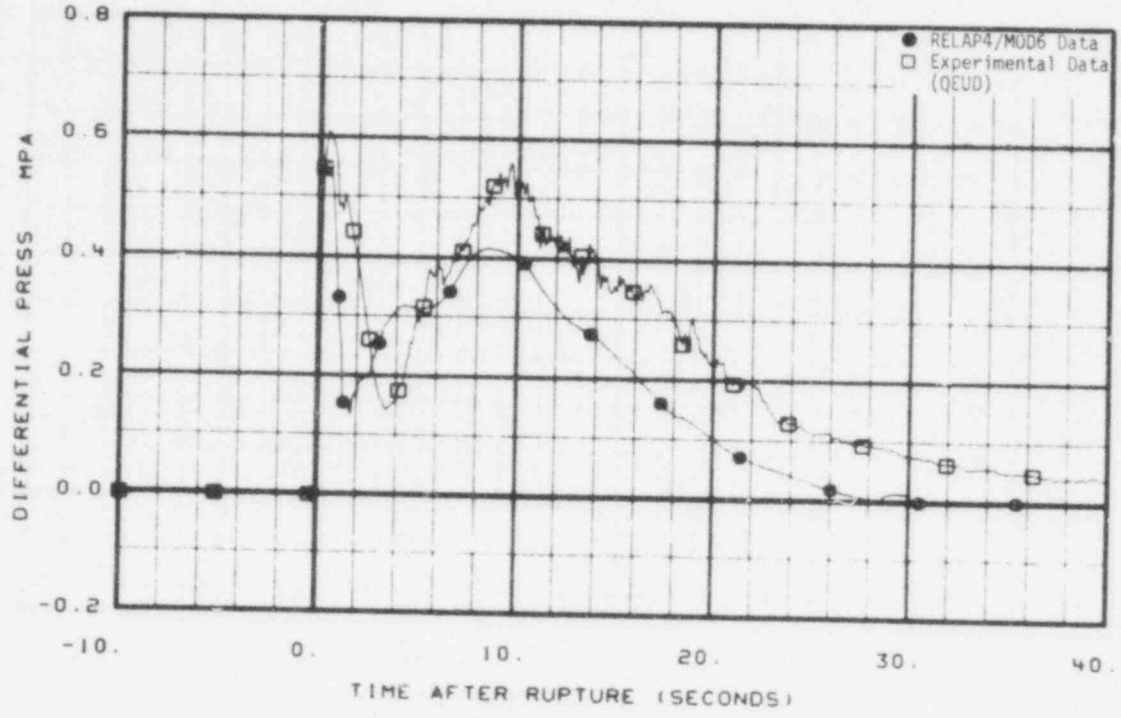

Fig. 7 Comparison of predicted and measured differential pressure across steam generator simulator (PDE-BL-7).

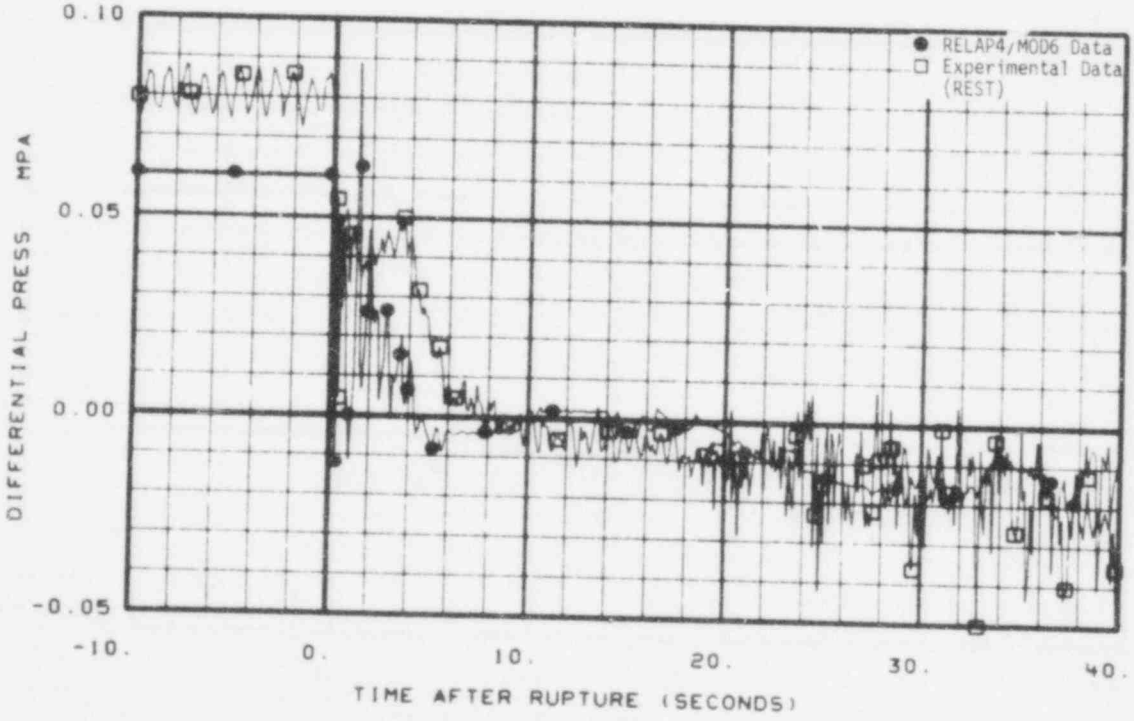

Fig. 8 Comparison of predicted and measured differential pressure across pumps (PDE-PC-1).

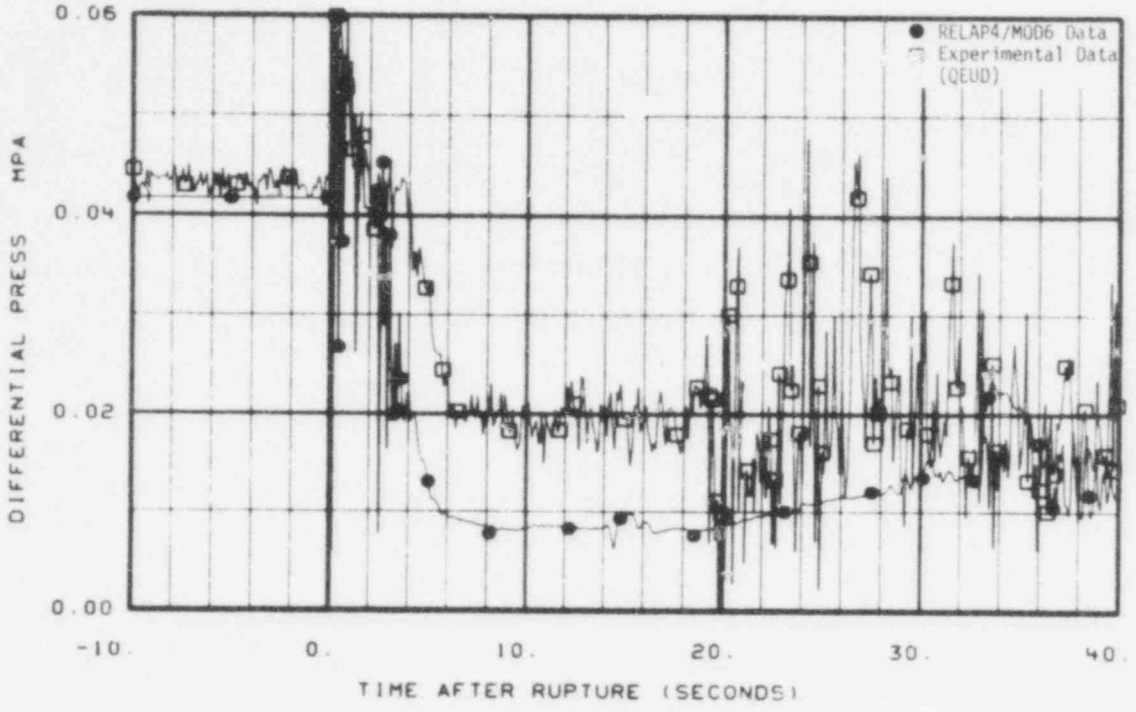

Fig. 9 Comparison of predicted and measured differential pressure across intact loop steam generator (PDE-PC-2).

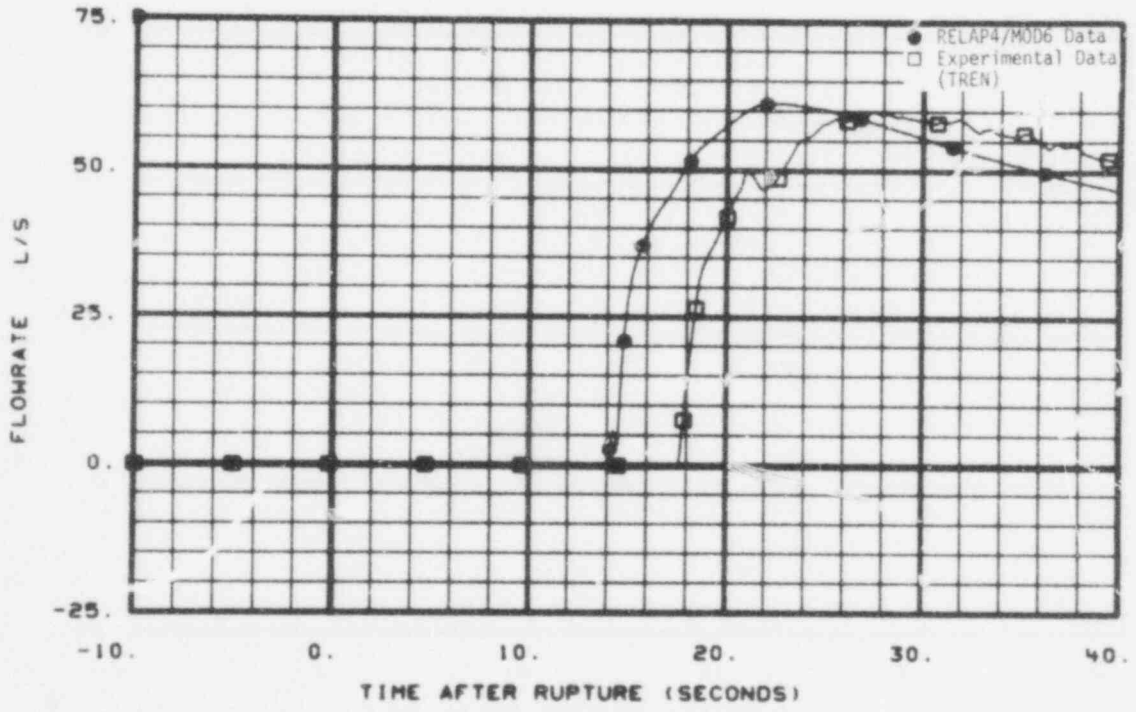

Fig. 10 Comparison of predicted and measured flow rate from accumulator (FT-P120-36-1).

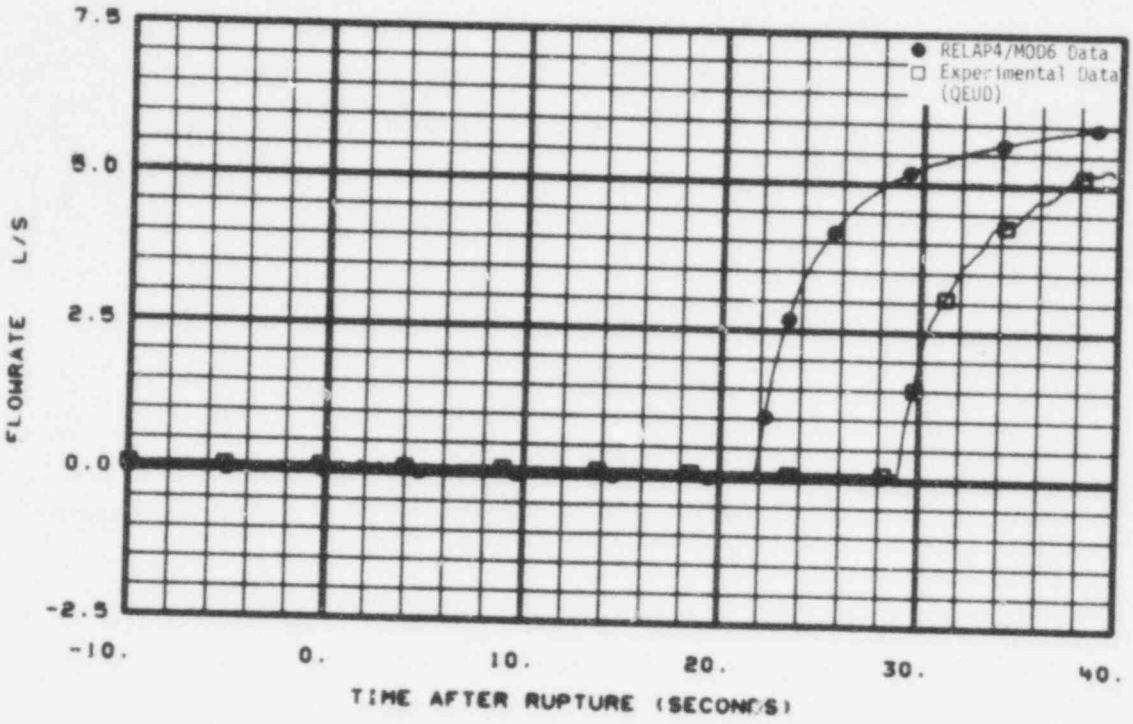

Fig. 11 Comparison of predicted and measured flow rate from LPIS pump (FT-P120-85).

function of system pressure. Assuming the functional relationship was accurately described, both comparisons indicate the calculated system pressure was low compared to the actual system for time greater than 14 s. Figure 12 shows the volumetric flow comparison for the high-pressure injection system (HPIS) pump. Since this pump is a positive displacement type, the flow rate is essentially constant with downstream pressure; and the comparison indicates the expected flow is close to the experimentally measured flow. Because the pump is started on a low pressurizer level, the comparison indicates the calculated pressurizer level trace is above the experimental values.

2.4 Level

The accumulator level comparison, shown in Figure 13, indicates the calculated time of accumulator flow initiation is early as mentioned previously; however, the data trends are in good agreement.

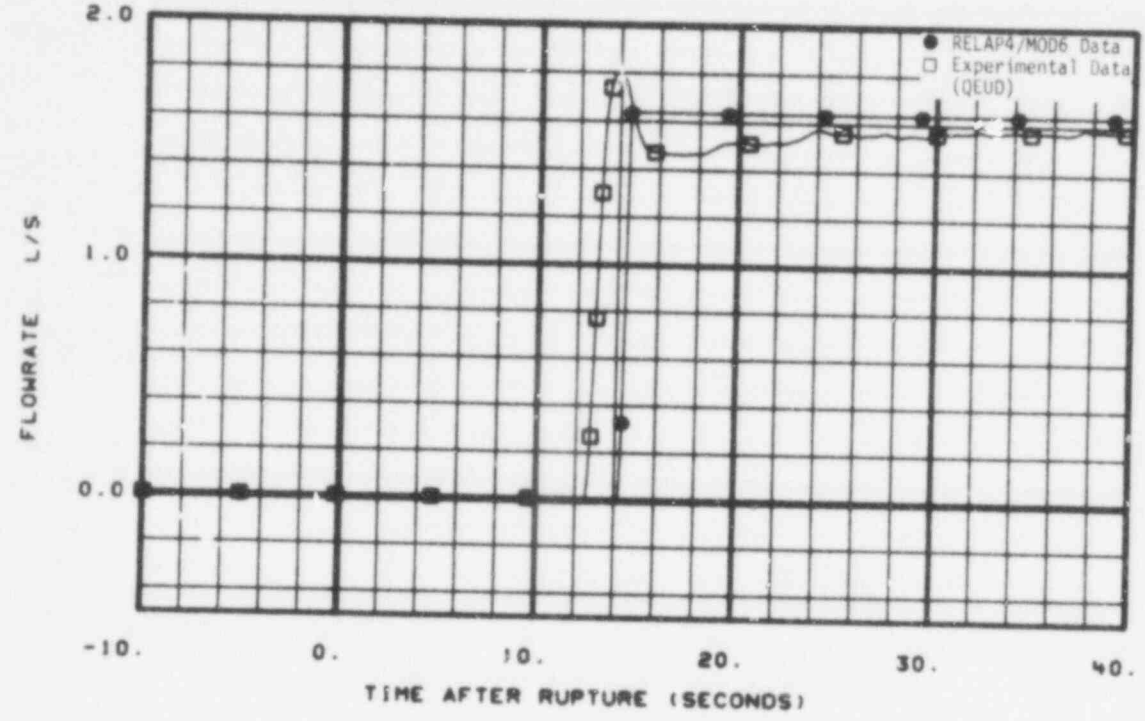

Fig. 12 Comparison of predicted and measured flow rate from HPIS pump (FT-P128-104).

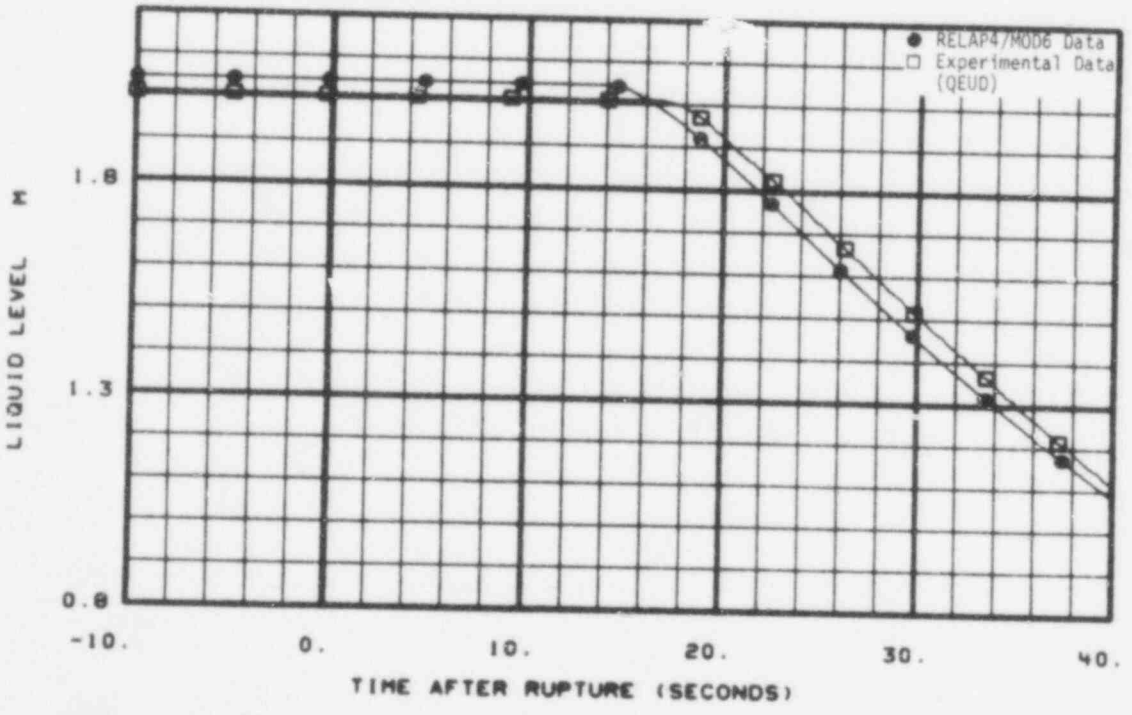

Fig. 13 Comparison of predicted and measured liquid level in accumulator (LIT-P120-44).

The levels in the steam generator secondary, Figure 14, do not compare well, indicating the boundary condition is not well stated at this point in the system.

Figure 15, showing the calculated pressurizer emptying time (15 s), agrees well with the measured data indicating the pressurizer behavior was well calculated.

2.5 Mass Flow

Since mass flow is not a directly measured parameter in LOFT, some algorithms have been developed at INEL to compute mass flow from other measurements. The comparison to one of these techniques is shown at each measurement location. The mass flow measurement shown is the best experimental mass flow available at this time.

Figure 16, a comparison of the mass flow in the broken loop cold leg, indicates the mass flow is generally less than or equal to the

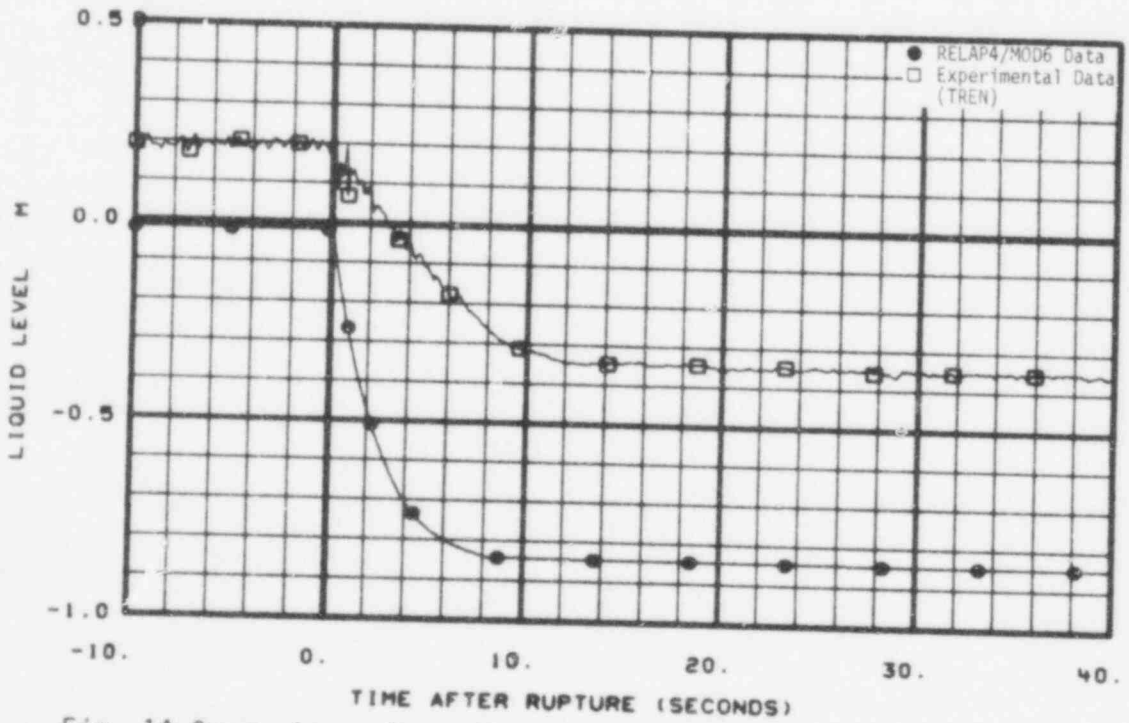

Fig. 14 Comparison of predicted and measured liquid level in steam generator secondary (LT-P004-8A).

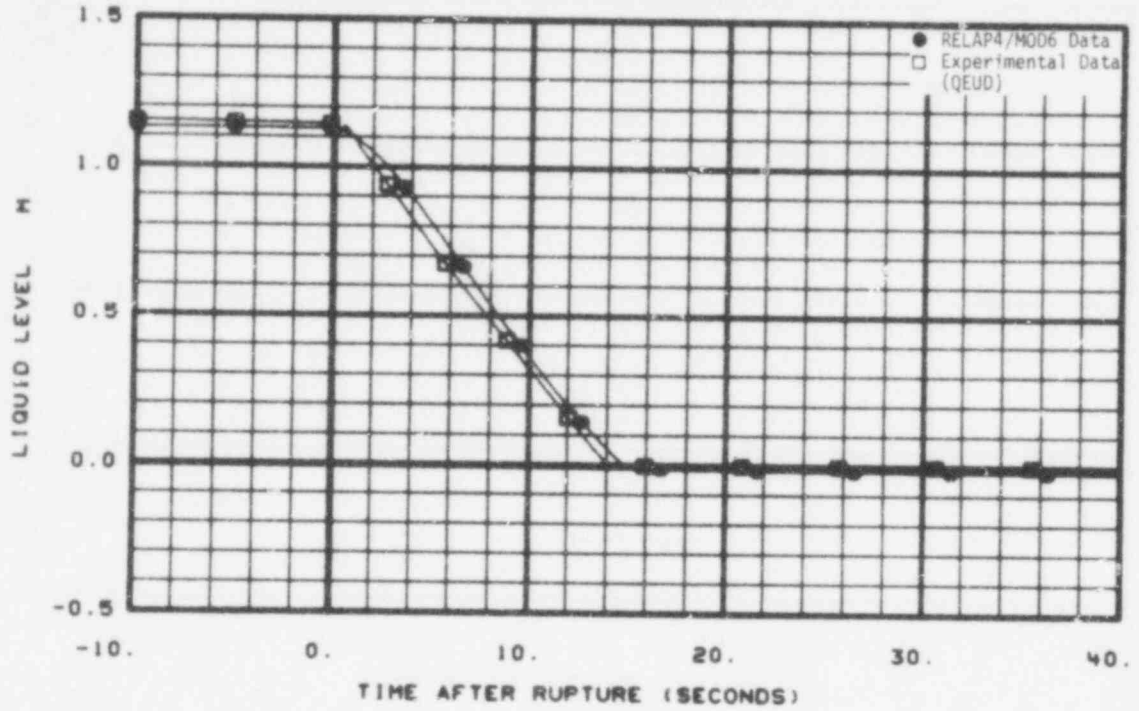

Fig. 15 Comparison of predicted and measured level in pressurizer Channel A (LT-P139-6).

RELAP4/MOD6 calculated values. On the basis of data previously presented (differential pressure and density), this result seems reasonable. The general trends in the experimental data are followed by the calculations.

For the broken loop hot leg, Figure 17, the calculated mass flow trends do not follow the data very well. This seems reasonable based on the differential pressure and density comparisons at this location.

In Figure 18 the general trend of the experimental data of the intact loop cold leg is followed by the RELAP4/MOD6 calculations. The expected decrease in experimental flow occurs approximately 2 s later than the calculations indicate. The mass flow comparison in the intact loop hot leg, Figure 19, shows the calculated flow is lower than the experimental values which is consistent with comparisons of differential pressure and density. The trends do not compare well after about 2 s.

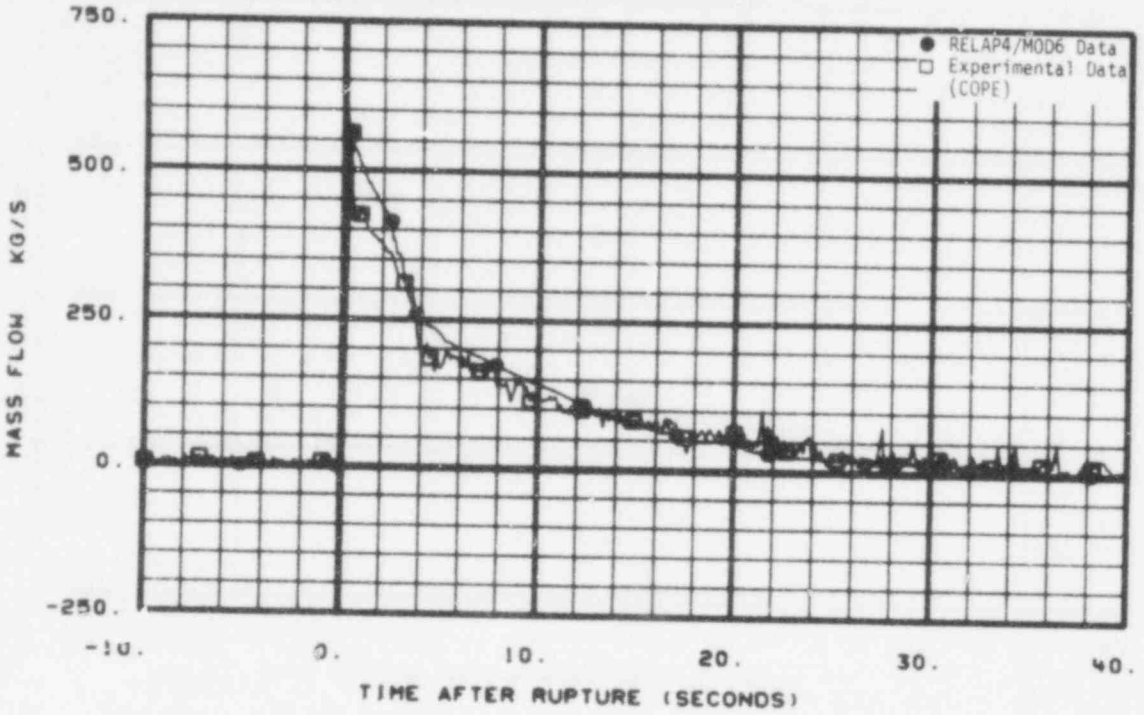

Fig. 16 Comparison of predicted and measured mass flow in broken loop cold leg (FR-BL-1).

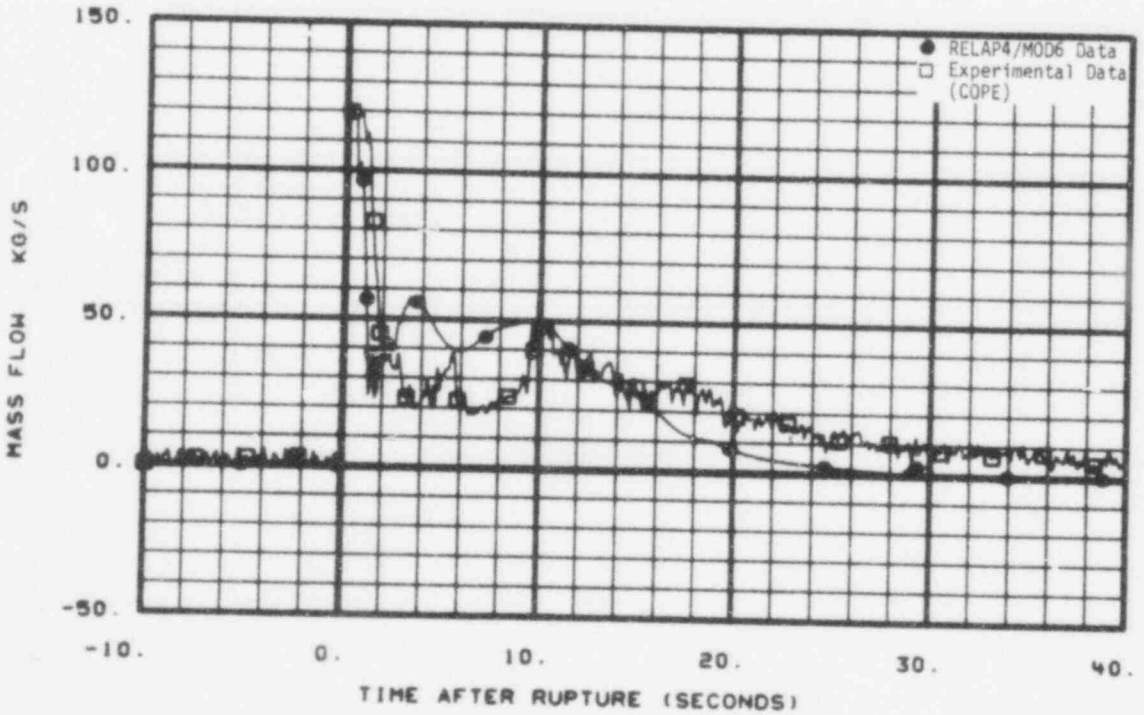

Fig. 17 Comparison of predicted and measured mass flow in broken loop hot leg (FR-BL-2).

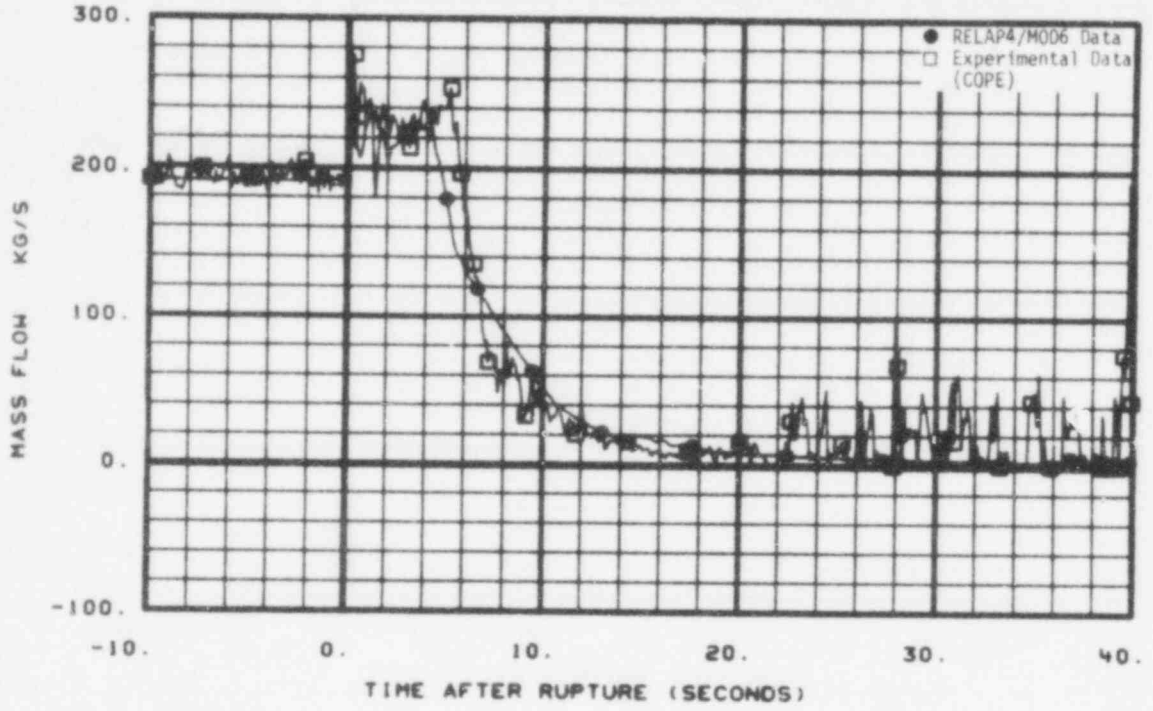

Fig. 18 Comparison of predicted and measured mass flow in intact loop cold leg (FR-PC-1).

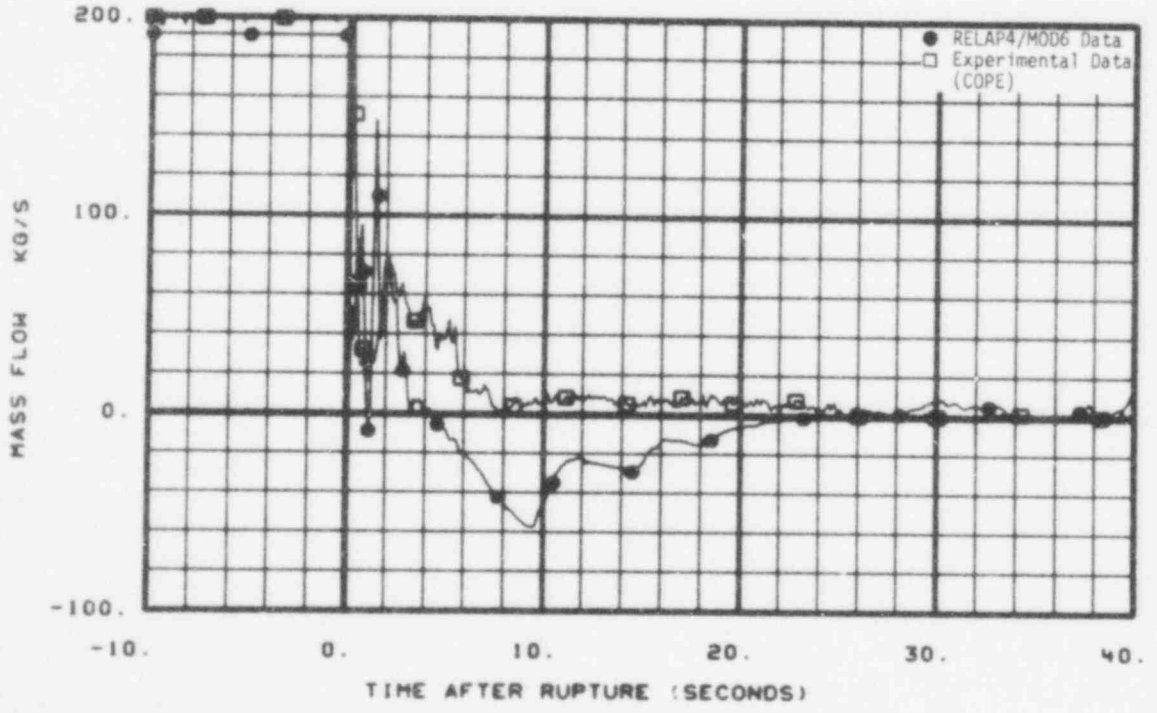

Fig. 19 Comparison of predicted and measured mass flow in intact loop hot leg (FR-PC-2).

2.6 Momentum Flux

The momentum flux comparison in the broken cold leg, Figure 20, is consistent with previous comparisons indicating high calculated values of breakflow at this location. A large disparity, shown in the 0- to 4-s range during the subcooled flow, indicates the calculation is different from the experimental values. The comparison in the broken hot leg, Figure 21, also seems consistent with other data at this location for time less than about 20 s. After 20 s the momentum flux in the experimental data indicates a flow reversal that is not indicated by the differential pressure measurements at this location. The behavior in the intact loop cold leg, Figure 22, seems consistent with the mass flow measurements. Figure 23 compares the momentum flux in the intact loop hot leg. This comparison supports other indications at this location and indicates the general trends in the intact loop hot leg were not calculated correctly. The comparison in Figure 24 shows the momentum flux at the bottom of the downcomer on

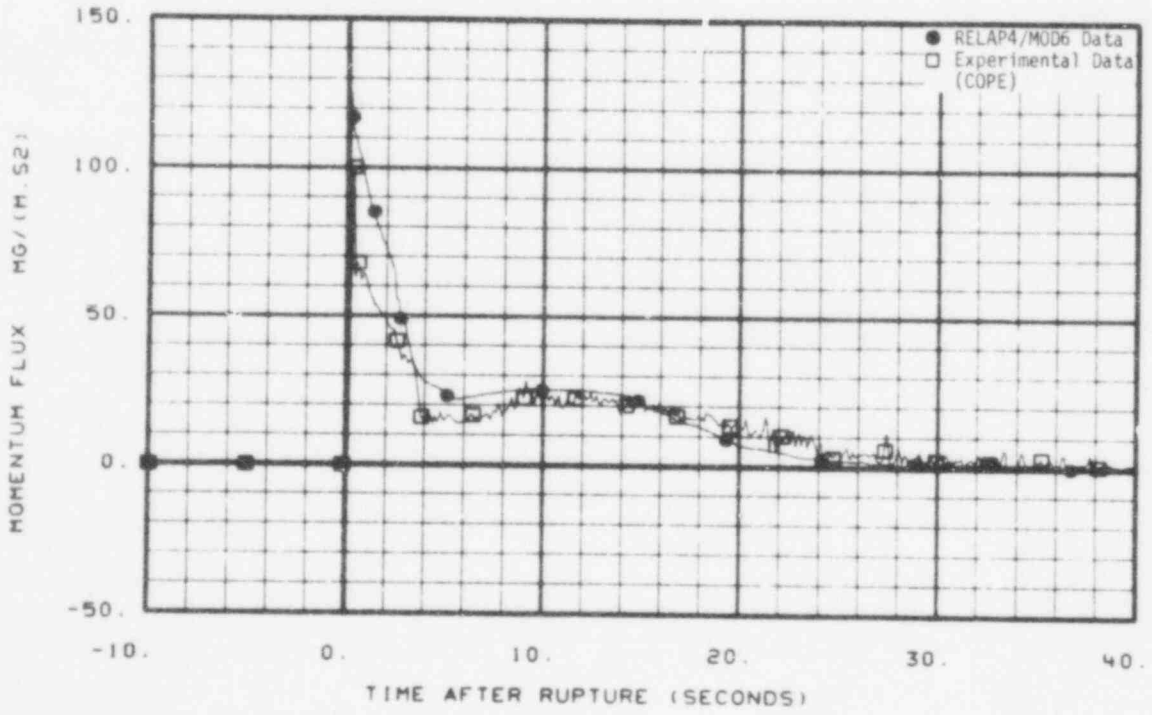

Fig. 20 Comparison of predicted and measured momentum flux in broken loop cold leg (ME-BL-1).

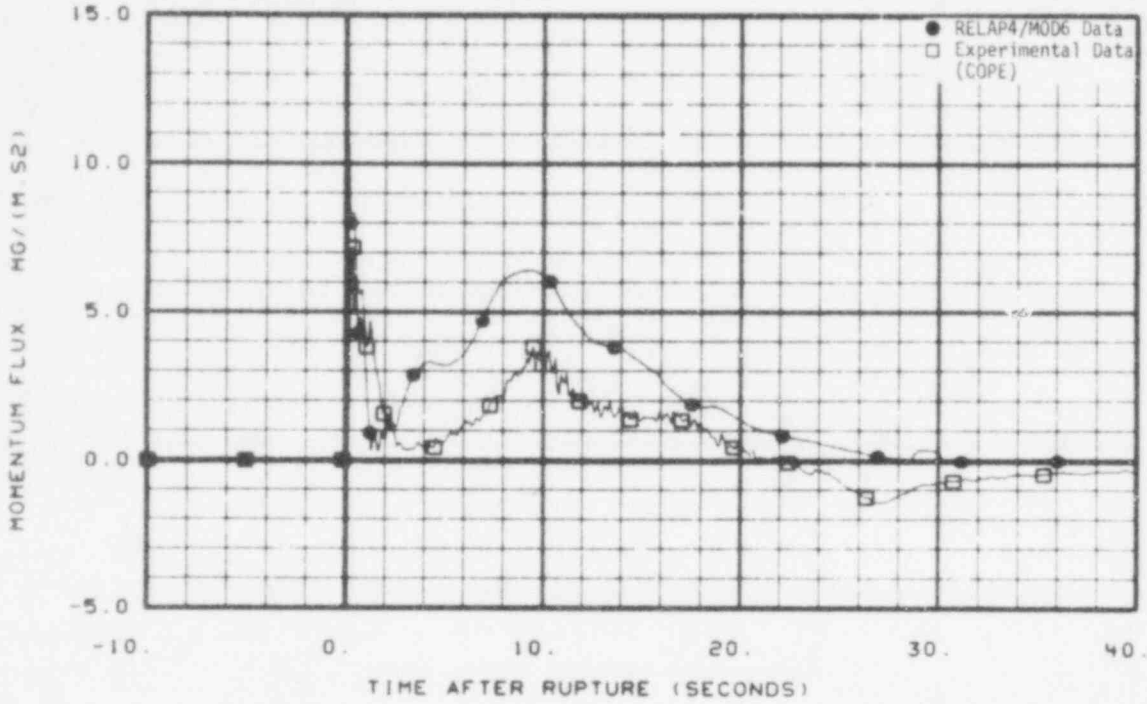

Fig. 21 Comparison of predicted and measured momentum flux in broken loop hot leg (ME-BL-2).

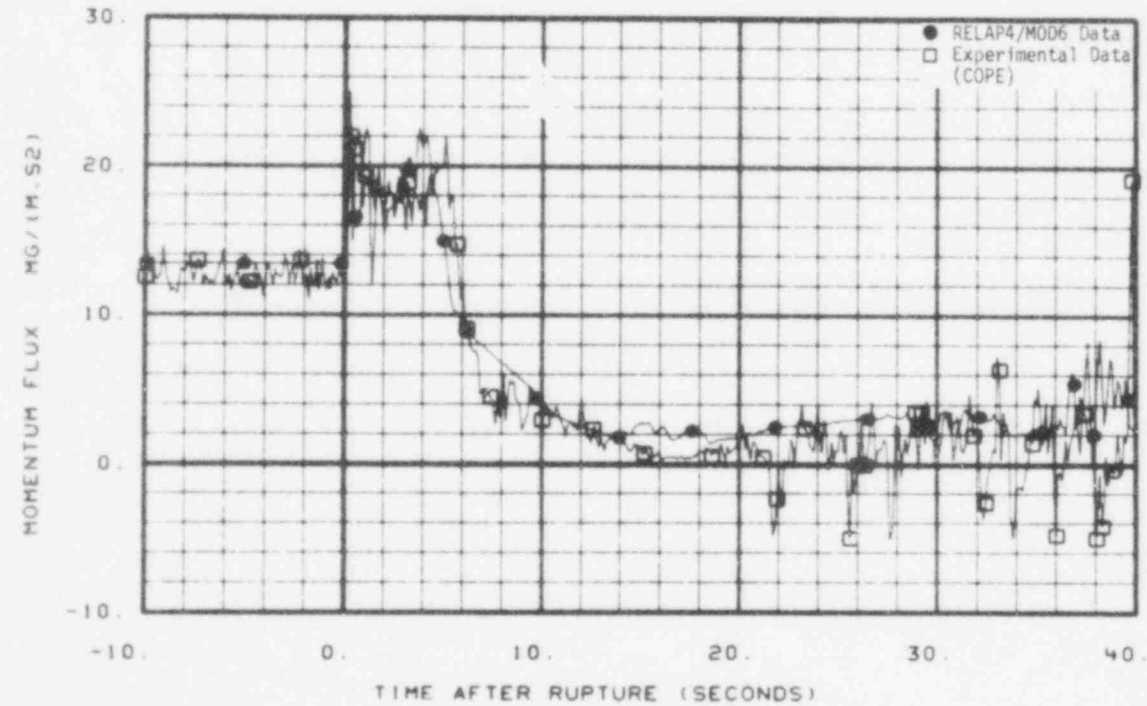

Fig. 22 Comparison of predicted and measured momentum flux in intact loop cold leg (ME-PC-1).

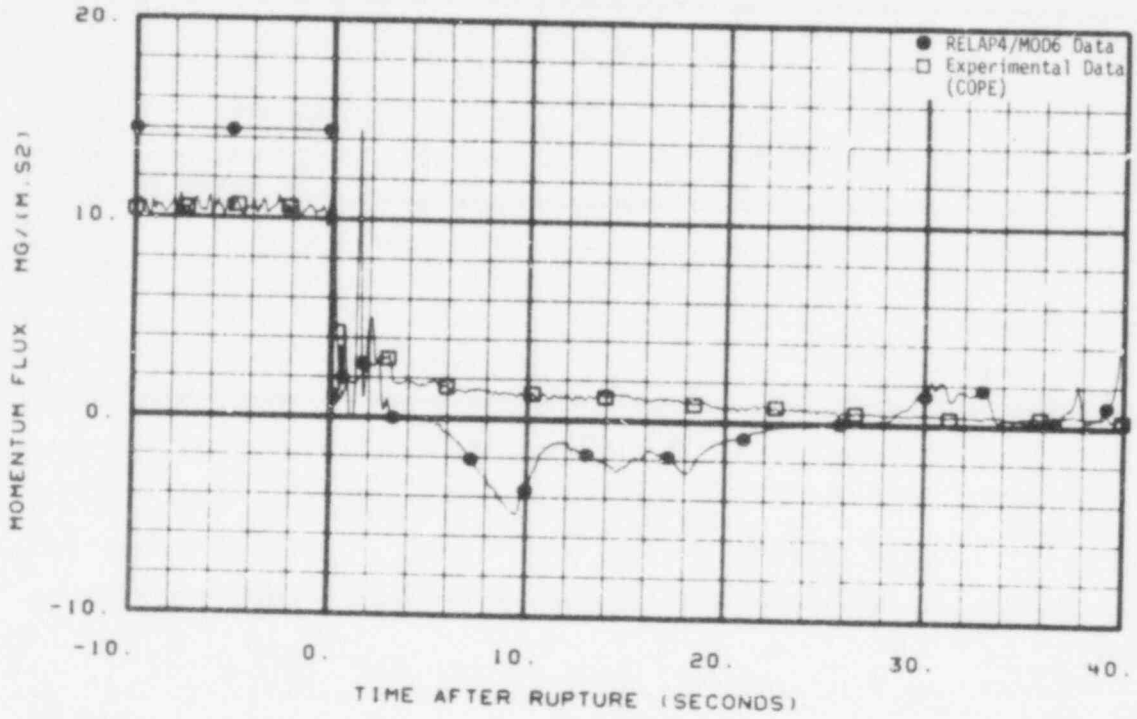

Fig. 23 Comparison of predicted and measured momentum flux in intact loop hot leg (ME-PC-2).

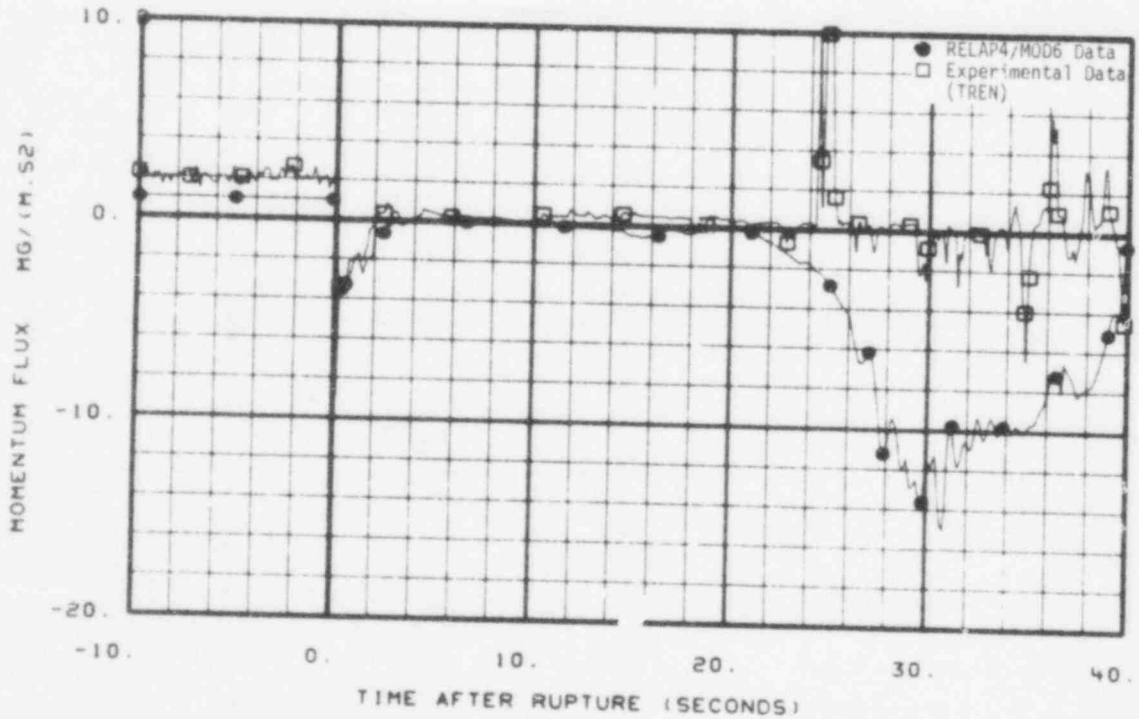

Fig. 24 Comparison of predicted and measured momentum flux at instrument stalk 1 (ME-1ST-1).

755 092

the broken loop side. The calculated and experimentally measured values agree well until about 22 s when the calculations indicate a large flow to the downcomer while the experimental data indicate a small oscillating flow.

At the top of fuel assembly 1, Figure 25 shows the experimental measurement of momentum flux has a sharp initial decrease followed by a large increase and then decays to 0 at about 18 s. This trend is followed in the calculations; however, the increase is not as large as the experimental data indicate. This same behavior is shown in Figure 26, the momentum flux above fuel assembly 3. Figure 27 shows the momentum flux on the intact loop side of the downcomer outlet to the lower plenum. The data compare favorably after 2 s. Before 2 s, a large flow to the downcomer is indicated by the experimental data but is not calculated to occur great in magnitude. The momentum flux comparison in Figures 24 and 27 are based on inconsistent flow areas which cause some of the magnitude differences.

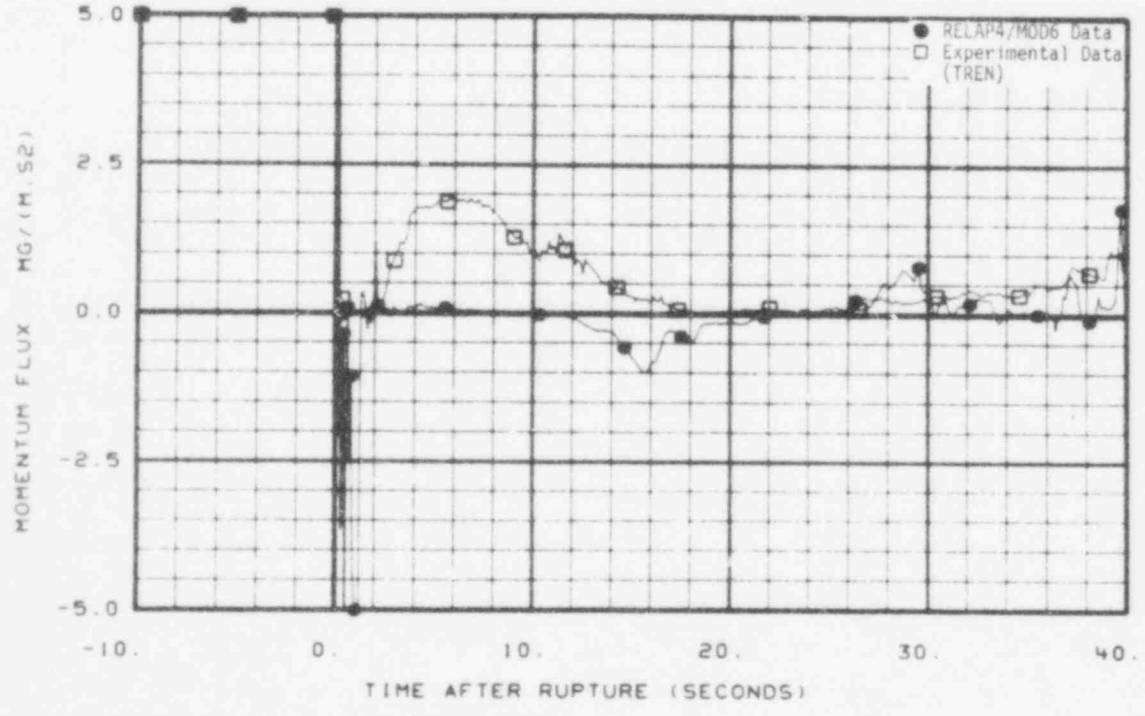

Fig. 25 Comparison of predicted and measured momentum flux in upper end box (ME-1UP-1).

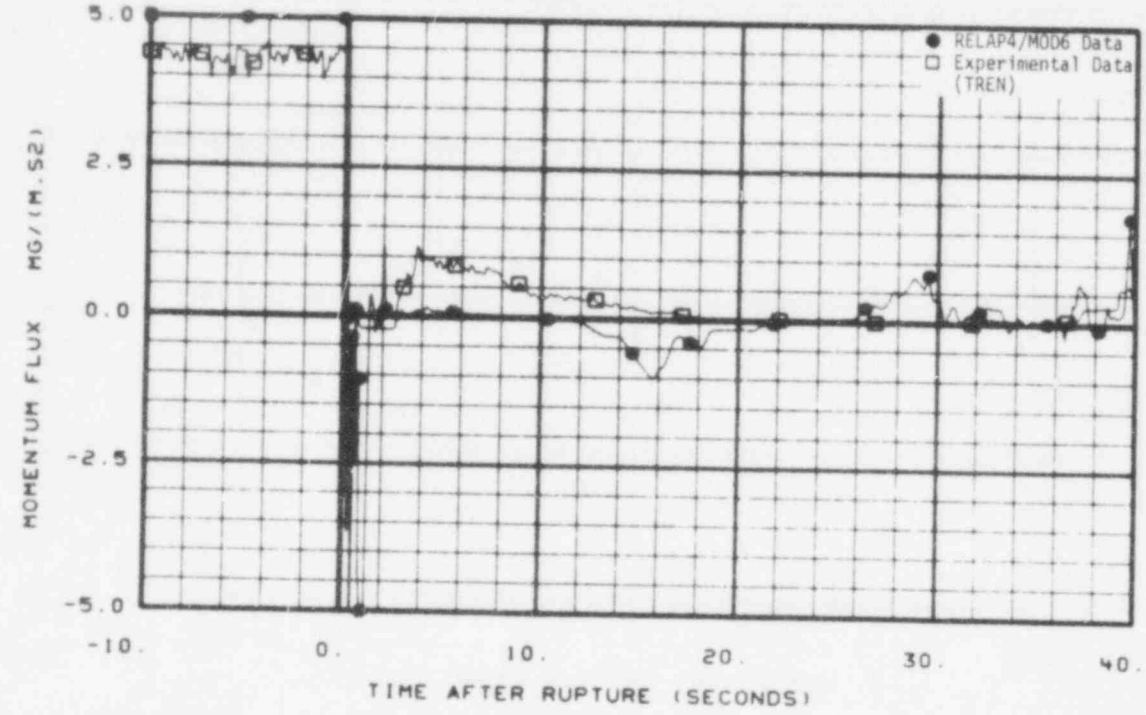

Fig. 26 Comparison of predicted and measured momentum flux in upper end box (ME-3UP-1).

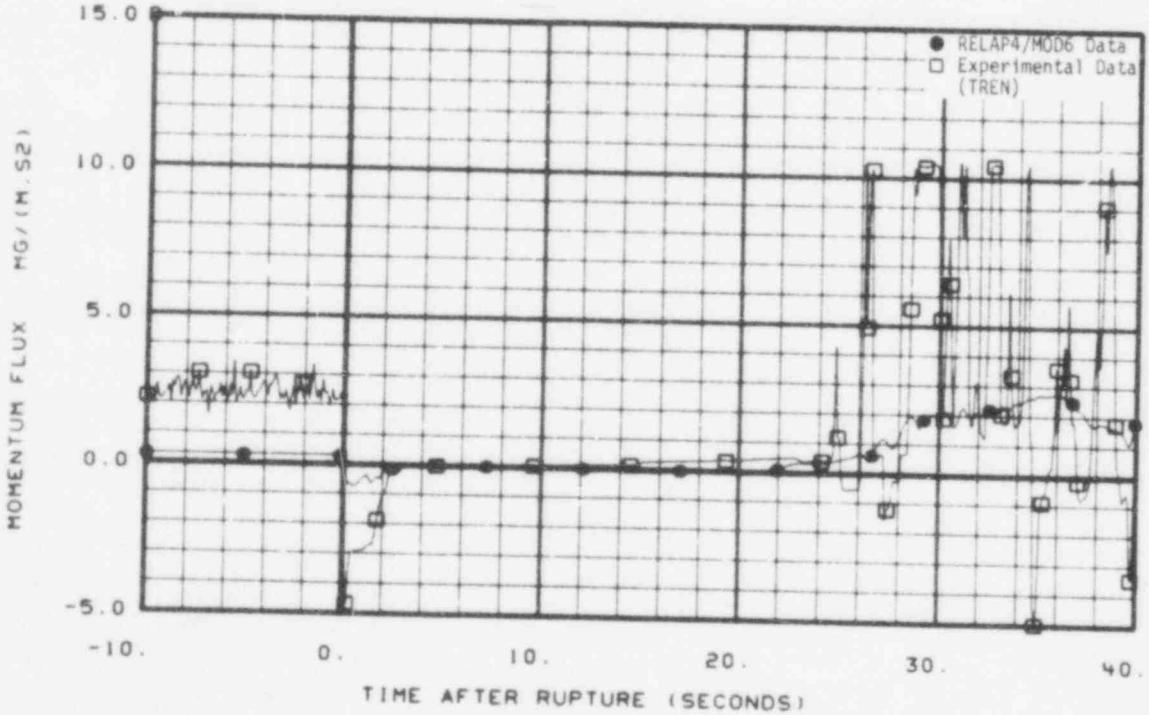

Fig. 27 Comparison of predicted and measured momentum flux at instrument stalk 2 (ME-2ST-1).

2.7 Pressure

Figures 28 through 36 show the pressure history comparisons at different locations in the system. These figures show that the calculated pressure agrees very well with the experimental data until about 7 s. After 7 s, the calculated pressure is lower than the experimental data. The calculated break flow is indicated high.

Figures 37 and 38 indicate the boundary conditions at the steam generator and suppression tank were probably improperly stated in the calculations. Figure 39 indicates the accumulator flow started later in the experiment than calculated and is consistent with flow and level comparisons.

2.8 Pump Speed

The primary coolant pump speed for pump 1 is shown in Figure 40. The experimental data indicate the pump begins to "unload" at about

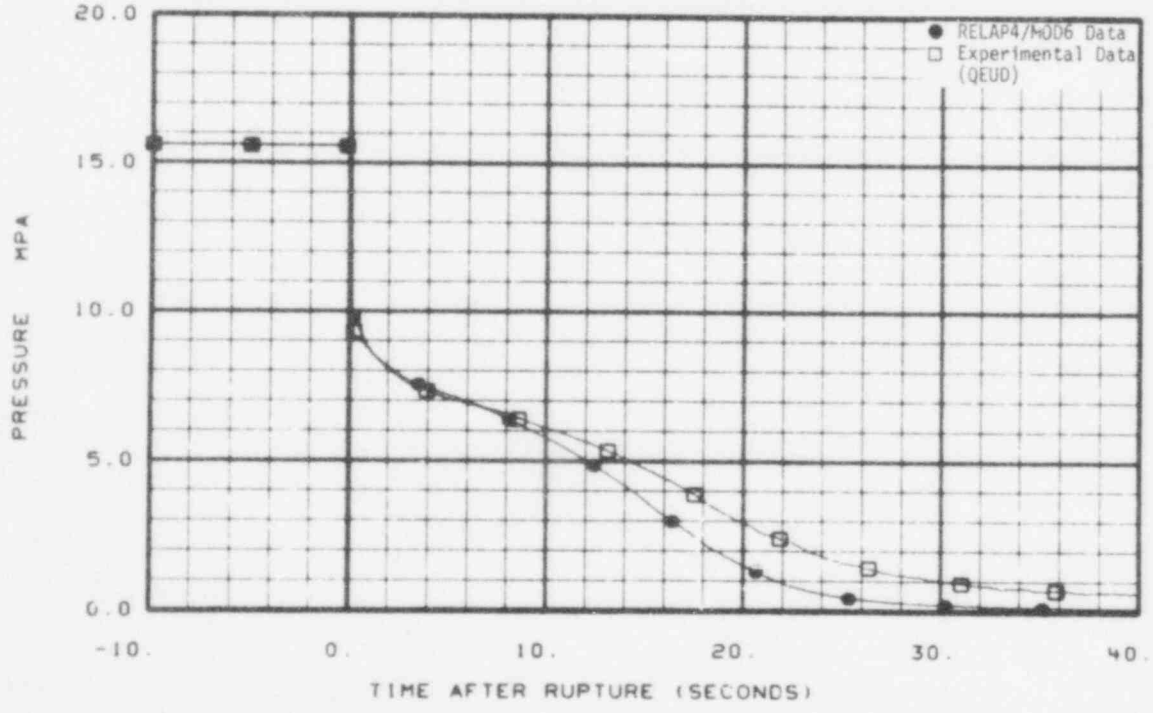

Fig. 28 Comparison of predicted and measured pressure in broken loop cold leg (PE-BL-1).

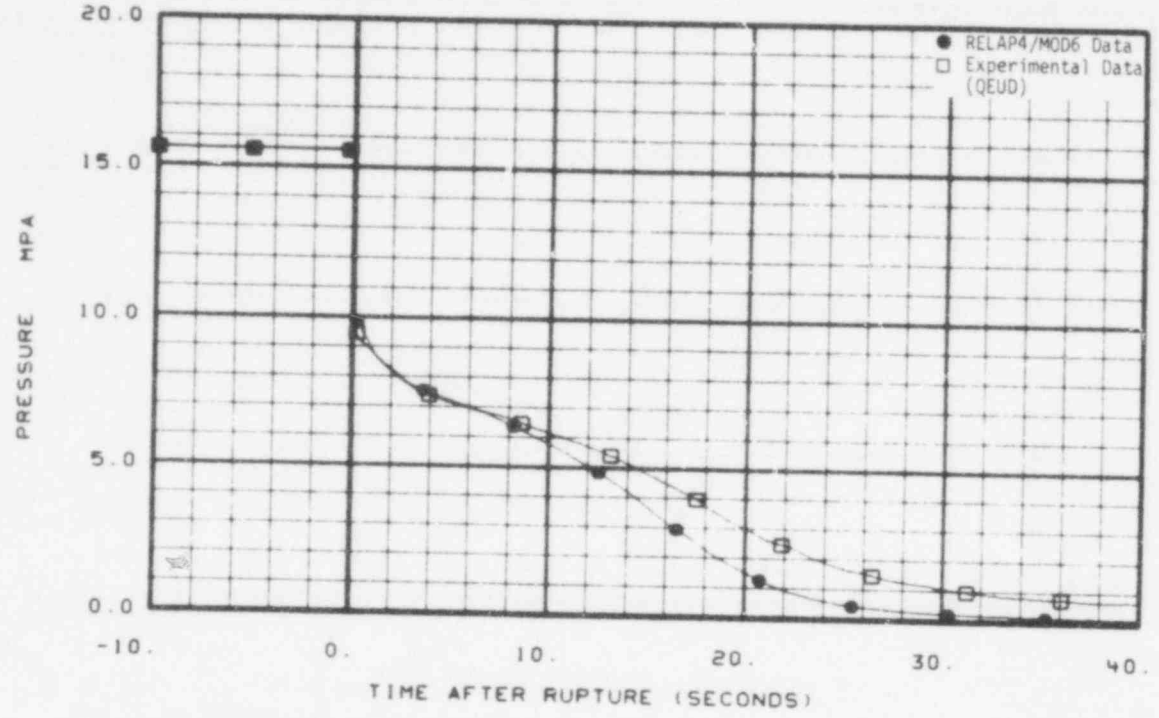

Fig. 29 Comparison of predicted and measured pressure in broken loop hot leg (PE-BL-2).

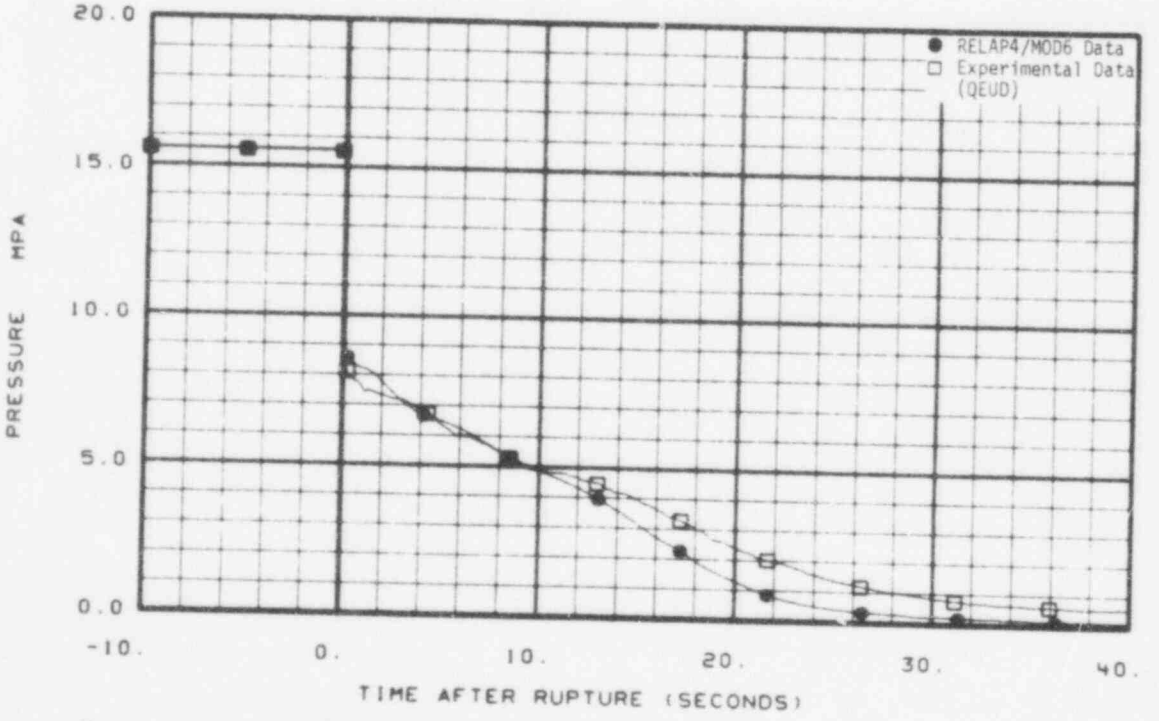

Fig. 30 Comparison of measured and predicted pressure at steam generator simulator outlet (PE-BL-6).

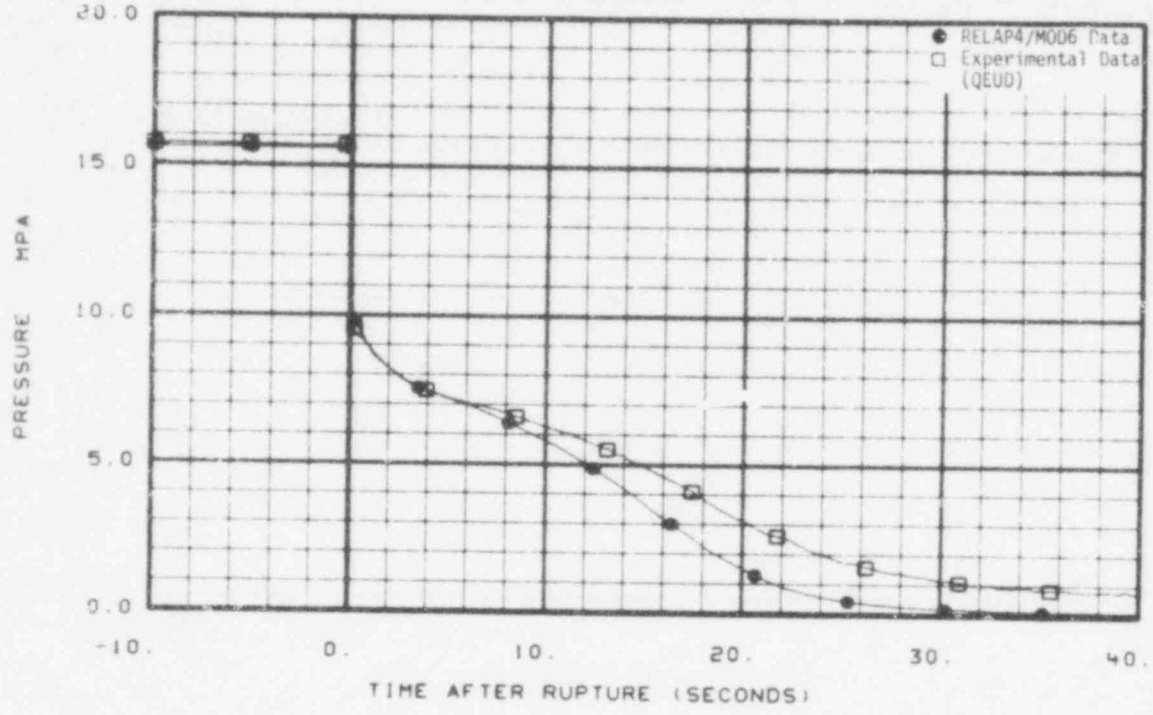

Fig. 31 Comparison of predicted and measured pressure in intact loop cold leg (PE-PC-1).

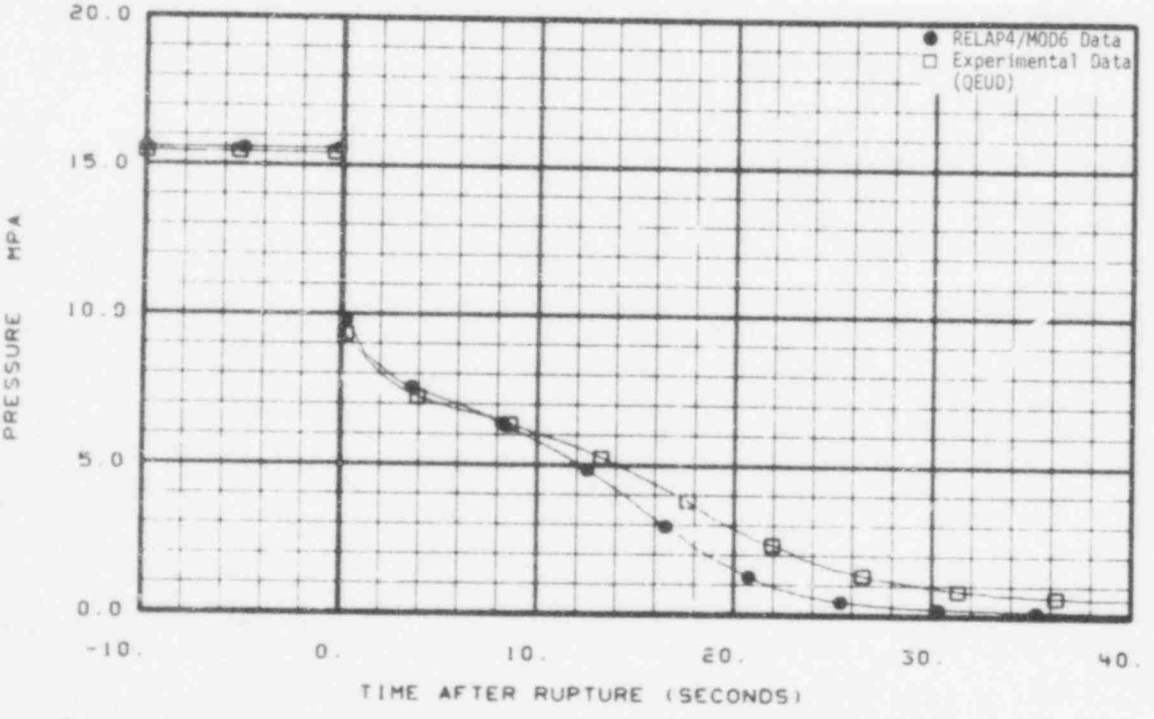

Fig. 32 Comparison of predicted and measured pressure in intact loop hot leg (PE-PC-2).

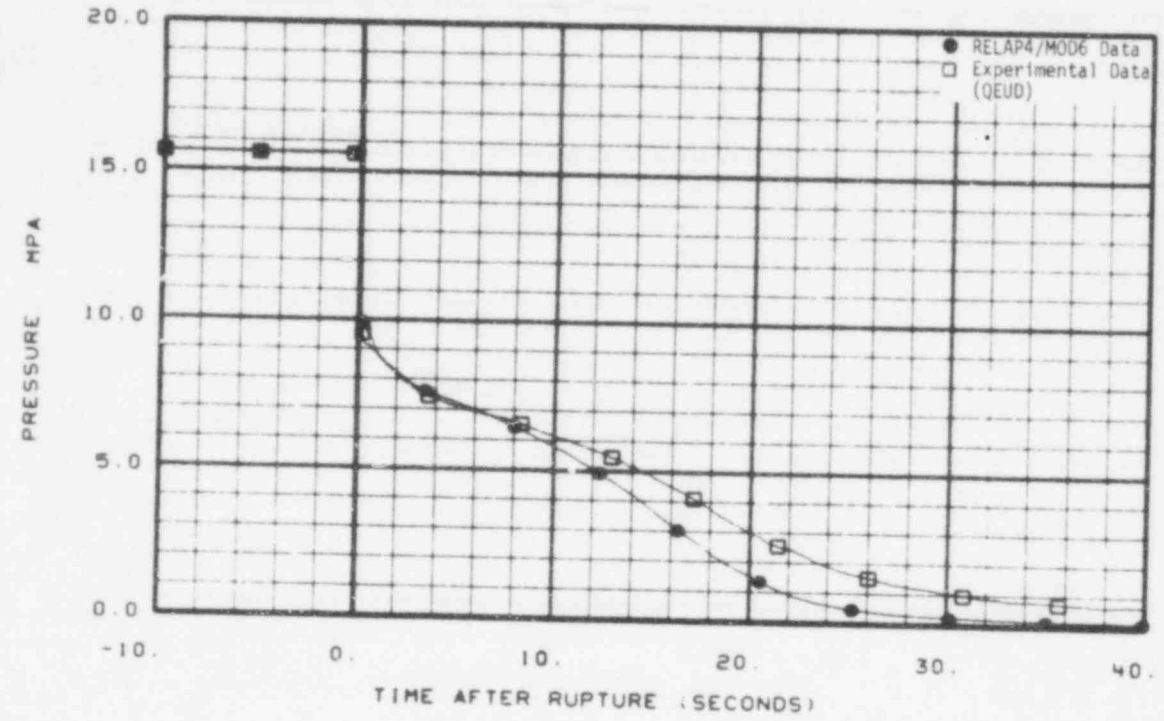

Fig. 33 Comparison of measured and predicted pressure at instrument stalk 1 (PE-1ST-1A).

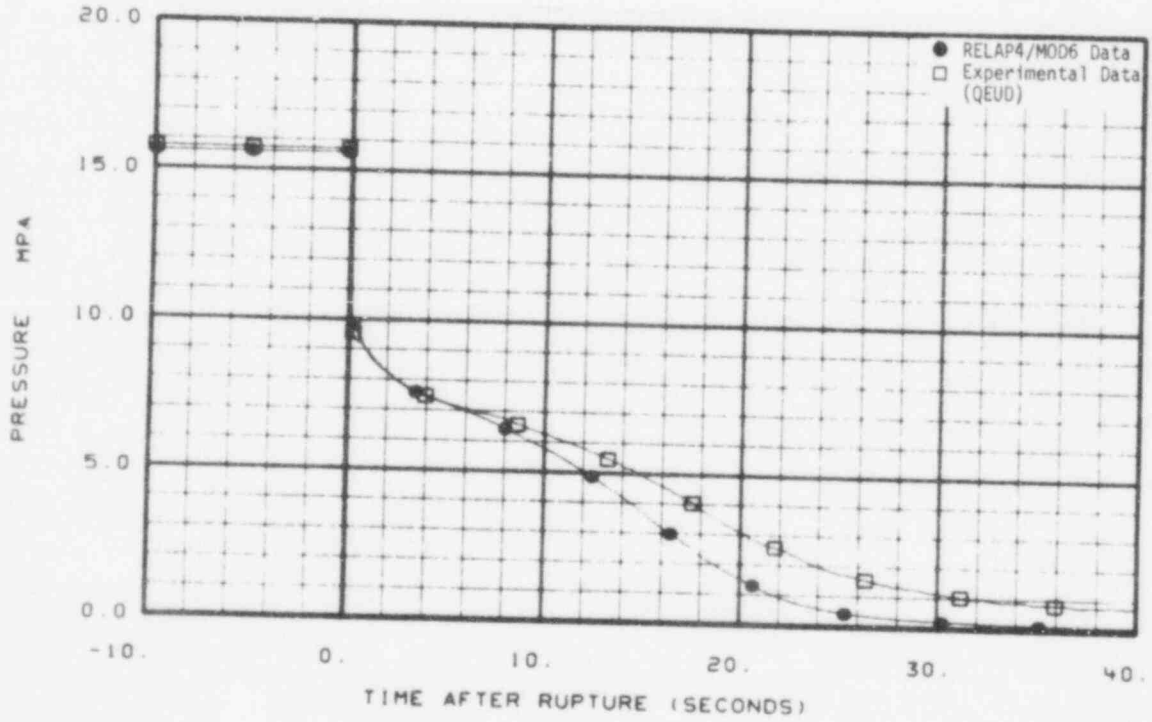

Fig. 34 Comparison of predicted and measured pressure at instrument stalk 1 (PE-1ST-3A).

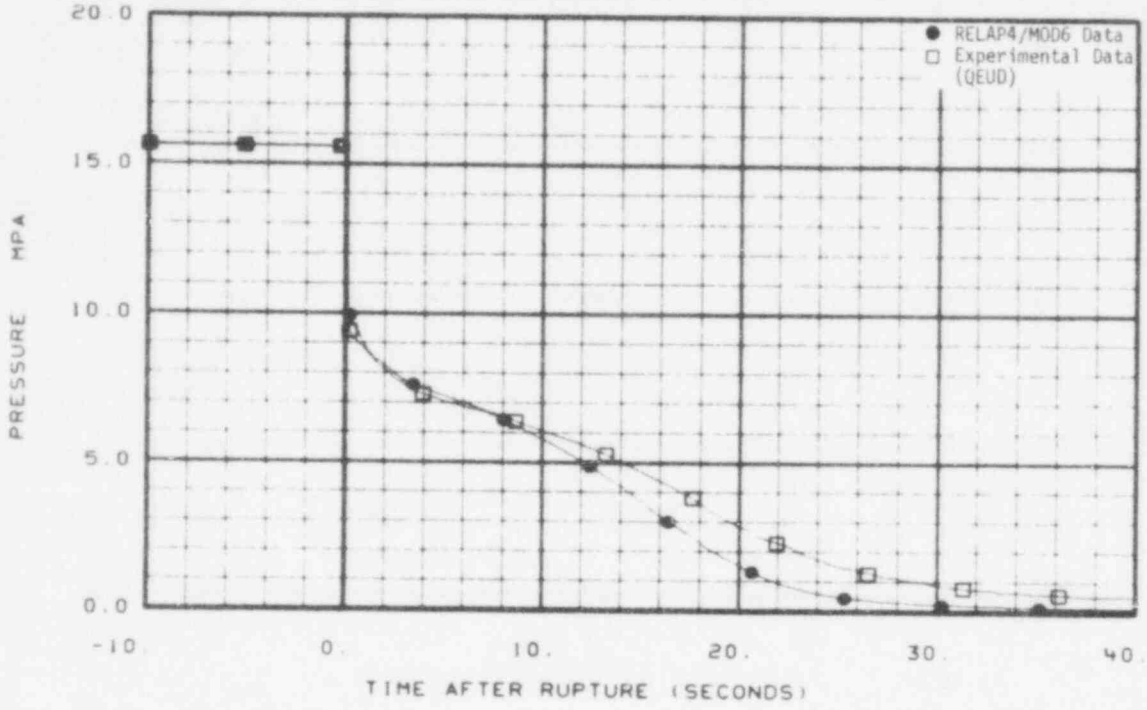

Fig. 35 Comparison of predicted and measured pressure in upper end box (PE-1UP-1A).

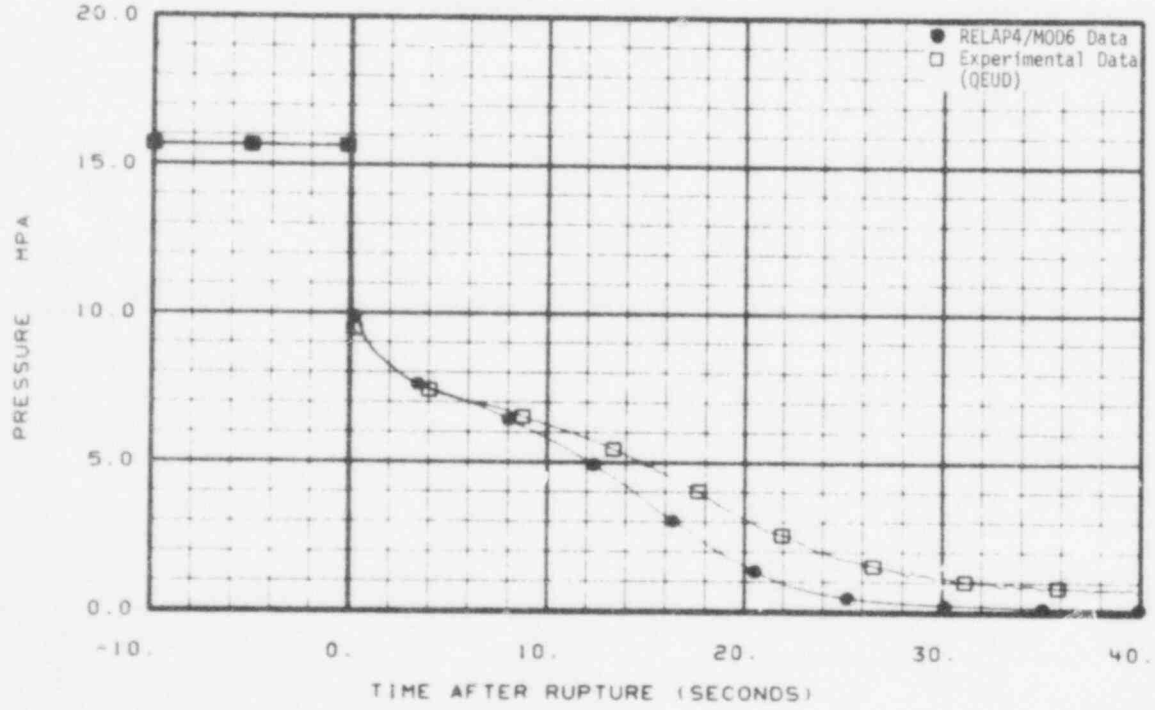

Fig. 36 Comparison of predicted and measured pressure at instrument stalk 2 (PE-2ST-1A).

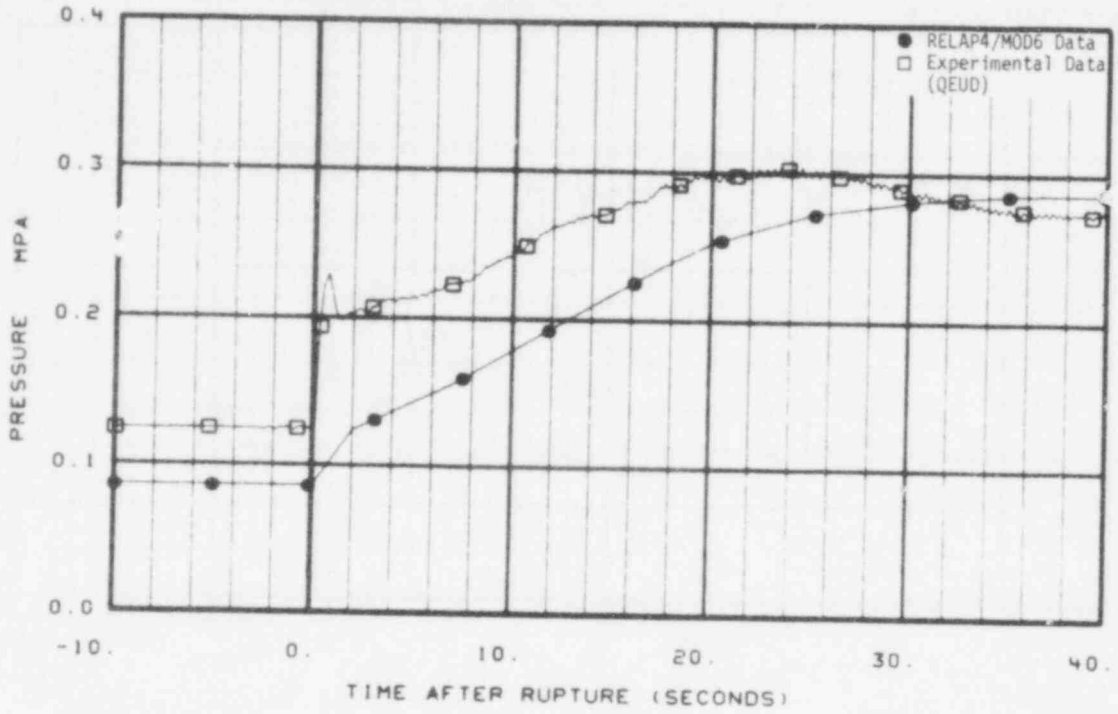

Fig. 37 Comparison of predicted and measured pressure in suppression tank (PE-SV-17).

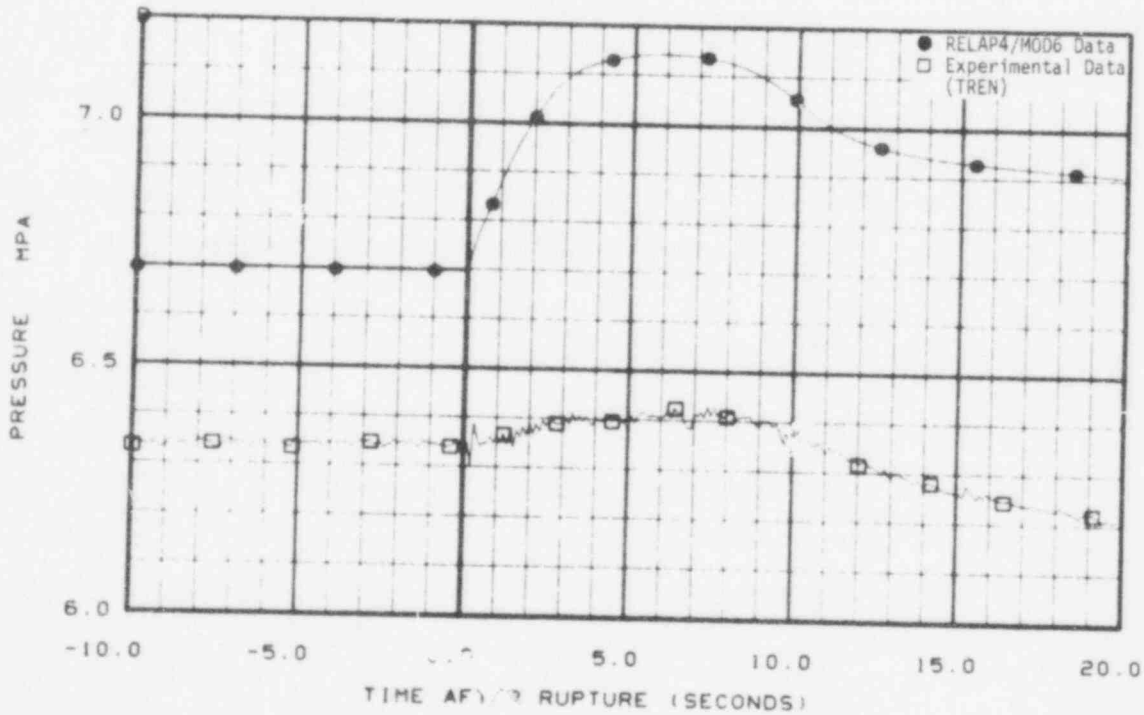

Fig. 38 Comparison of predicted and measured pressure in steam generator secondary (PT-P004-10A).

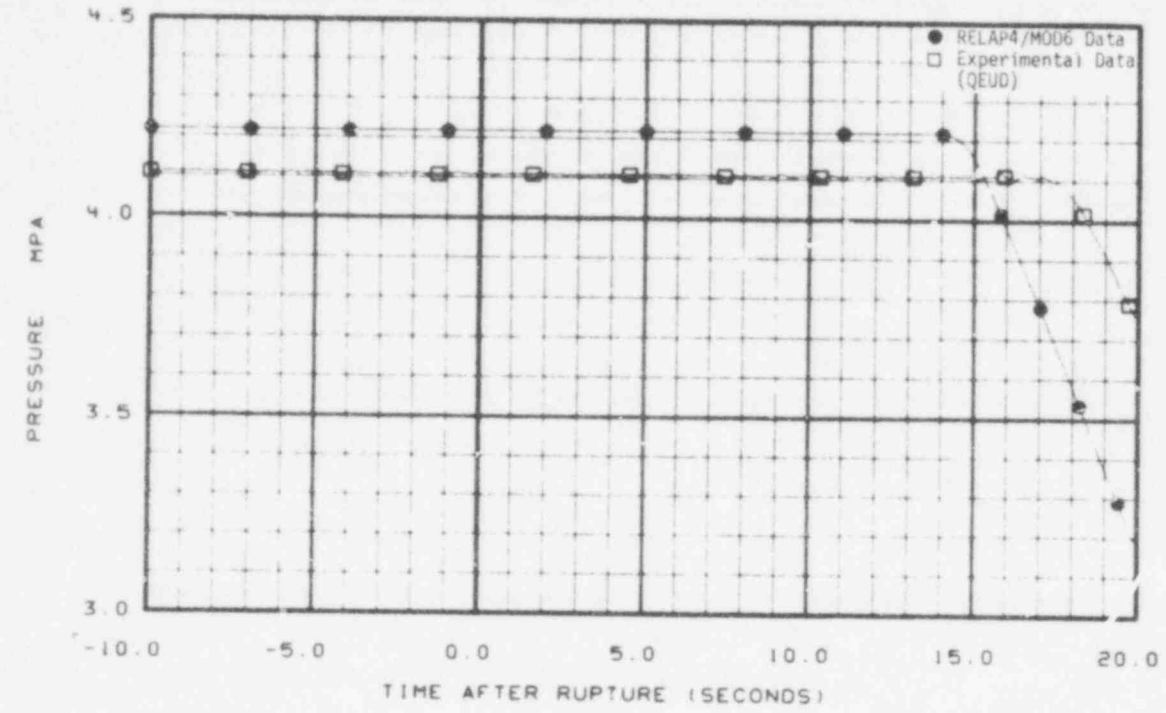

Fig. 39 Comparison of predicted and measured pressure in accumulator (PT-P120-43).

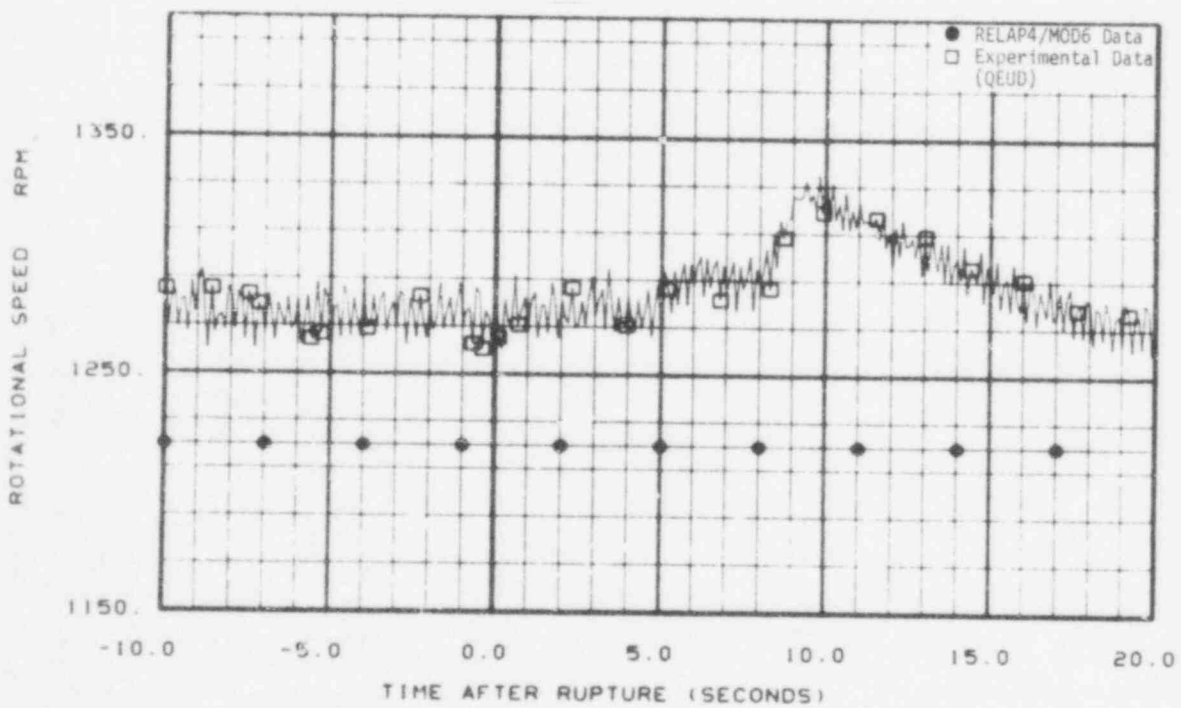

Fig. 40 Comparison of predicted and measured pump speed for pump 2 (RPE-PC-2).

4 s which agrees with a coincident measured pump differential pressure degradation. The constant pump speed used in the calculations does not follow the experimental data trend and is lower than the experimental values.

2.9 Velocity

The coolant velocity comparison in the broken cold leg, Figure 41, shows the calculated velocity is higher than the measured velocity for a time period less than 20 s. An overprediction of broken cold leg mass flow is again indicated. The broken hot leg velocity comparison in Figure 42 supports indications in other measurements that a flow reduction experienced in the experimental facility at about 4 s is calculated to occur about 2 s early. The trends in the experimental data are generally not well followed by the calculations.

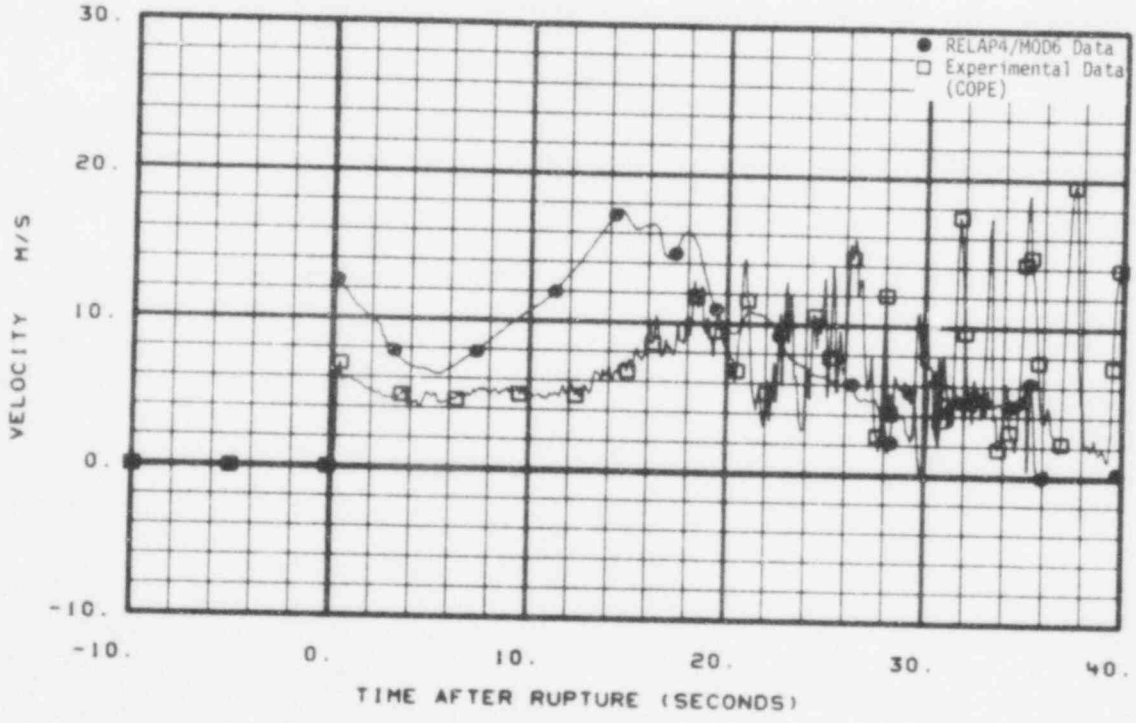

Fig. 41 Comparison of predicted and measured average velocity in broken loop cold leg (FE-BL-1).

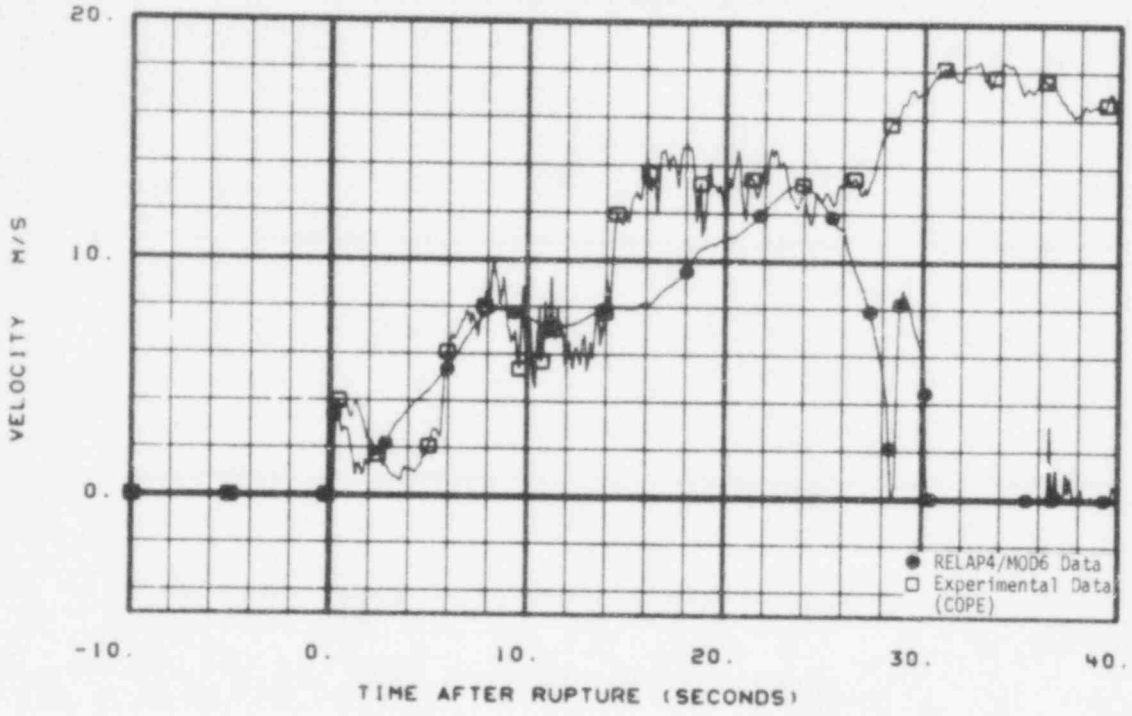

Fig. 42 Comparison of predicted and measured average velocity in broken loop hot leg (FE-BL-2).

The intact cold leg velocity comparison, Figure 43, is very good until 6 s at which time the calculated values begin diverging from the experimental data. The velocity comparison in the intact hot leg, shown in Figure 44, indicates the physical processes occurring in this area are not well accounted for in the calculations since neither the trends nor the magnitudes of the experimental measurement are followed by the calculations.

2.10 Temperatures

Figures 45 and 46 compare the coolant temperatures in the broken cold leg and broken hot leg. These comparisons indicate that a larger initial subcooling existed in these areas than was used in the calculations. The larger initial subcooling is particularly true for the broken hot leg. For the intact loops, Figures 47 and 48, the temperatures compared well until about 10 s when the calculated values begin to fall below the measured data. Figures 49 through 60 compare the coolant temperatures on the broken leg side of the downcomer. The

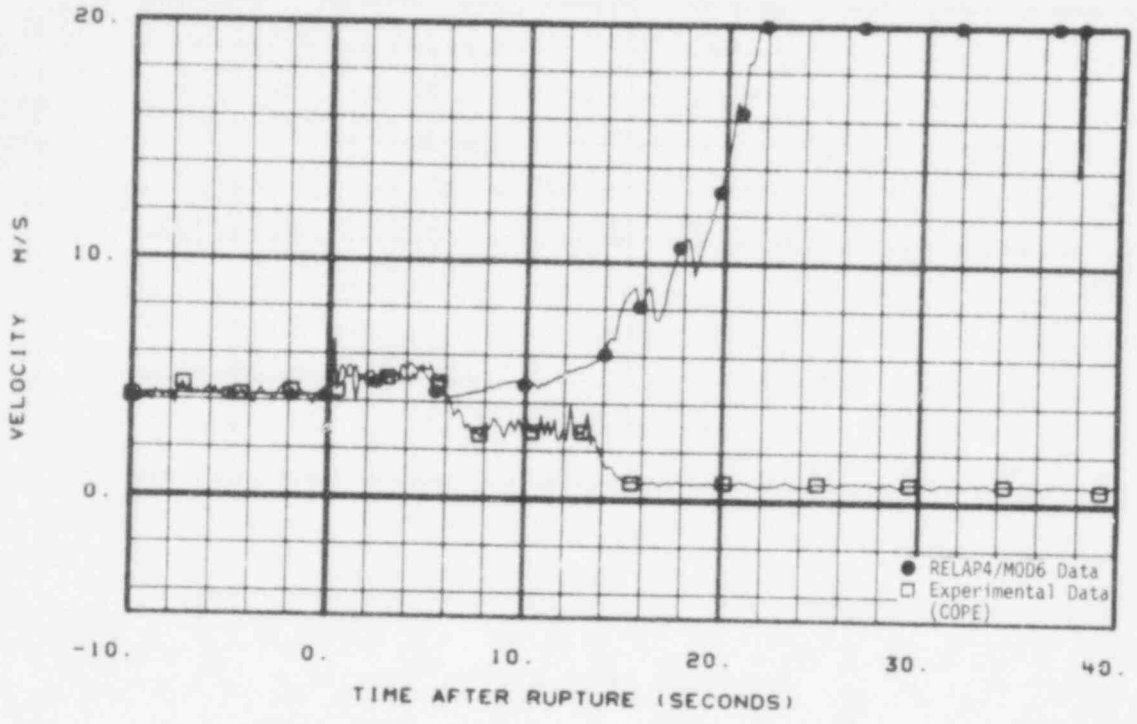

Fig. 43 Comparison of predicted and measured average velocity in intact loop cold leg (FE-PC-1).

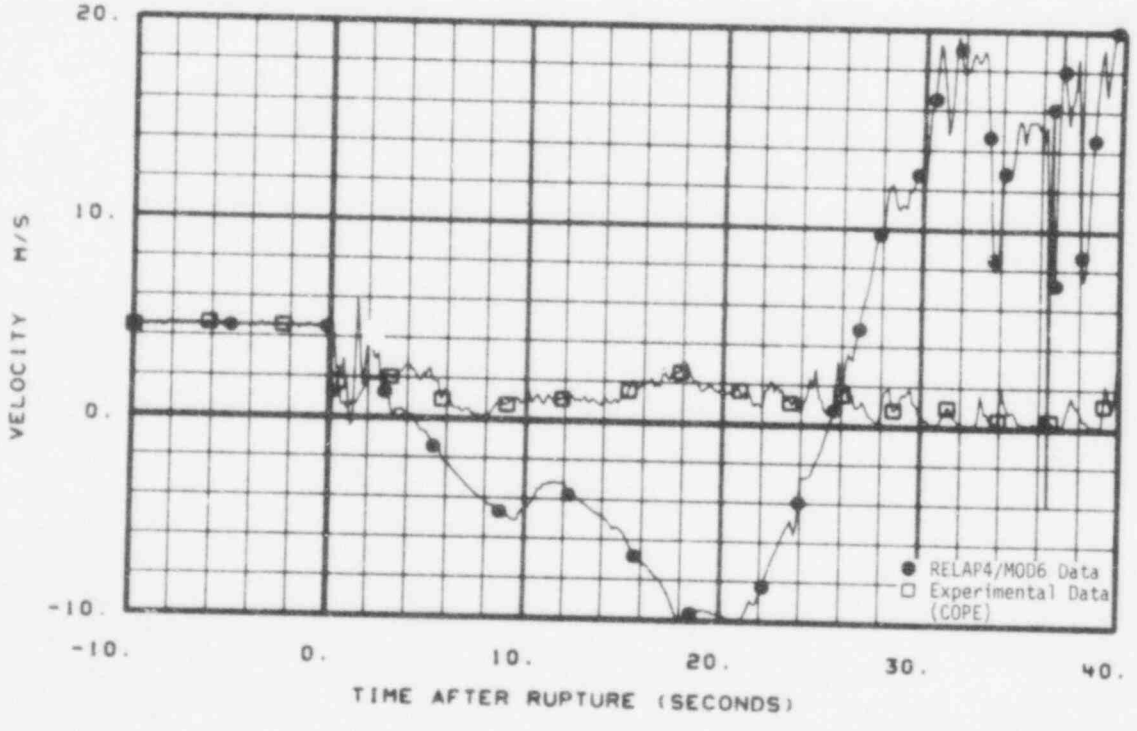

Fig. 44 Comparison of predicted and measured average velocity in intact loop hot leg (FE-PC-2).

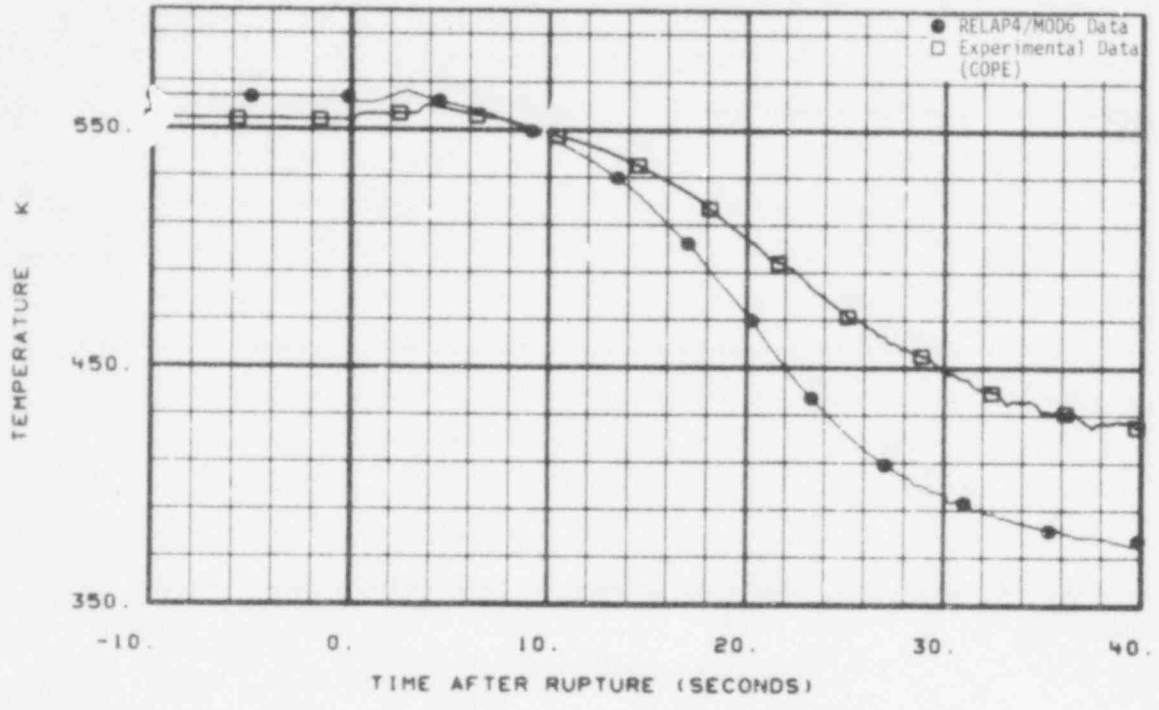

Fig. 45 Comparison of predicted and measured average temperature in broken loop cold leg (TE-BL-1).

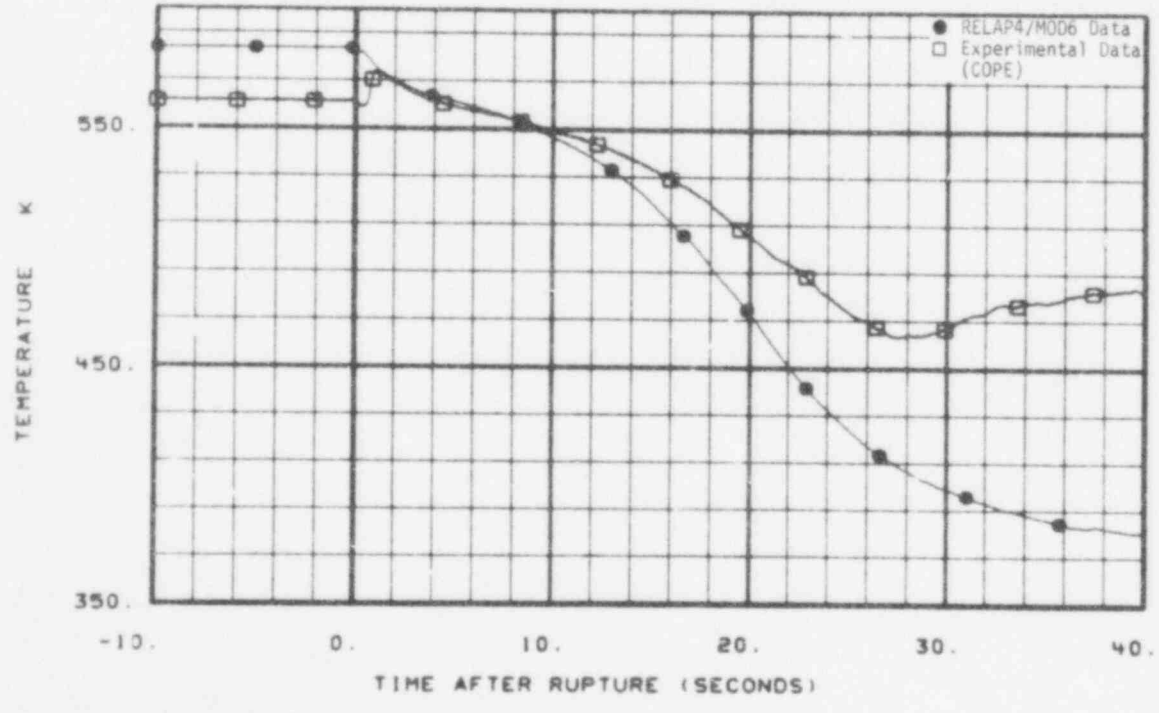

Fig. 46 Comparison of predicted and measured average coolant temperature in broken loop hot leg (TE-BL-2).

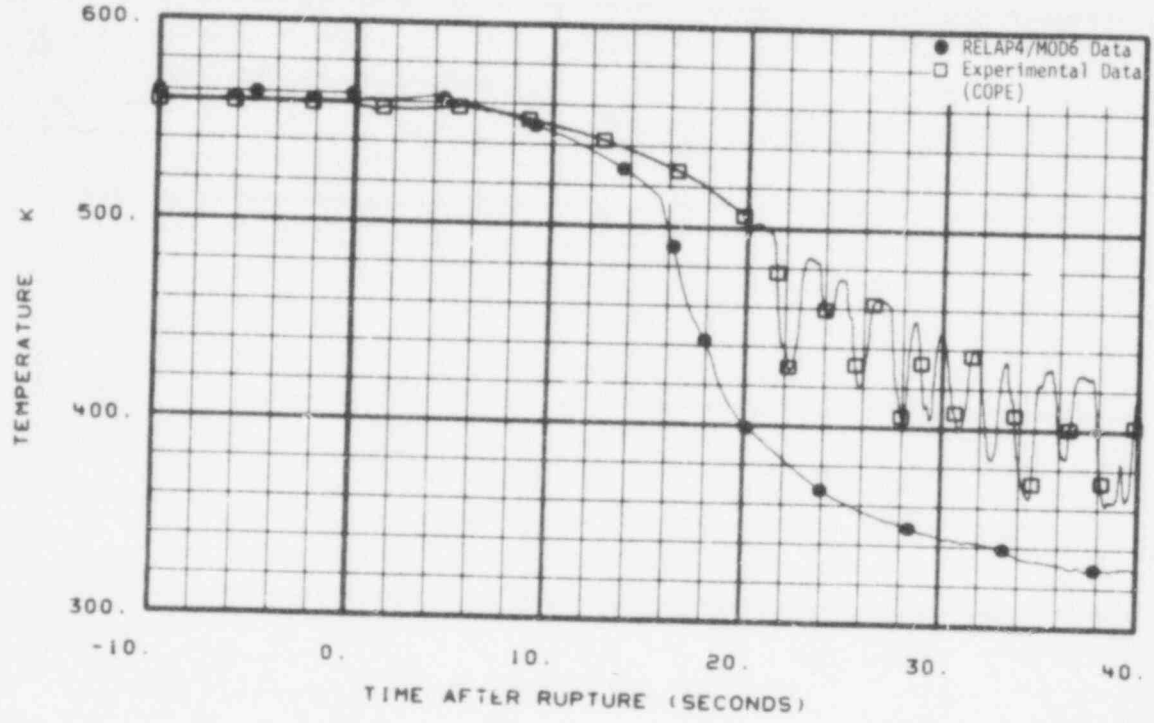

Fig. 47 Comparison of predicted and measured average temperature in intact loop cold leg (TE-PC-1).

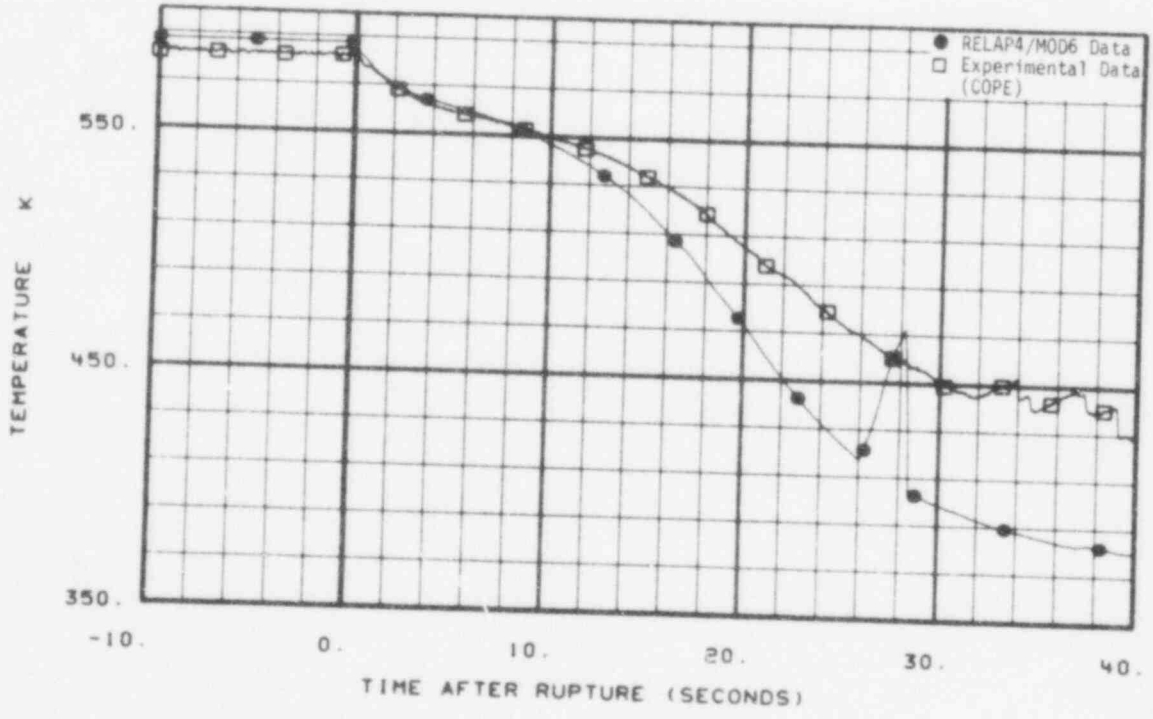

Fig. 48 Comparison of predicted and measured average coolant temperature in intact loop hot leg (TE-PC-2).

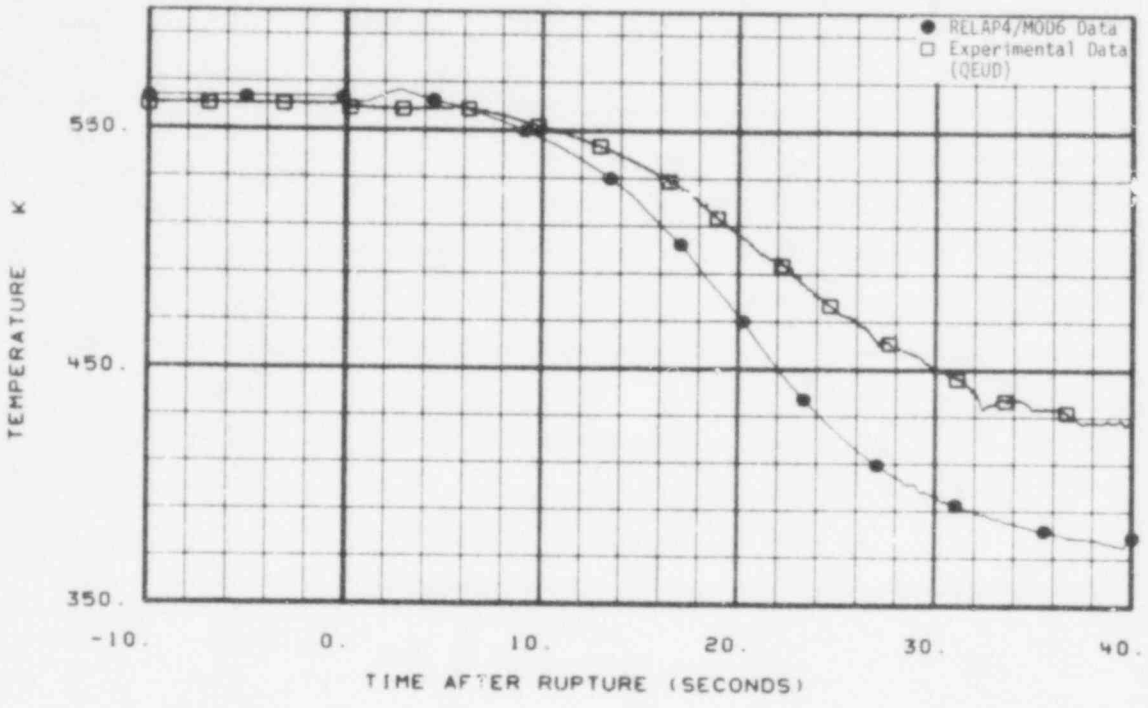

Fig. 49 Comparison of predicted and measured coolant temperature on instrument stalk 1 (TE-1ST-1).

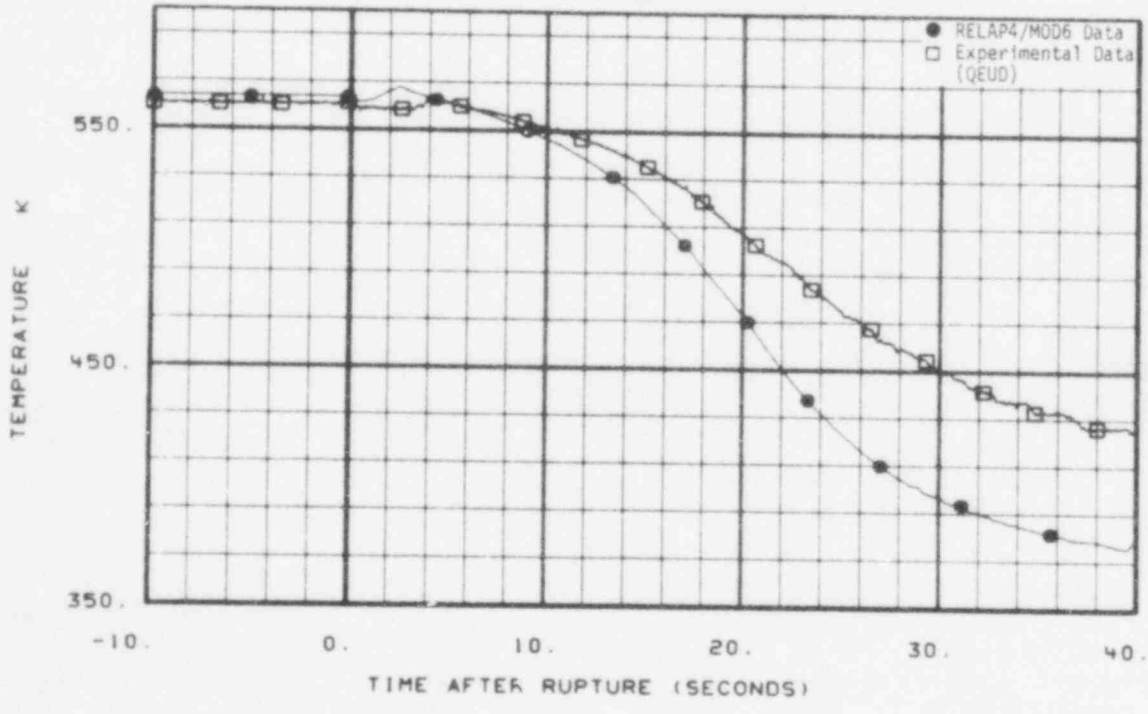

Fig. 50 Comparison of predicted and measured coolant temperature on instrument stalk 1 (TE-1ST-2).

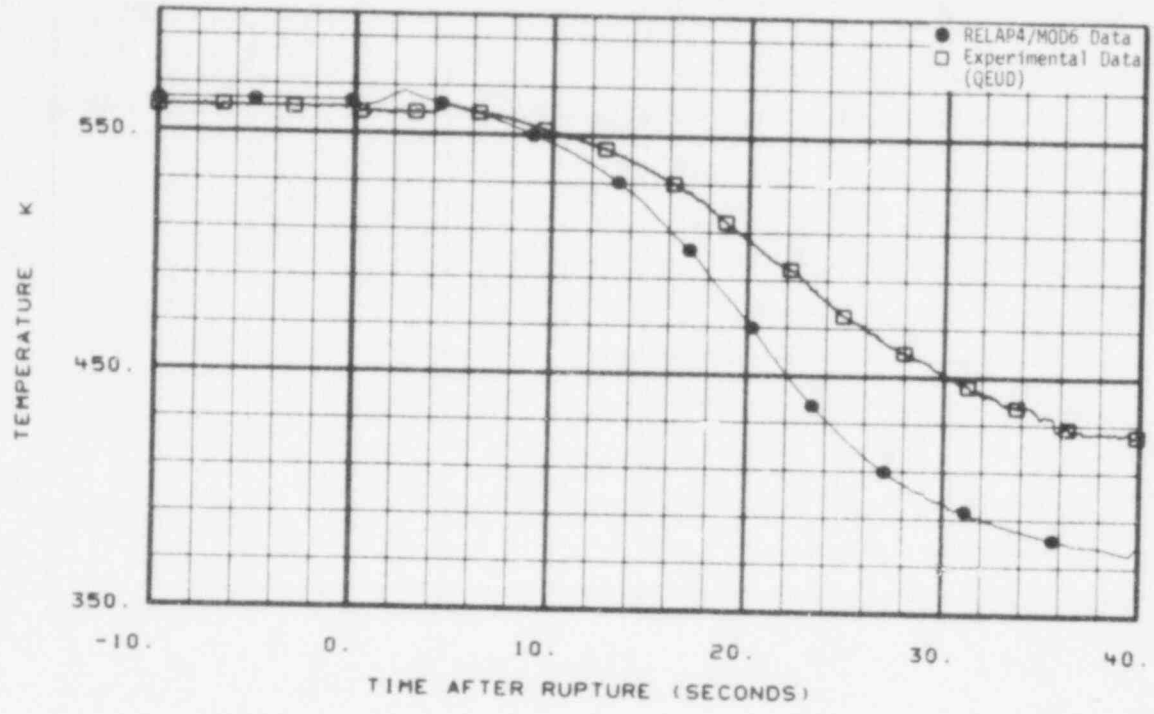

Fig. 51 Comparison of predicted and measured coolant temperature on instrument stalk 1 (TE-1ST-3).

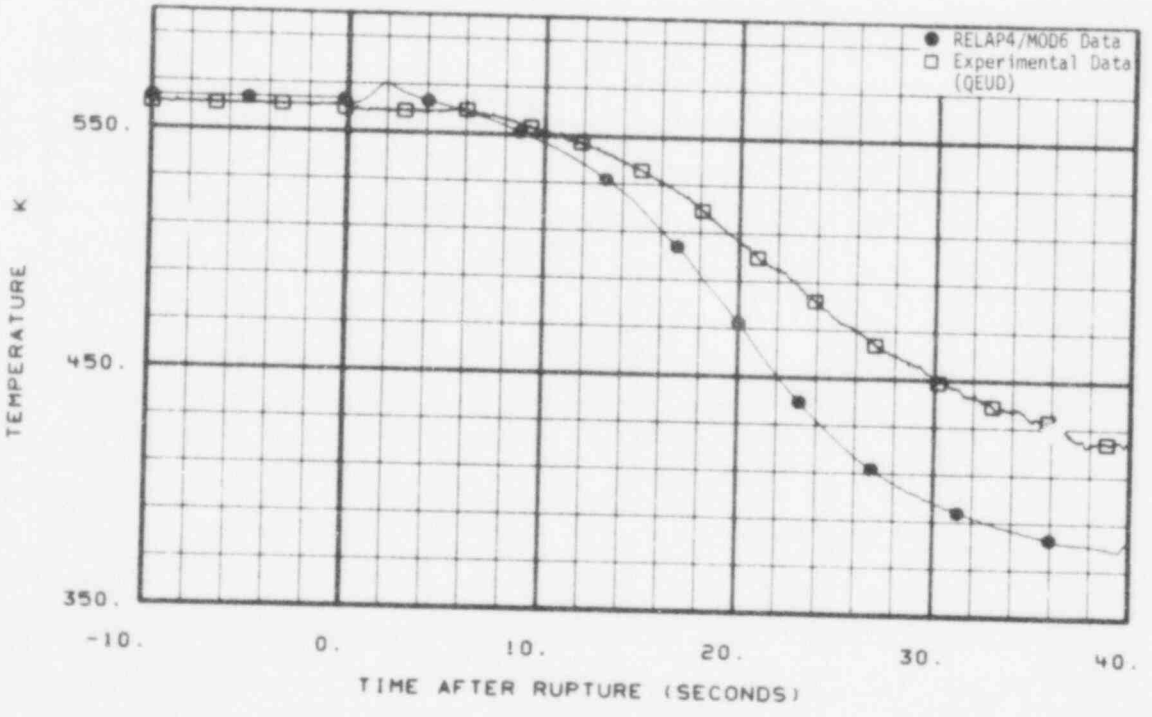

Fig. 52 Comparison of predicted and measured coolant temperature on instrument stalk 1 (TE-1ST-4).

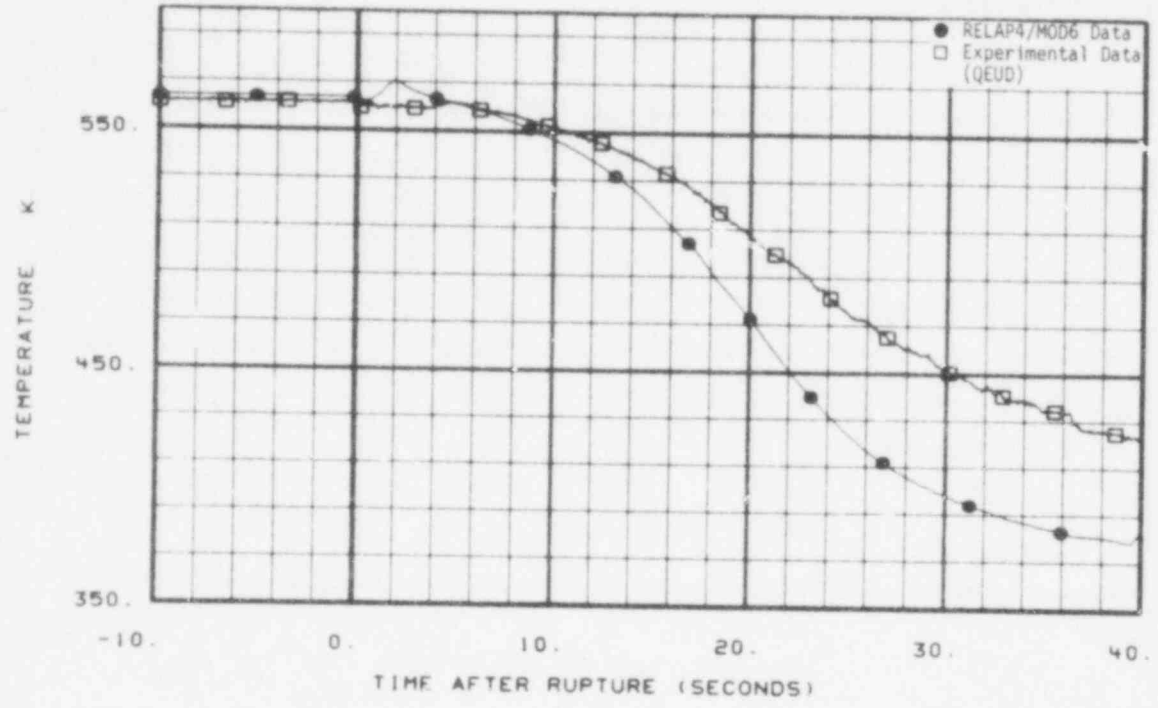

Fig. 53 Comparison of predicted and measured coolant temperature on instrument stalk 1 (TE-1ST-5).

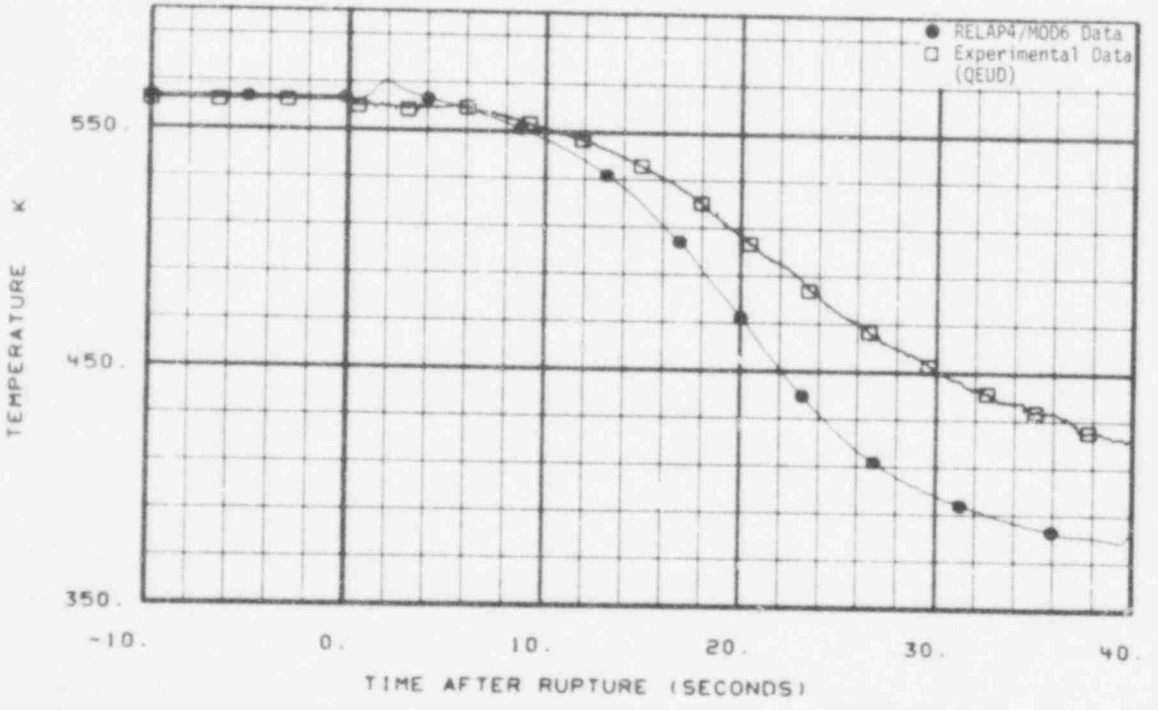

Fig. 54 Comparison of predicted and measured coolant temperature on instrument stalk 1 (TE-1ST-6).

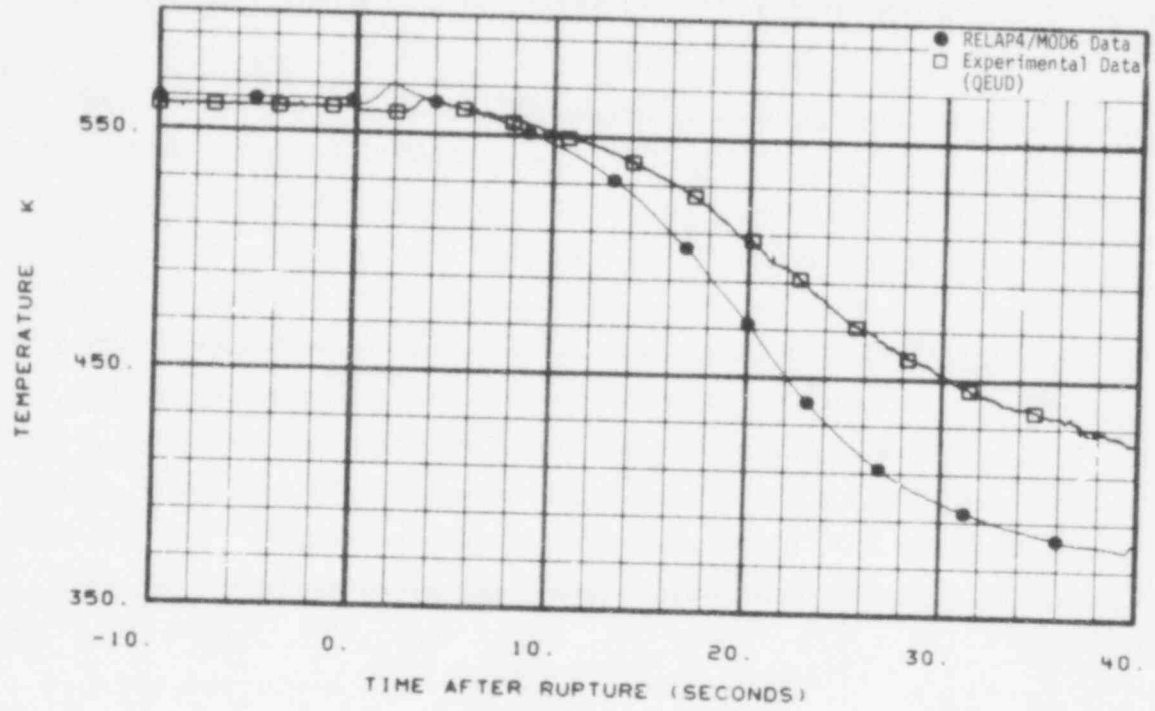

Fig. 55 Comparison of predicted and measured coolant temperature on instrument stalk 1 (TE-1ST-8).

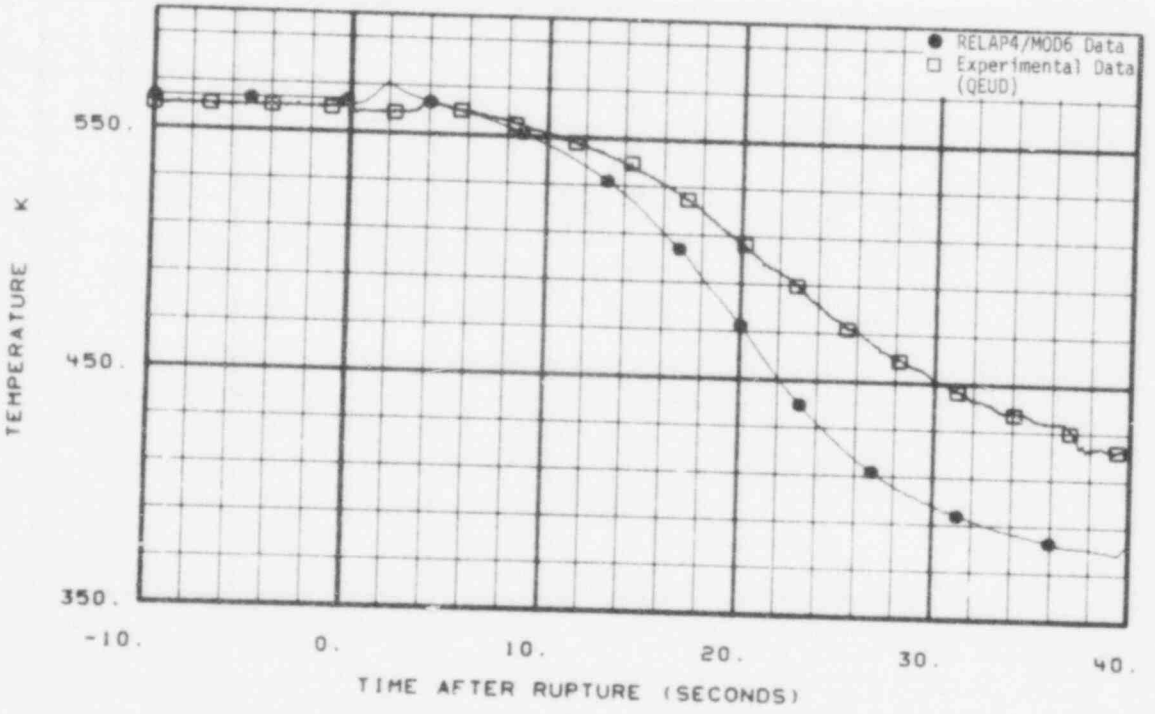

Fig. 56 Comparison of predicted and measured coo nt temperature on instrument stalk 1 (TE-1ST-9).

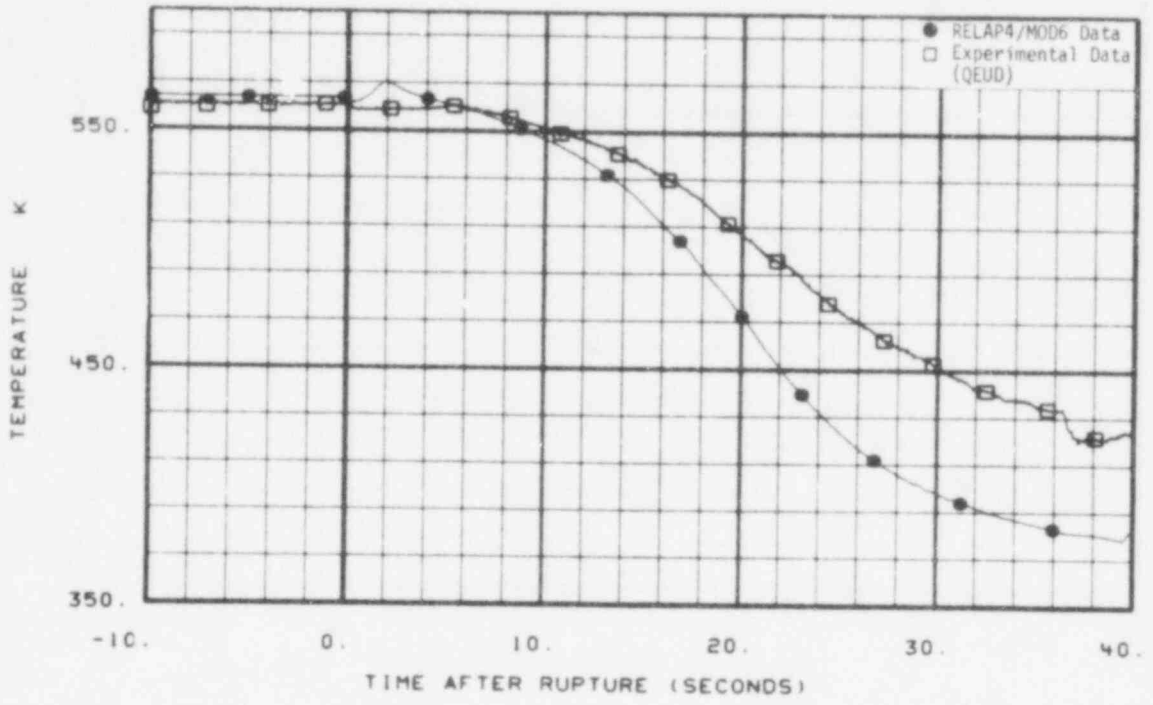

Fig. 57 Comparison of predicted and measured coolant temperature on instrument stalk 1 (TE-1ST-11).

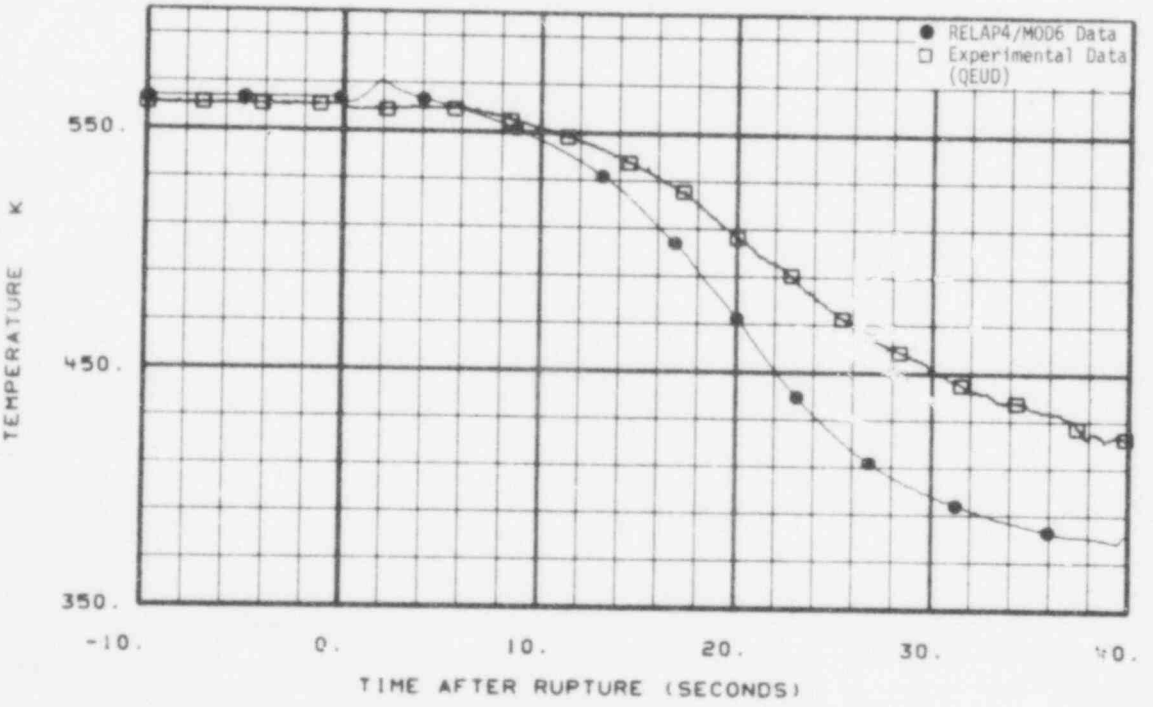

Fig. 58 Comparison of predicted and measured coolant temperature on instrument stalk 1 (TE-1ST-12).

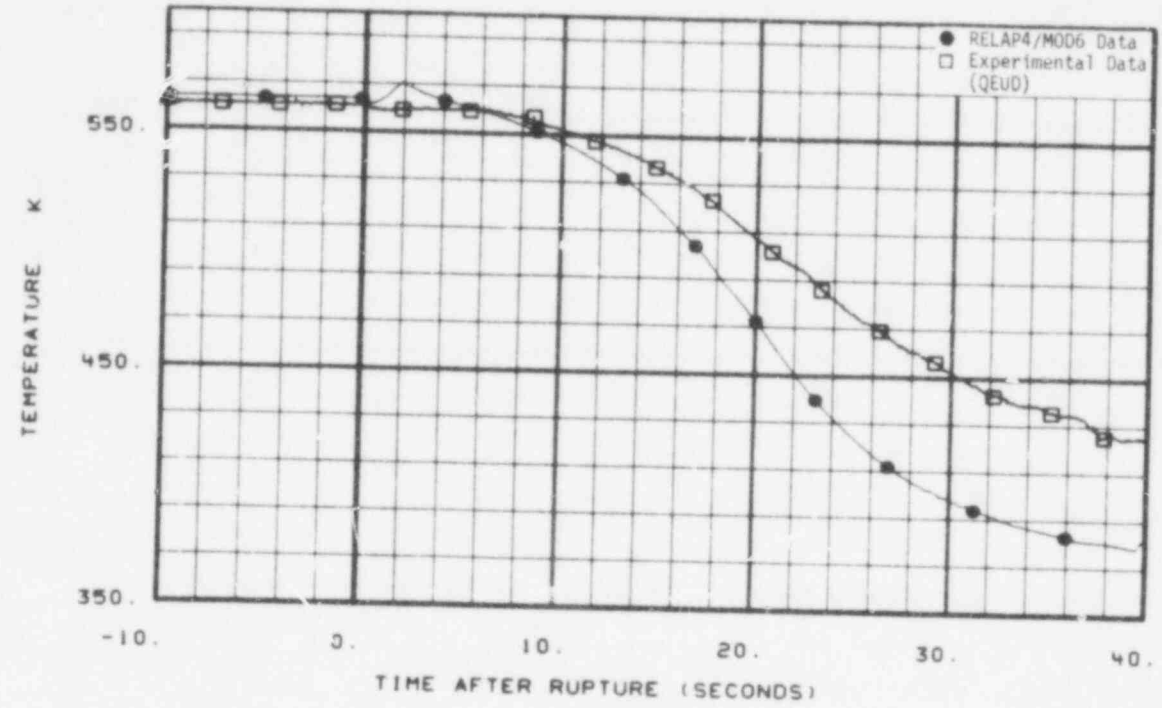

Fig. 59 Comparison of predicted and measured coolant temperature on instrument stalk 1 (TE-1ST-12).

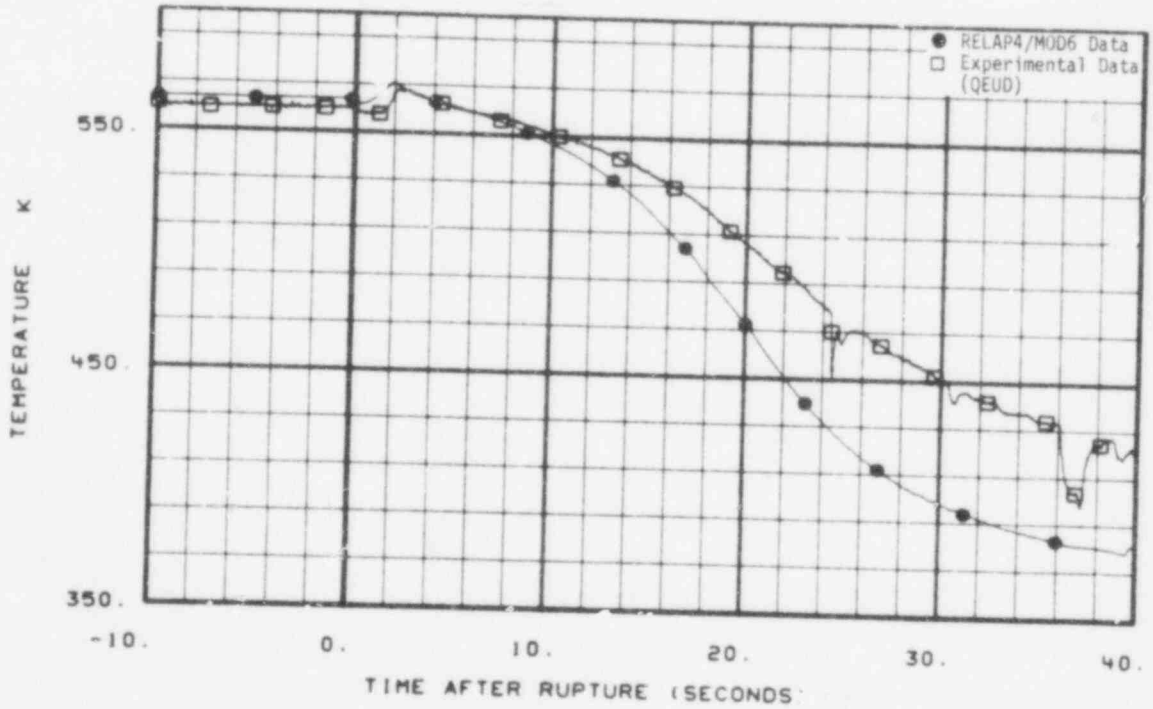

Fig. 60 Comparison of predicted and measured coolant temperature on instrument stalk 1 (TE-1ST-14).

temperature rise calculated at about 2 s at all locations was only measured on the lowest thermocouple (Figure 60). The same general behavior is shown in Figures 61 through 69 on the intact loop side of the downcomer. The effects of the early core flow reversal in the experiment probably did not propagate much farther than the lower plenum. Late time disparities are due to the undercalculation of pressure.

The comparisons, shown in Figures 70 through 72, for the lower end box are very good until about 10 s and indicate an early core flow reversal took place as indicated by other measurements. Above the core, Figures 73 through 80, comparisons are also very good until about 10 s with the exception of Figure 94 which indicates a measured local temperature rise just above the center fuel assembly from 2 to 8 s not followed by the calculations. Some flow of superheated steam to the upper plenum from the center assembly was not accounted for in the calculations.

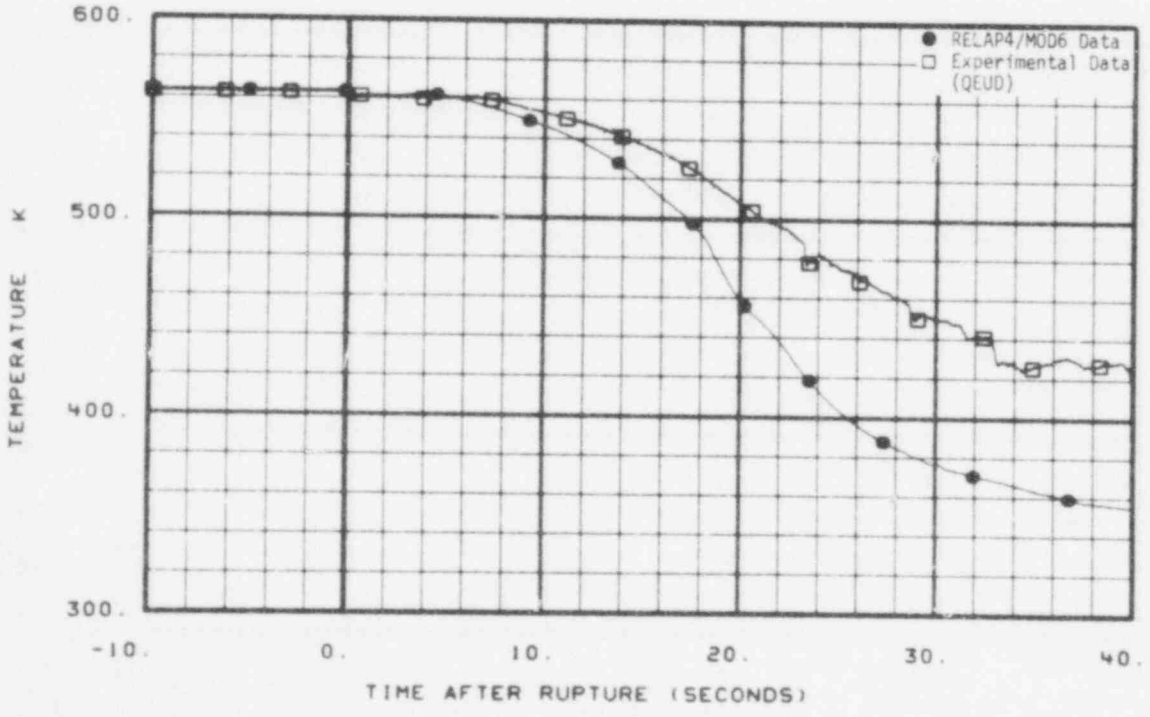

Fig. 61 Comparison of predicted and measured coolant temperature on instrument stalk 2 (T ' 1).

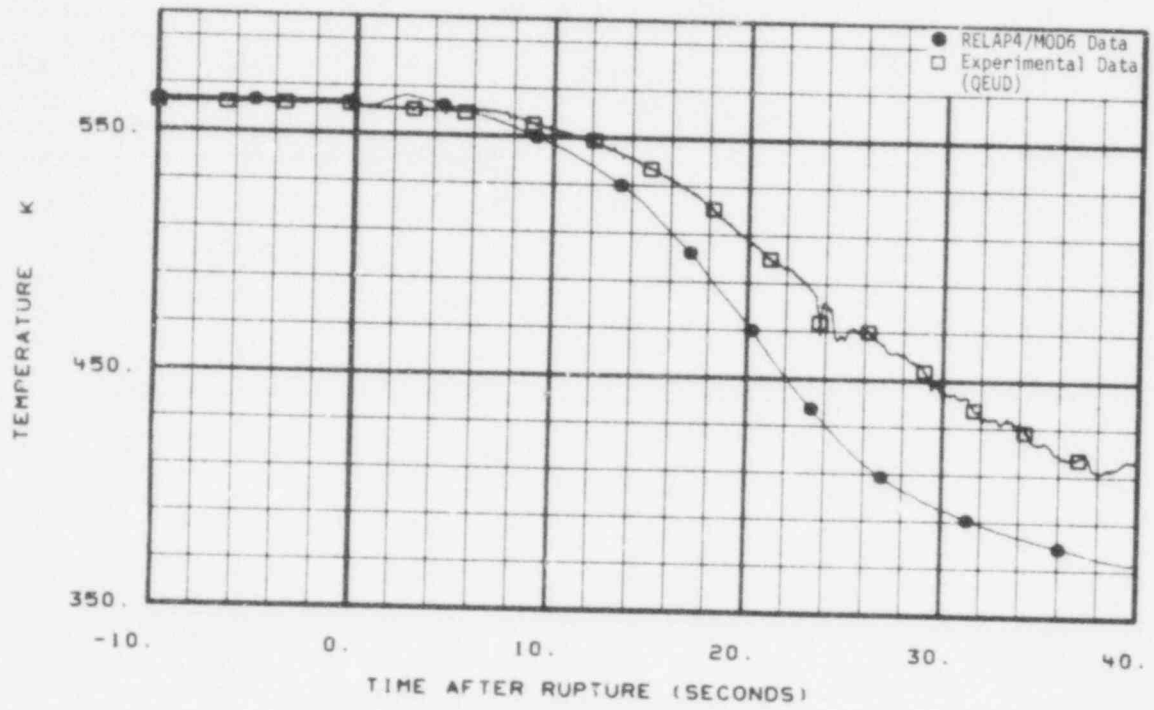

Fig. 62 Comparison of predicted and measured coolant temperature on instrument stalk 2 (TE-2ST-2).

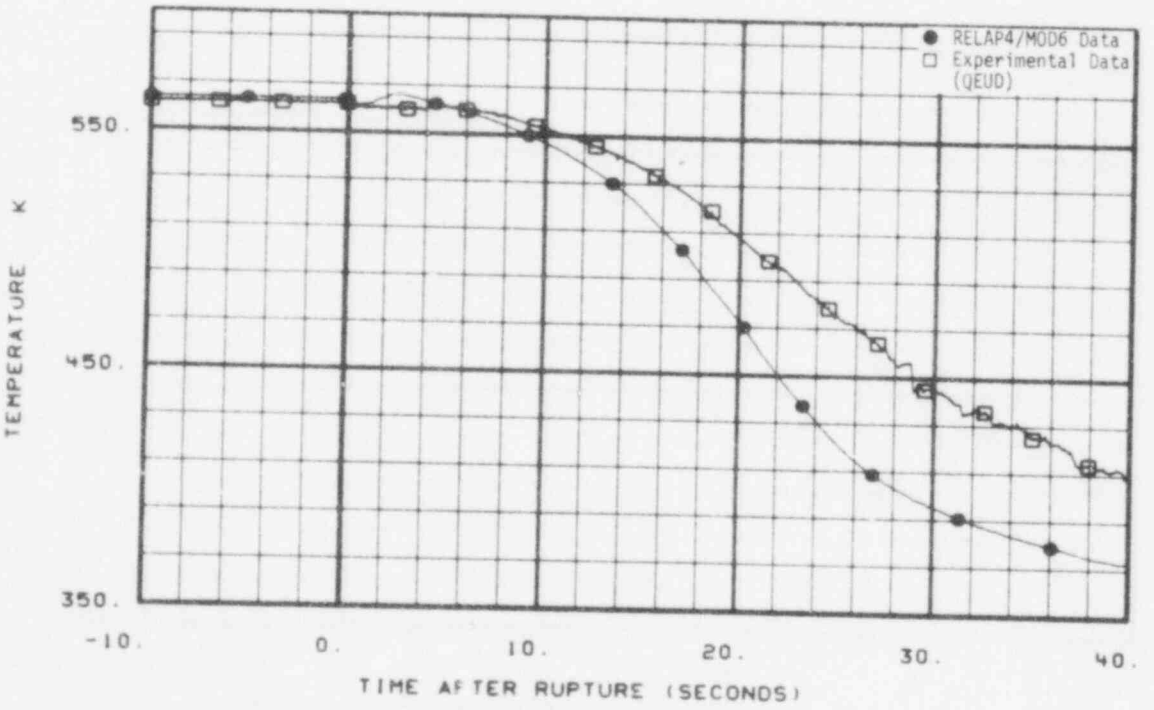

Fig. 63 Comparison of predicted and measured coolant temperature on instrument stalk 2 (TE-2ST-3).

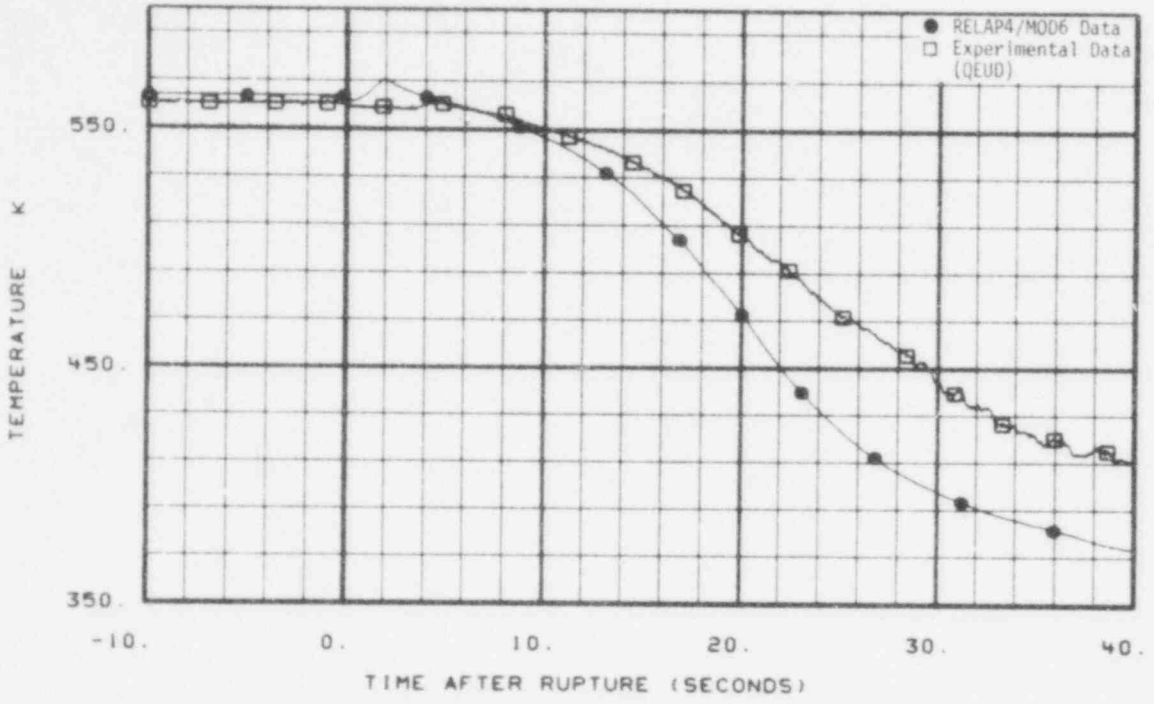

Fig. 64 Comparison of predicted and measured coolant temperature on instrument stalk 2 (TE-2ST-5).

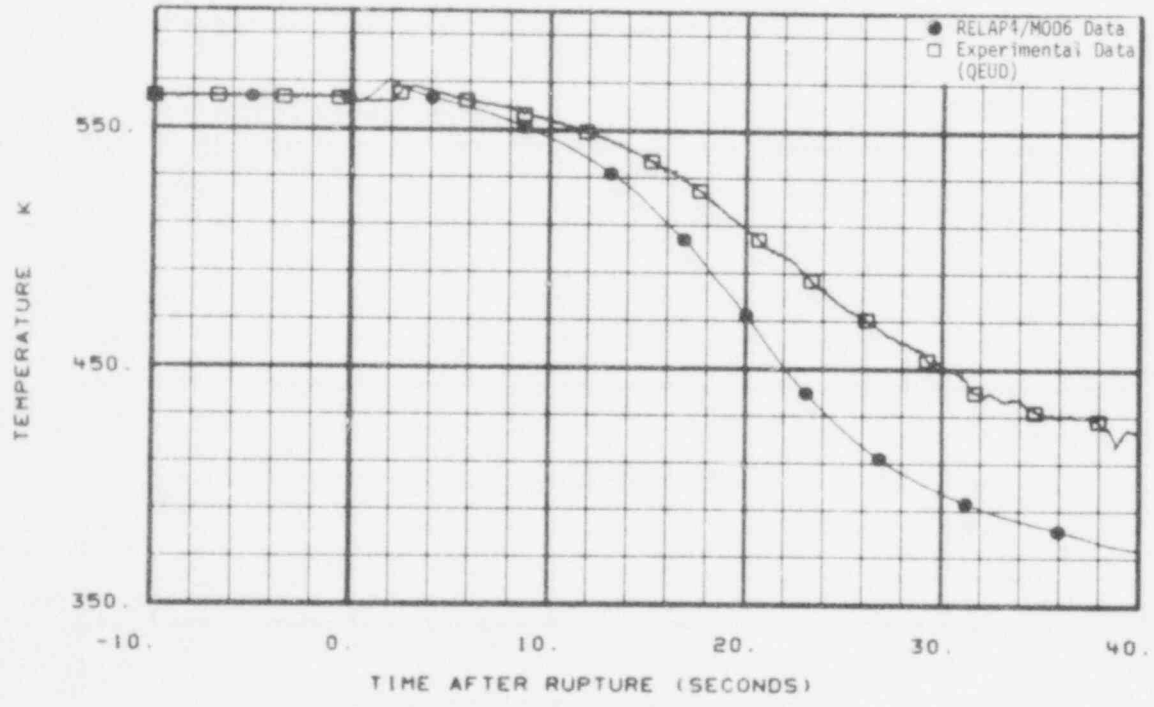

Fig. 65 Comparison of predicted and measured coolant temperature on instrument stalk 2 (TE-2ST-7).

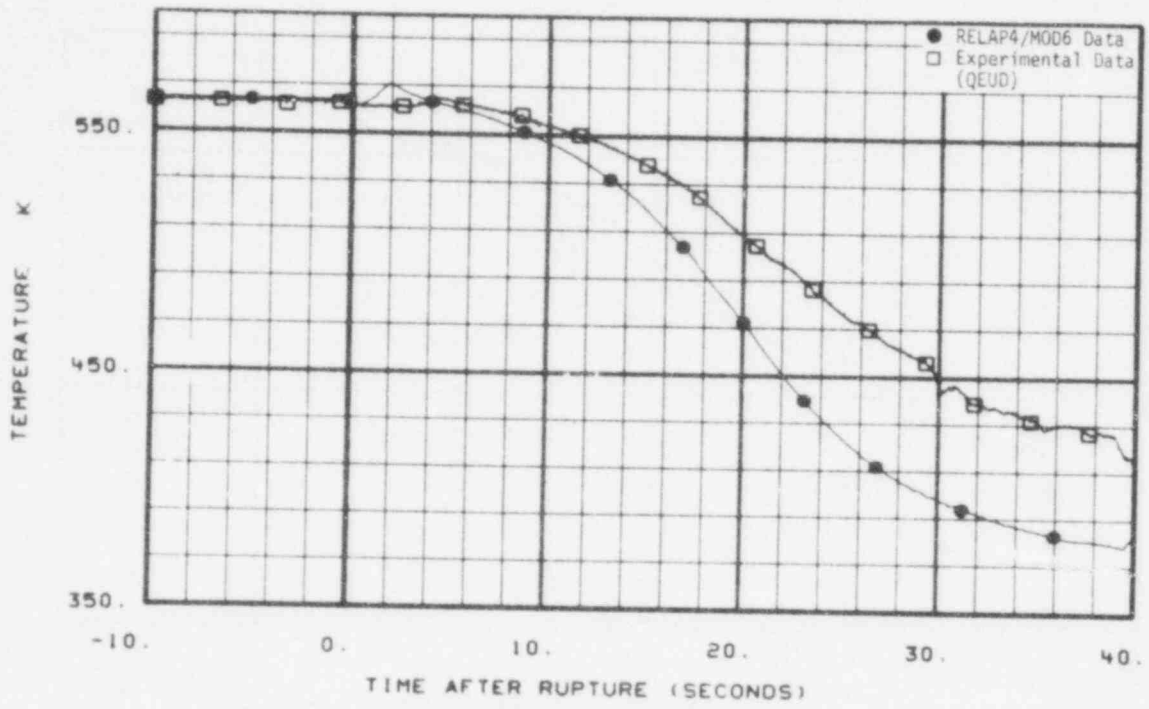

Fig. 66 Comparison of predicted and measured coolant temperature on instrument stalk 2 (TE-2ST-9).

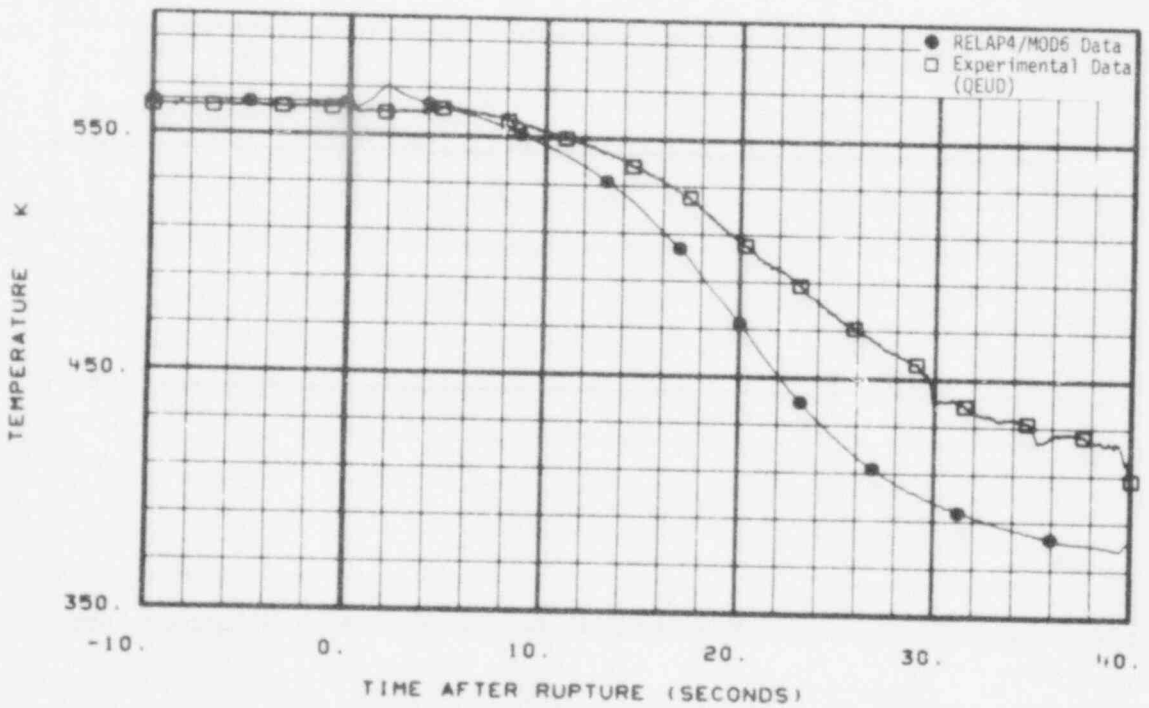

Fig. 67 Comparison of predicted and measured coolant temperature on instrument stalk 2 (TE-2ST-10).

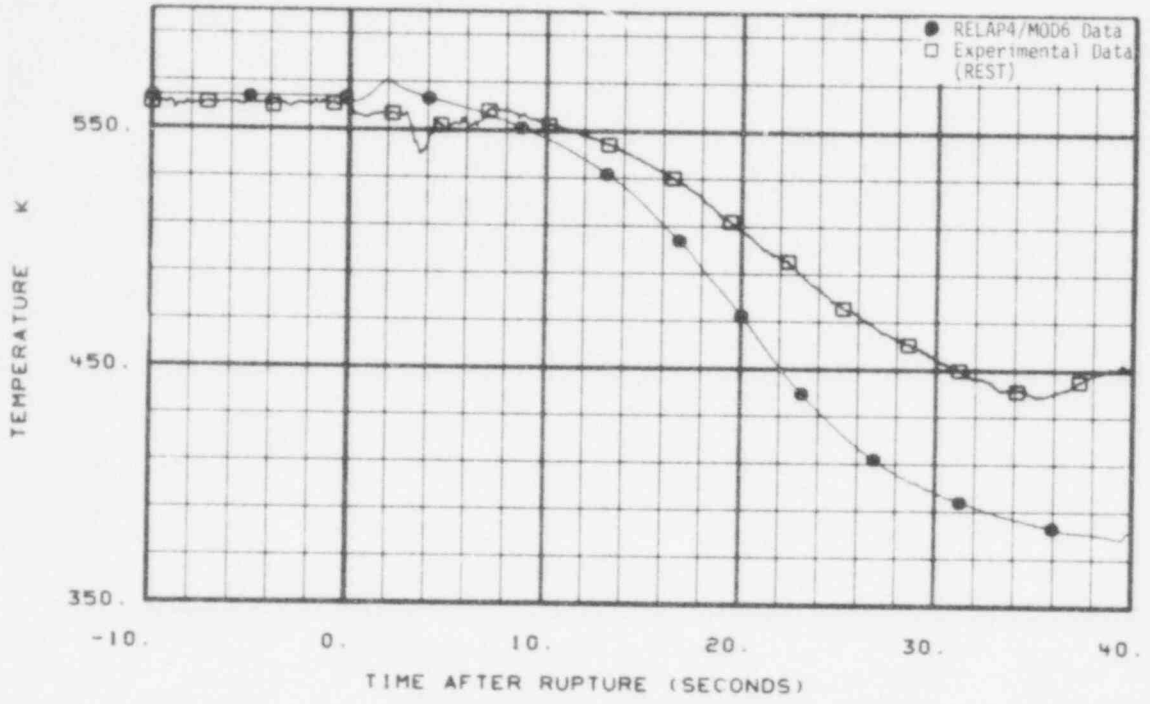

Fig. 68 Comparison of predicted and measured coolant temperature on instrument stalk 2 (TE-2ST-11).

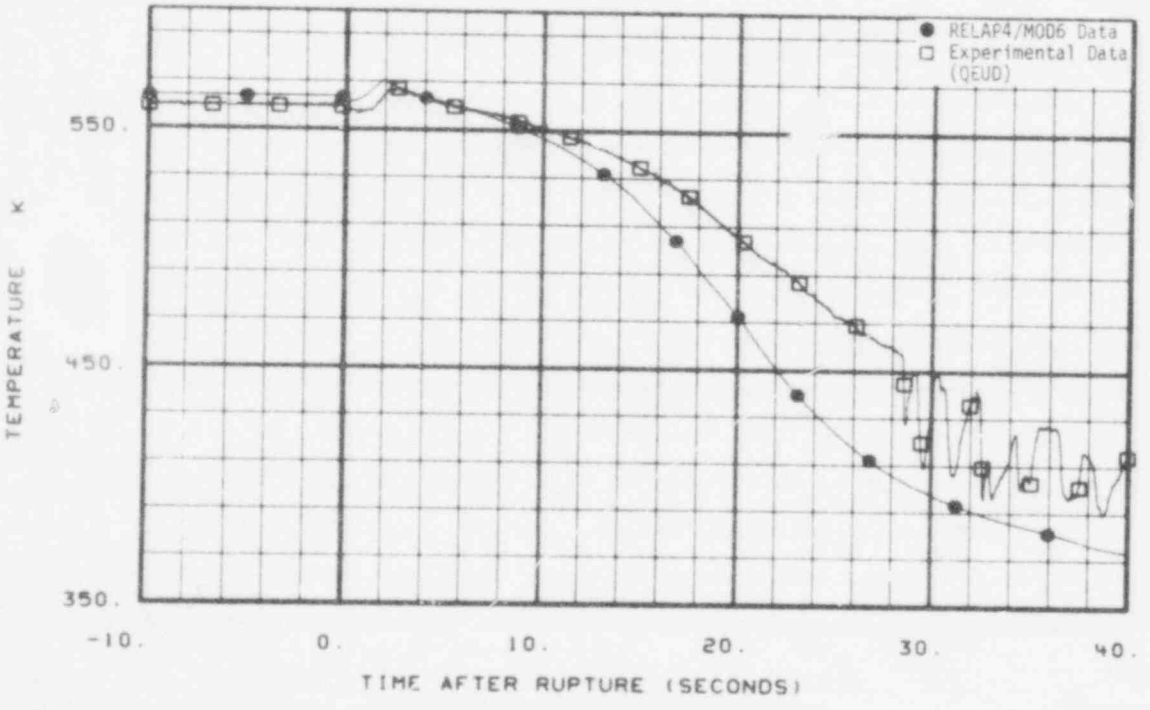

Fig. 69 Comparison of predicted and measured coolant temperature on instrument stalk 2 (TE-2ST-14).

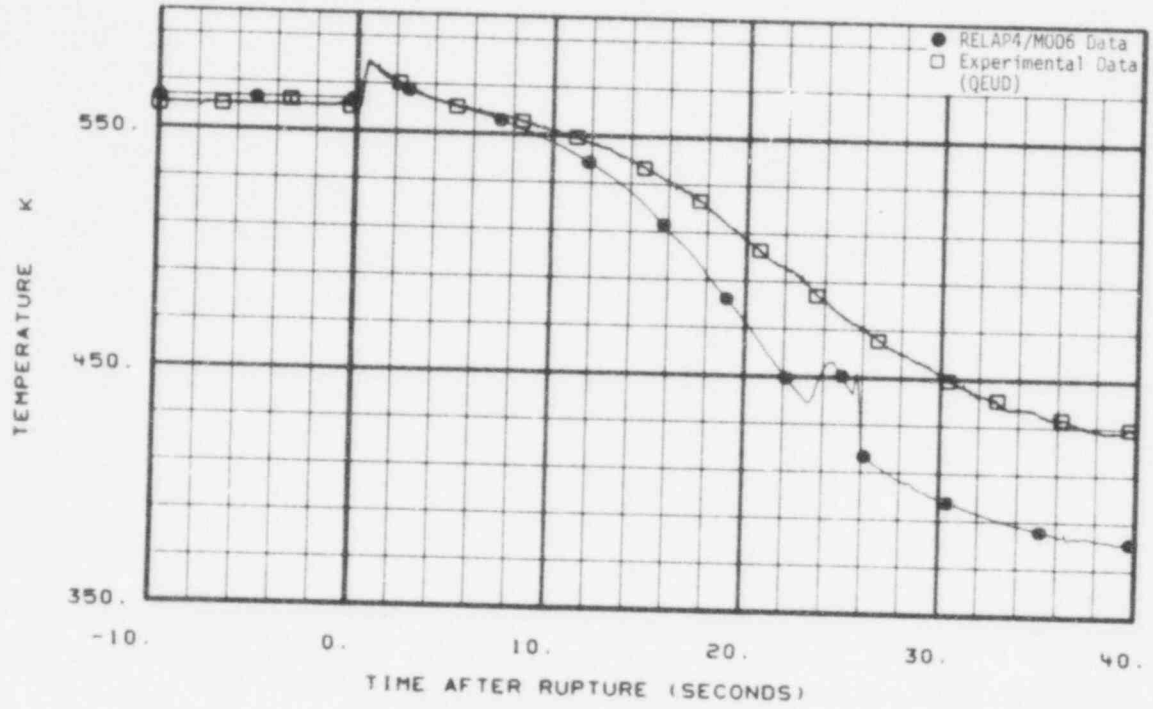

Fig. 70 Comparison of predicted and measured coolant temperature in lower end box (TE-1LP-1).

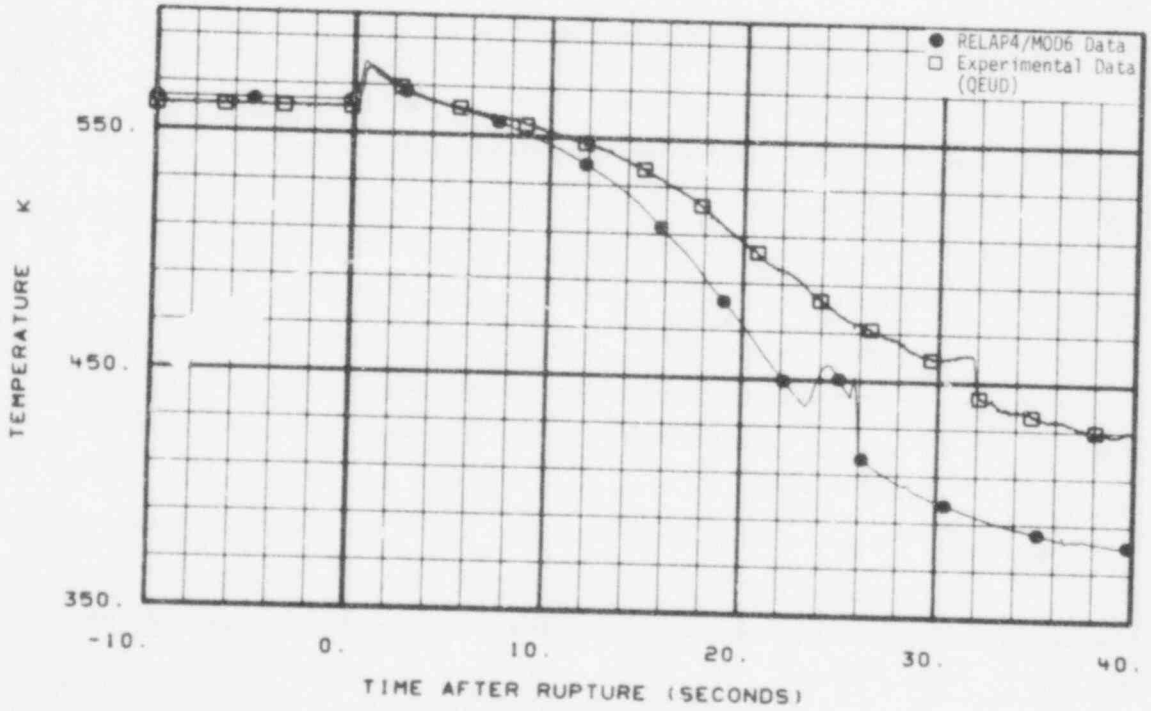

Fig. 71 Comparison of predicted and measured coolant temperature in lowe- end box (TE-2LP-1).

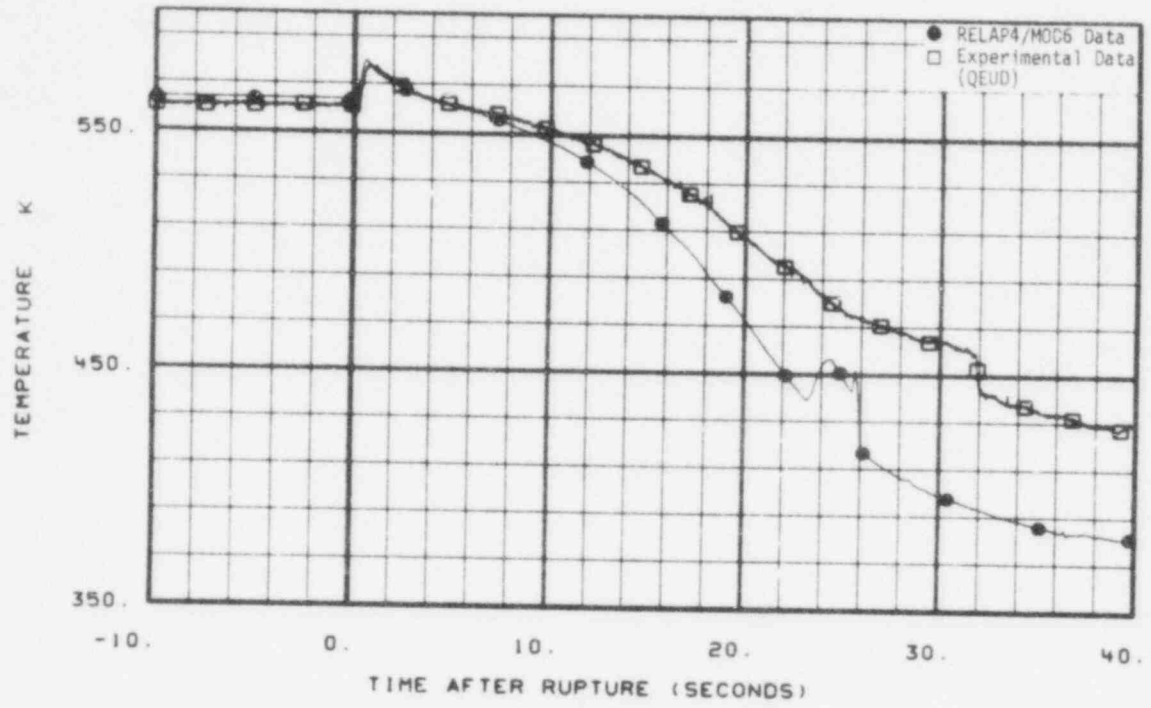

Fig. 72 Comparison of predicted and measured coolant temperature in lower end box (TE-6LP-1).

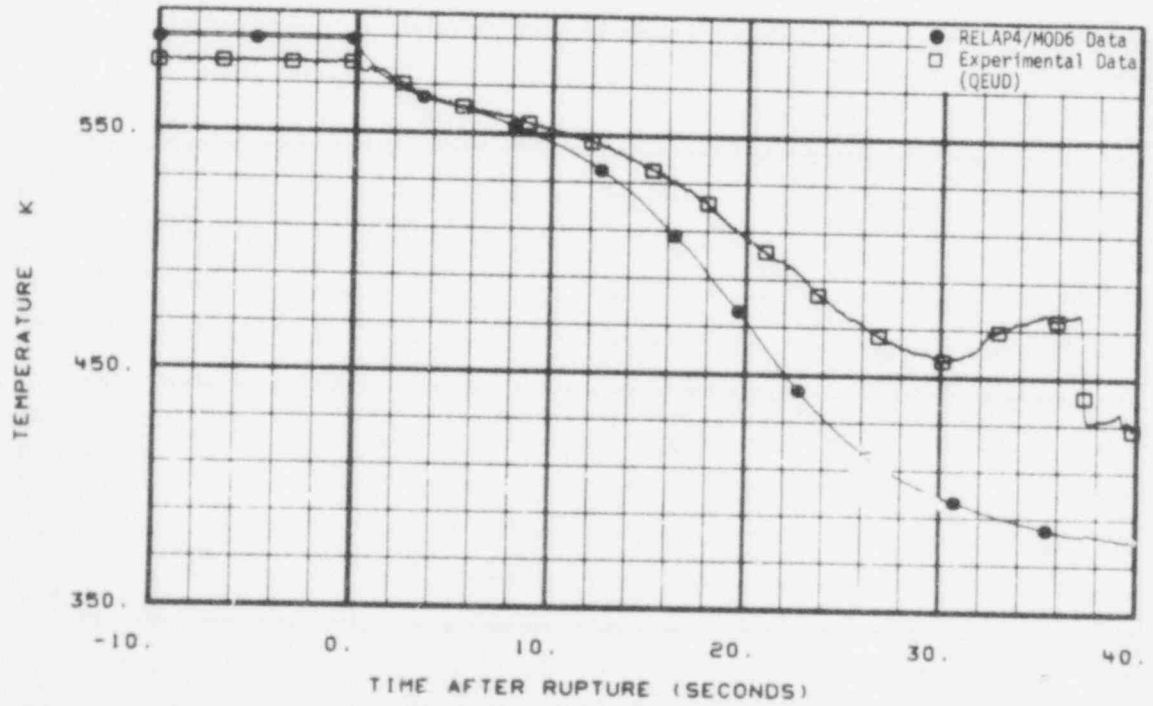

Fig. 73 Comparison of predicted and measured coolant temperature in upper end box (TE-2UP-1).

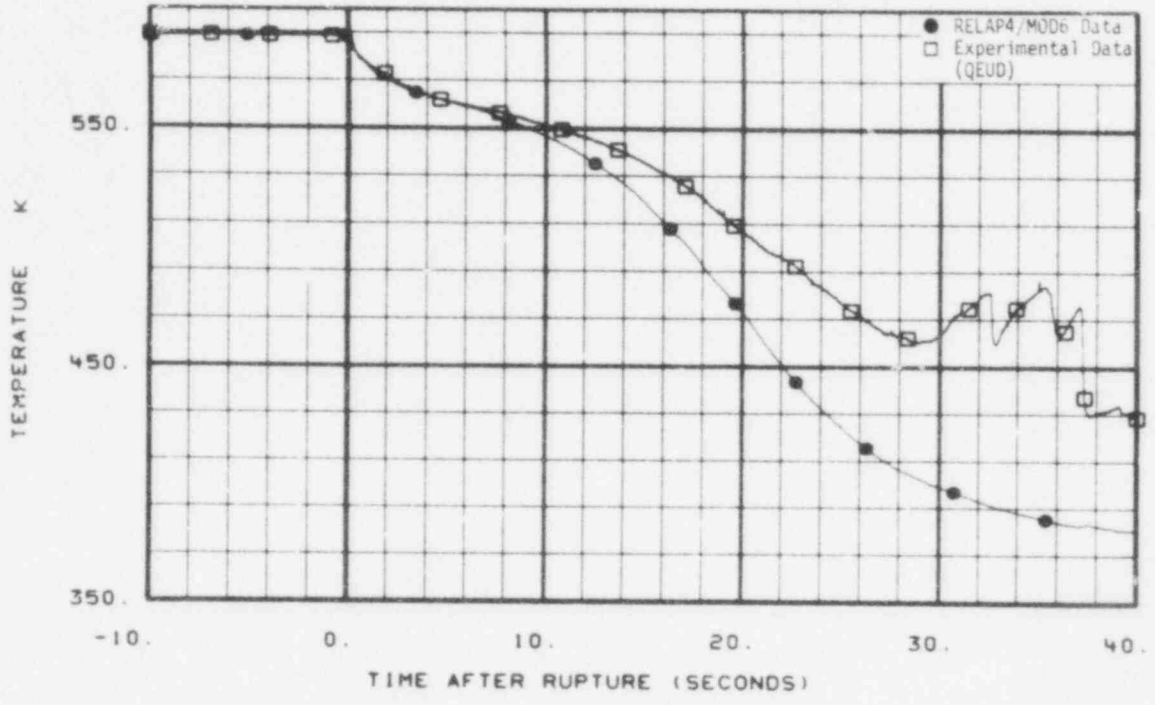

Fig. 74 Comparison of predicted and measured coolant temperature in upper end box (TE-3UP-4).

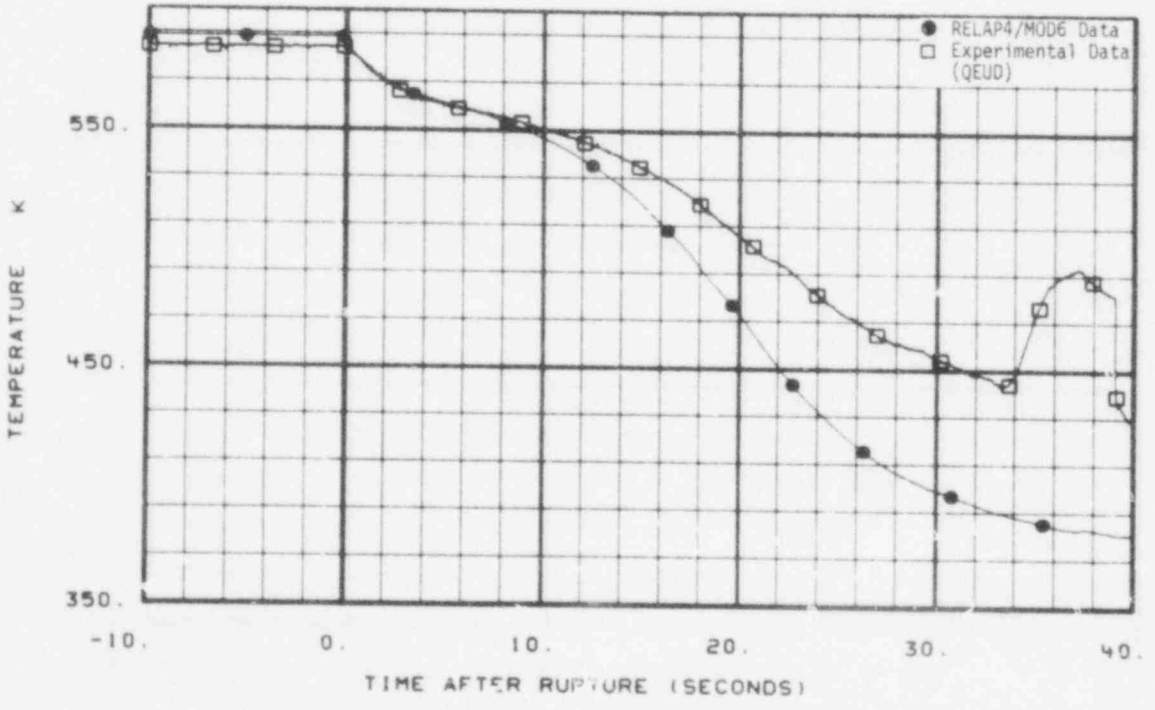

Fig. 75 Comparison of predicted and measured coolant temperature on drag-disc turbine transducer FE-3UP-1 (TE-3UP-5).

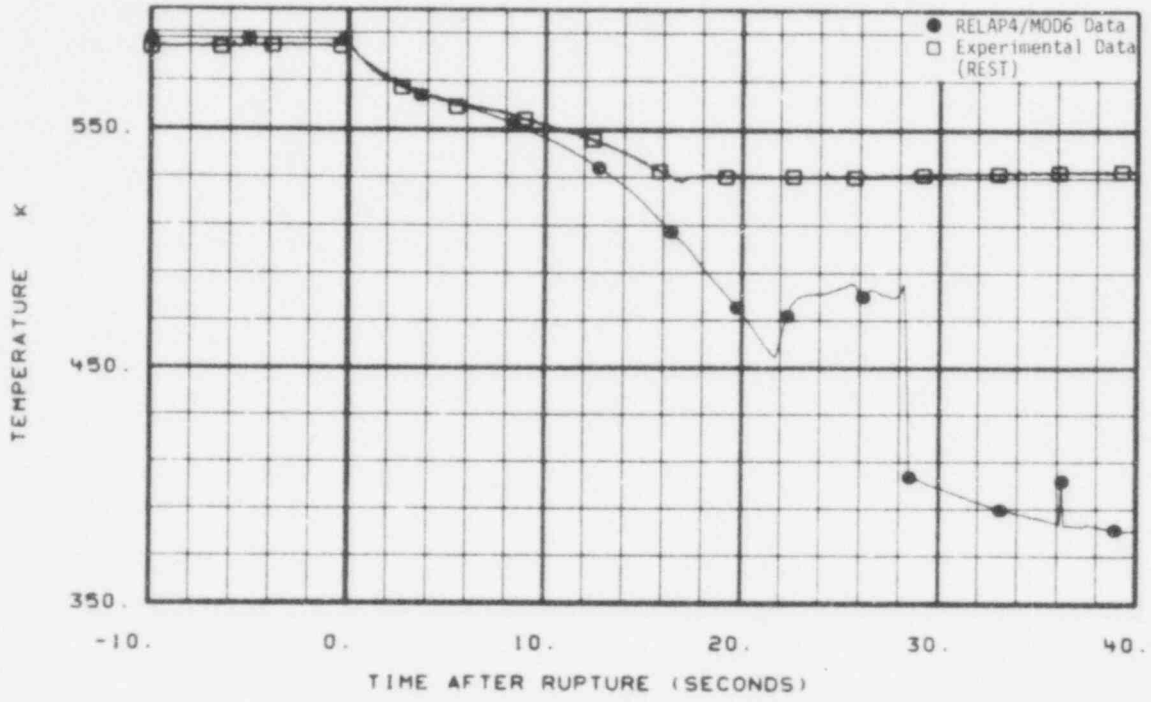

Fig. 76 Comparison of predicted and measured coolant temperature liquid level transducer above FA3 (TE-3UP-8).

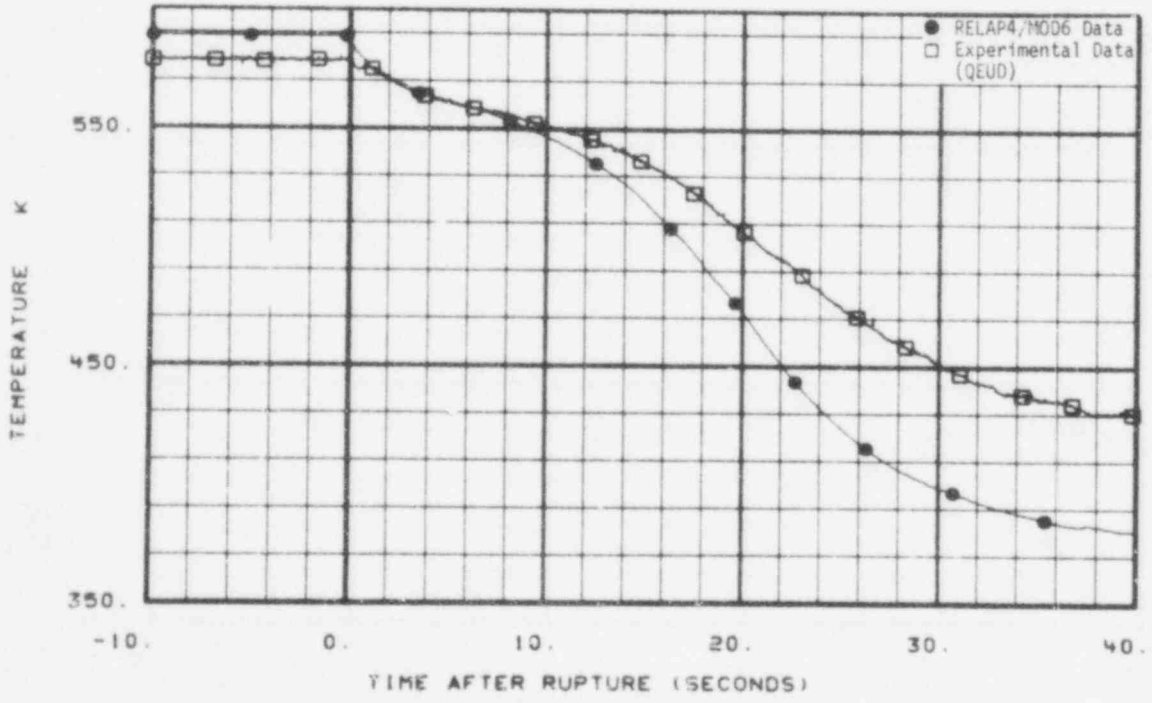

Fig. 77 Comparison of predicted and measured coolant temperature in upper end box (TE-4UP-1).

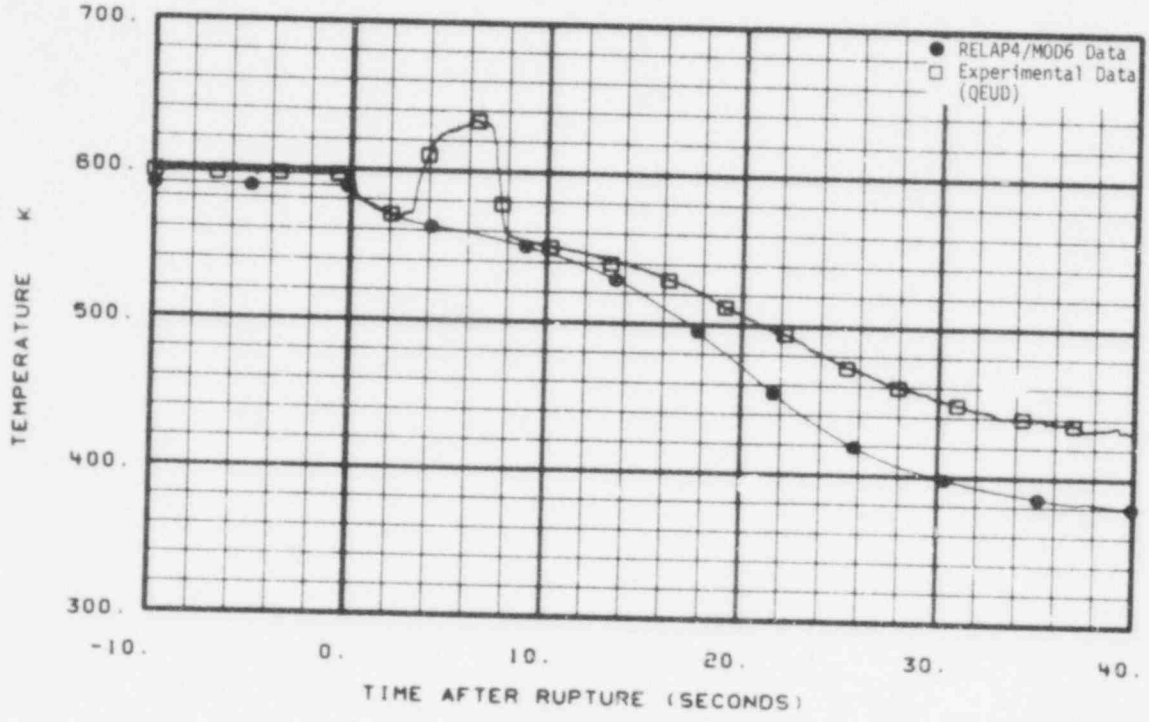

Fig. 78 Comparison of predicted and measured coolant temperature in upper end box (TE-5UP-1).

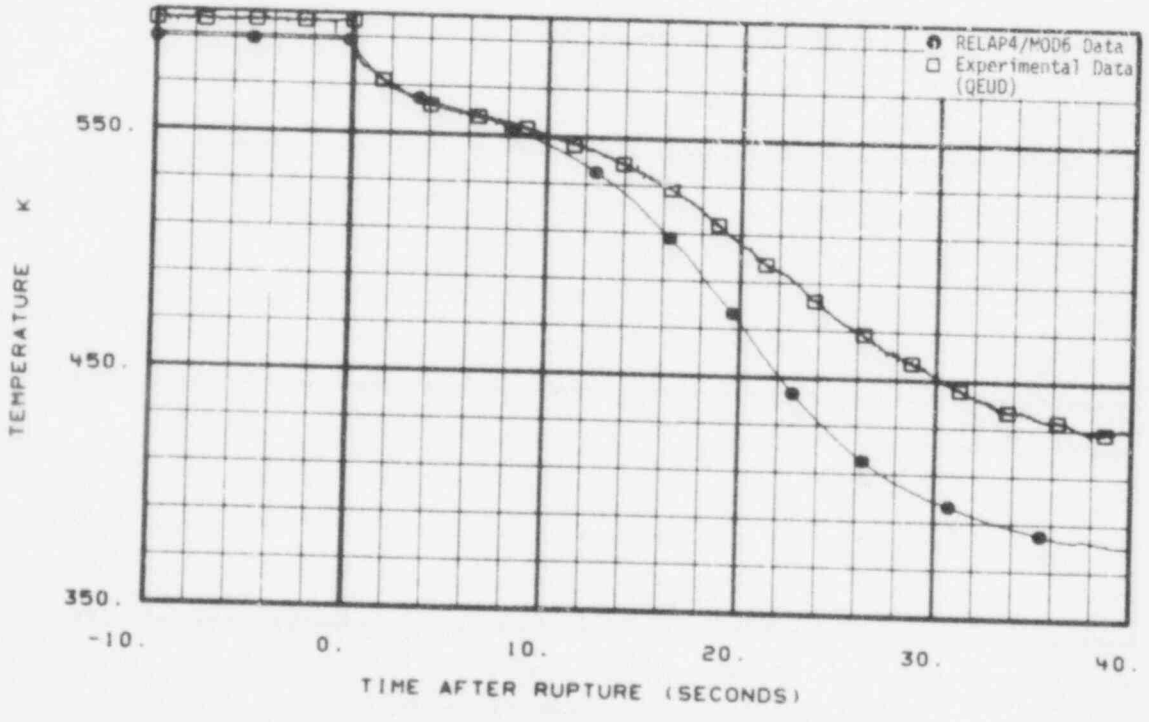

Fig. 79 Comparison of predicted and measured coolant temperature on drag-disc turbine transducer FE-5UP-1 (TE-5UP-9).

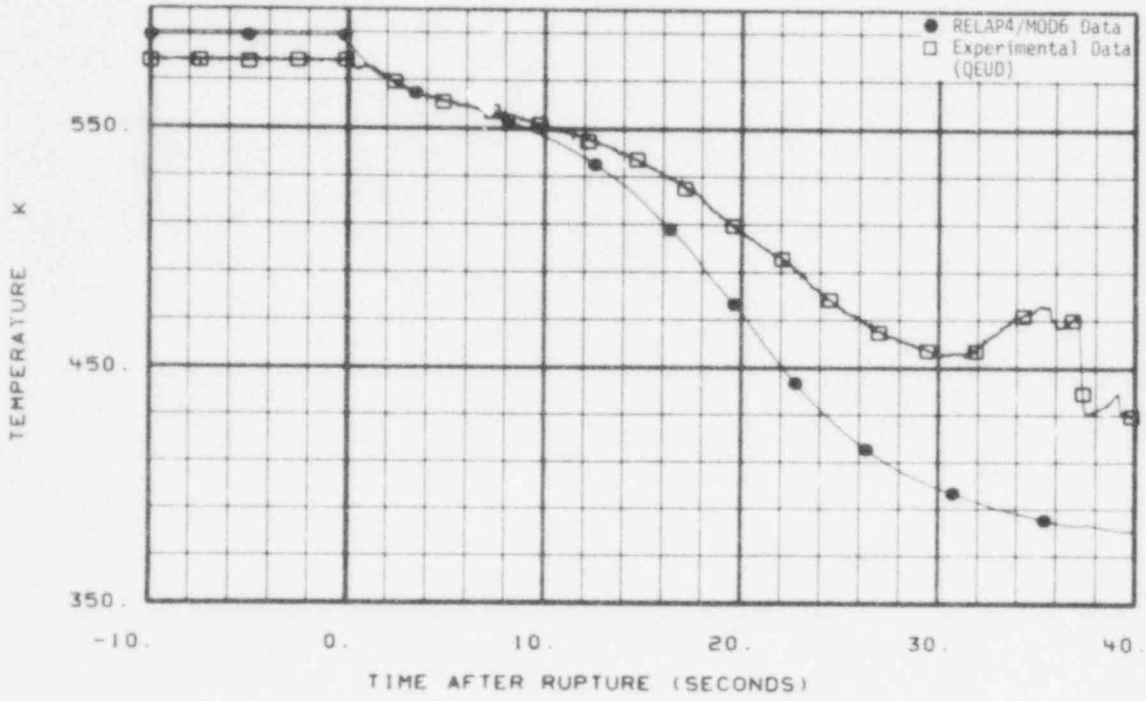

Fig. 80 Comparison of predicted and measured coolant temperature in upper end box (TE-6UP-1).

The final set of temperature comparisons are the fuel rod cladding surface response at various locations in the core. Figure 81 shows the response for a low powered rod at the 26-in. elevation. The trends in the measured data are followed very well by the calculations; however, the calculated data are essentially shifted back about 2 s. In a control assembly, Figure 82 shows that the calculations are in very poor agreement with the data after about 2 s. The measured data are below the calculated values and the trends do not compare. Figures 83 through 97 are the comparisons for the high powered fuel assembly. These comparisons are all very similar. In the first 4 s, the comparisons are very good. After 4 s, the measured data diverge from the calculated values and remain less than the calculations. Furthermore, the measured data trends are not reflected in the calculations after 4 s. The measured data indicate that core heat transfer was much higher than what was used in the calculations at least in the 4- to 10-s range. These comparisons support other comparisons throughout the system that indicate a low calculated mass inventory and low core flow, both of which are needed to accommodate the large energy release indicated in these figures by the measured data.

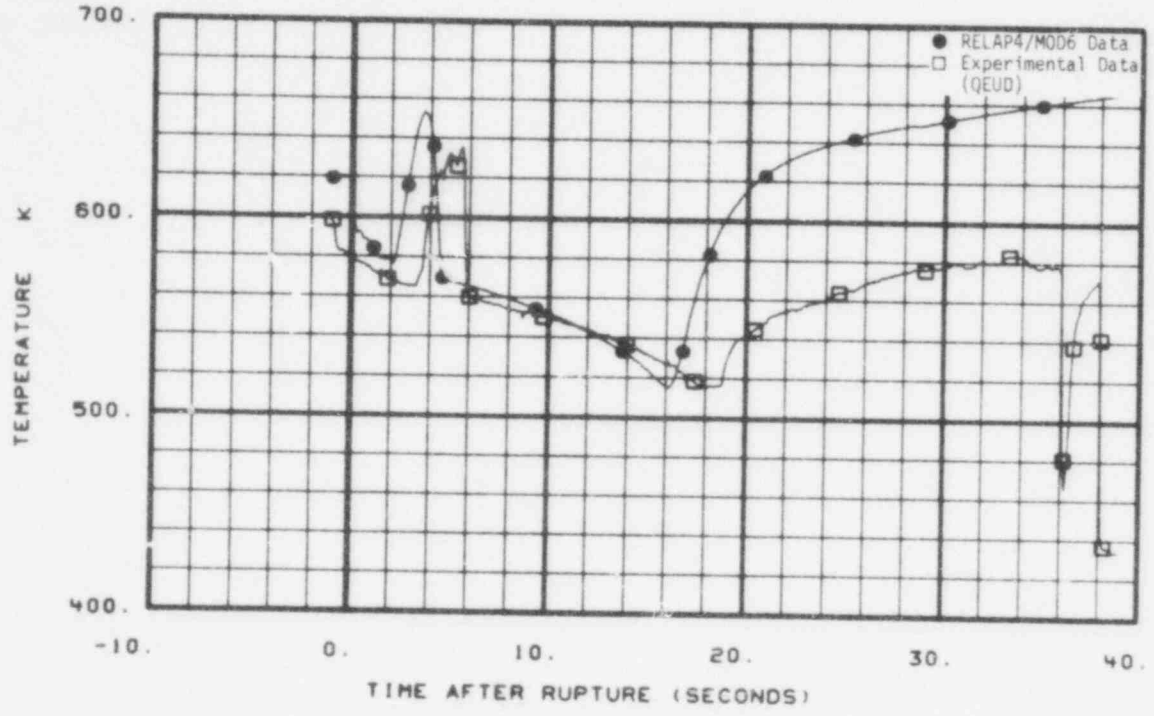

Fig. 81 Comparison of predicted and measured cladding temperature on FA3 pin B12 at 26 in. (TE-3B12-26).

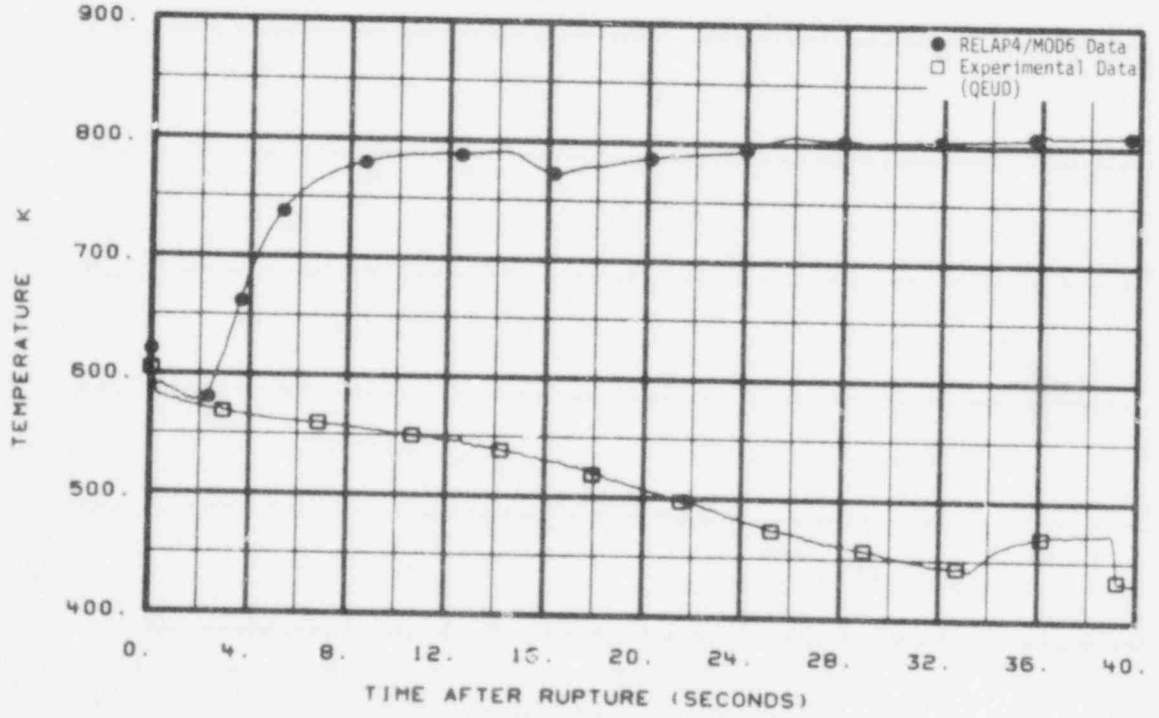

Fig. 82 Comparison of predicted and measured cladding temperature on FA4 pin H13 at 37 in. (TE-4H13-37).

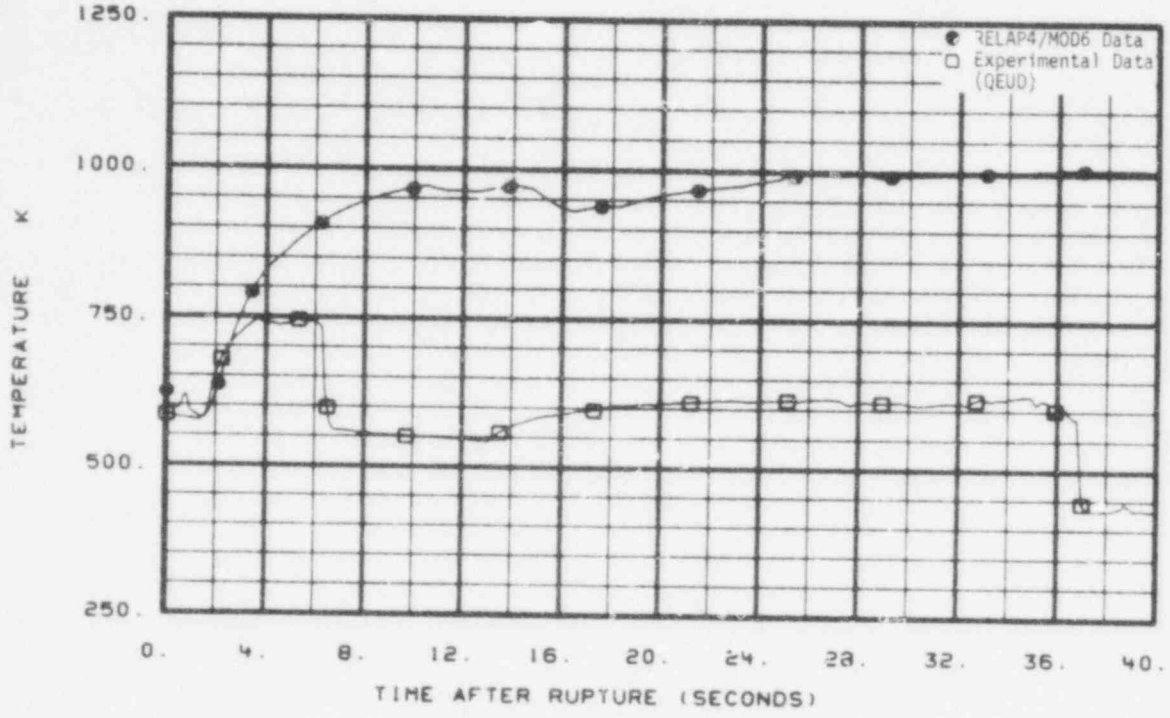

Fig. 83 Comparison of predicted and measured cladding temperature on FA5 pin F4 at 15 in. (TE-5F4-15).

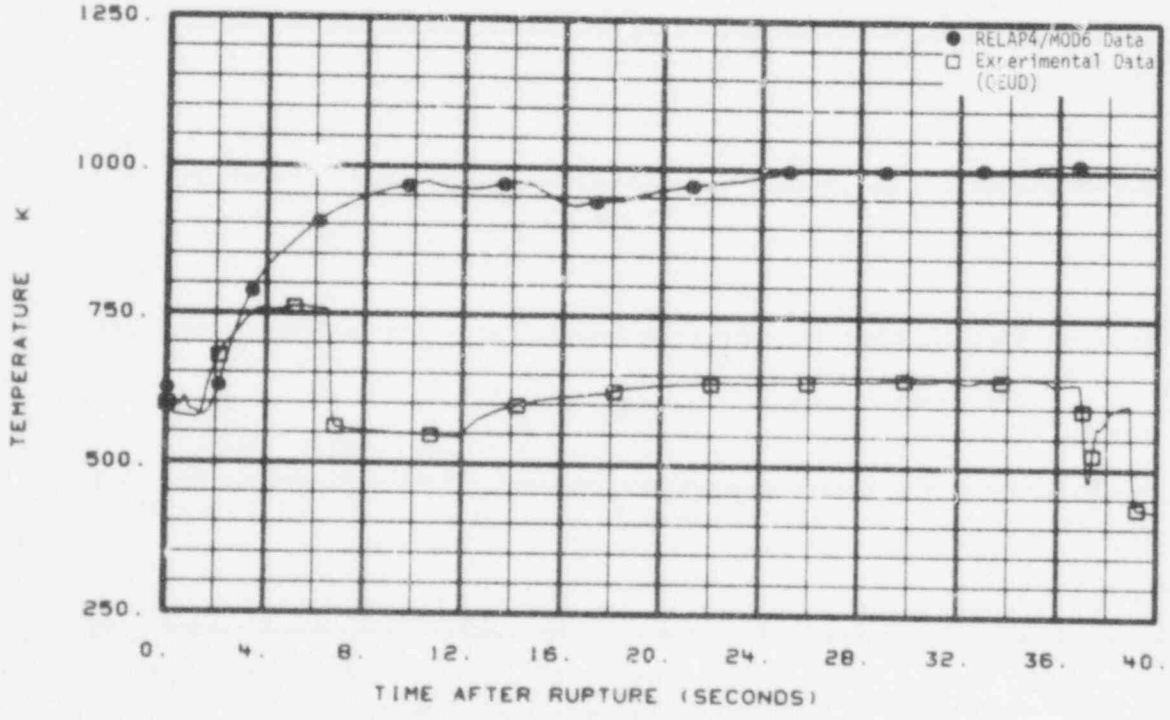

Fig. 84 Comparison of predicted and measured cladding temperature on FA5 pin F4 at 21 in. (TE-5F4-21).

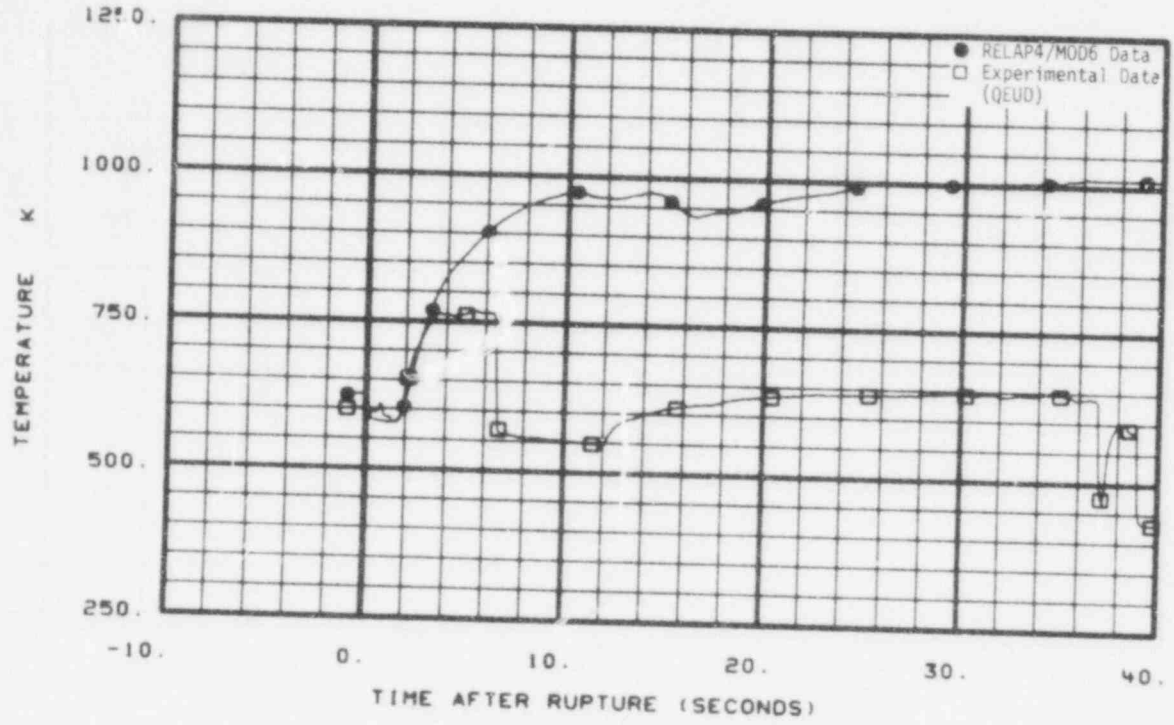

Fig. 85 Comparison of predicted and measured cladding temperature on FA5 pin J4 at 21 in. (TE-5J4-21).

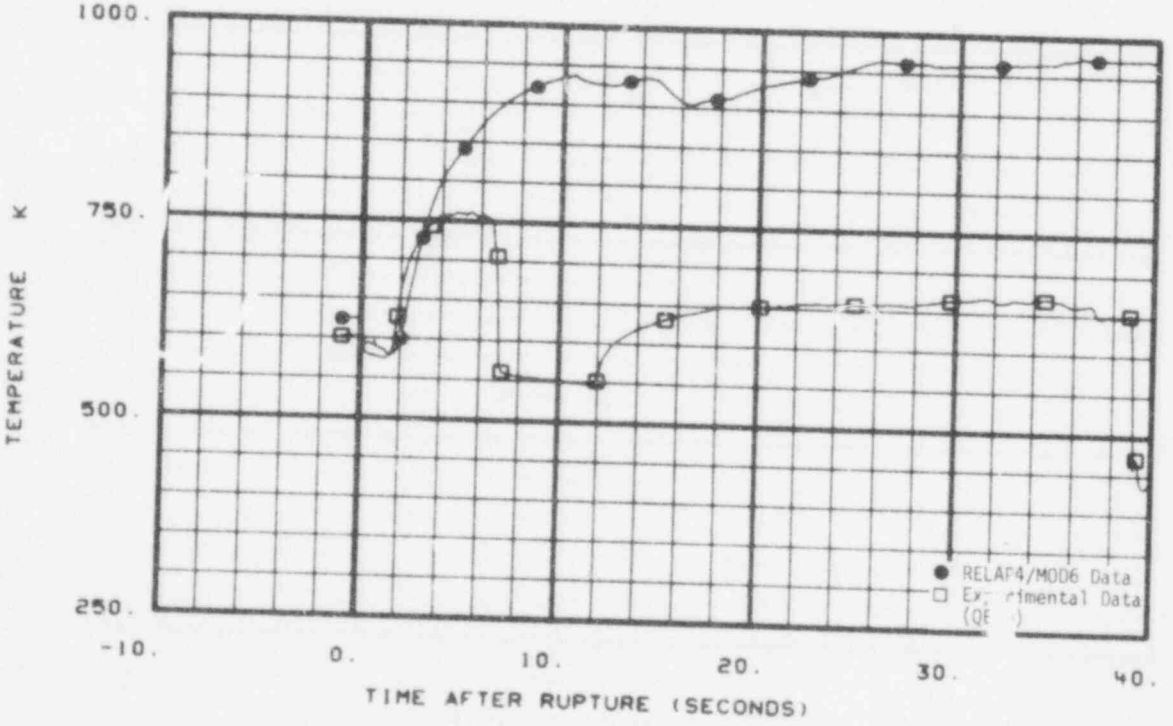

Fig. 86 Comparison of predicted and measured cladding temperature on FA5 pin J4 at 26 in. (TE-5J4-26).

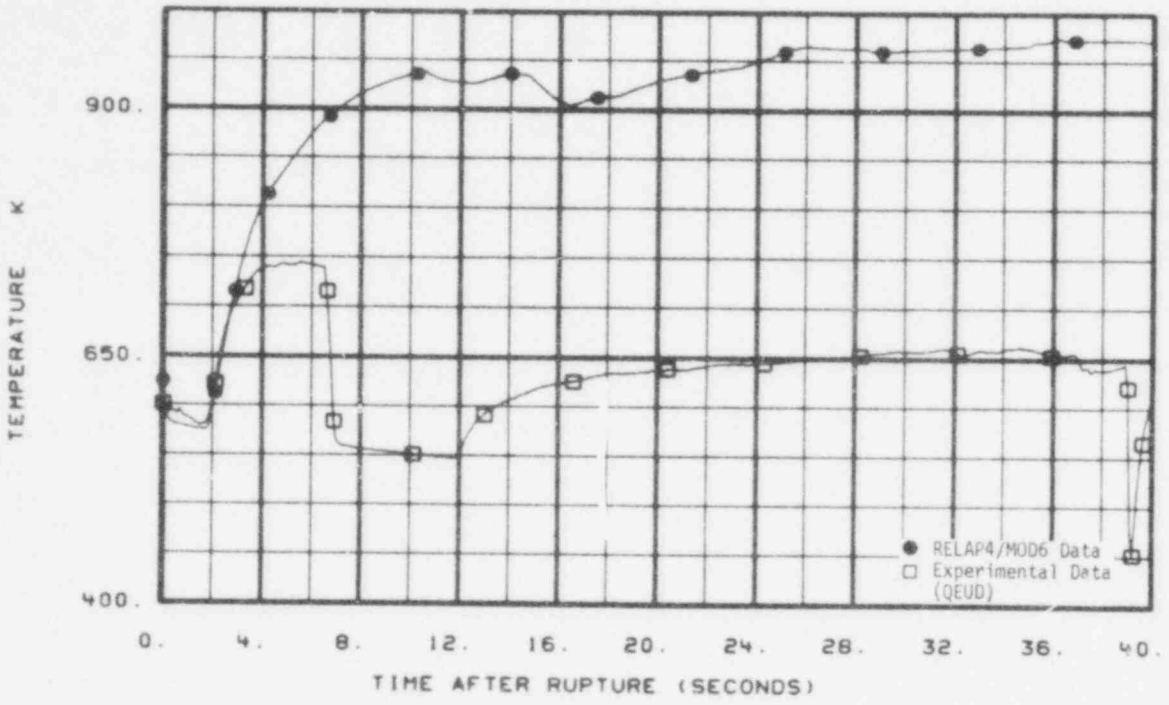

Fig. 87 Comparison of predicted and measured cladding temperature on FA5 pin F4 at 26 in. (TE-5F4-26).

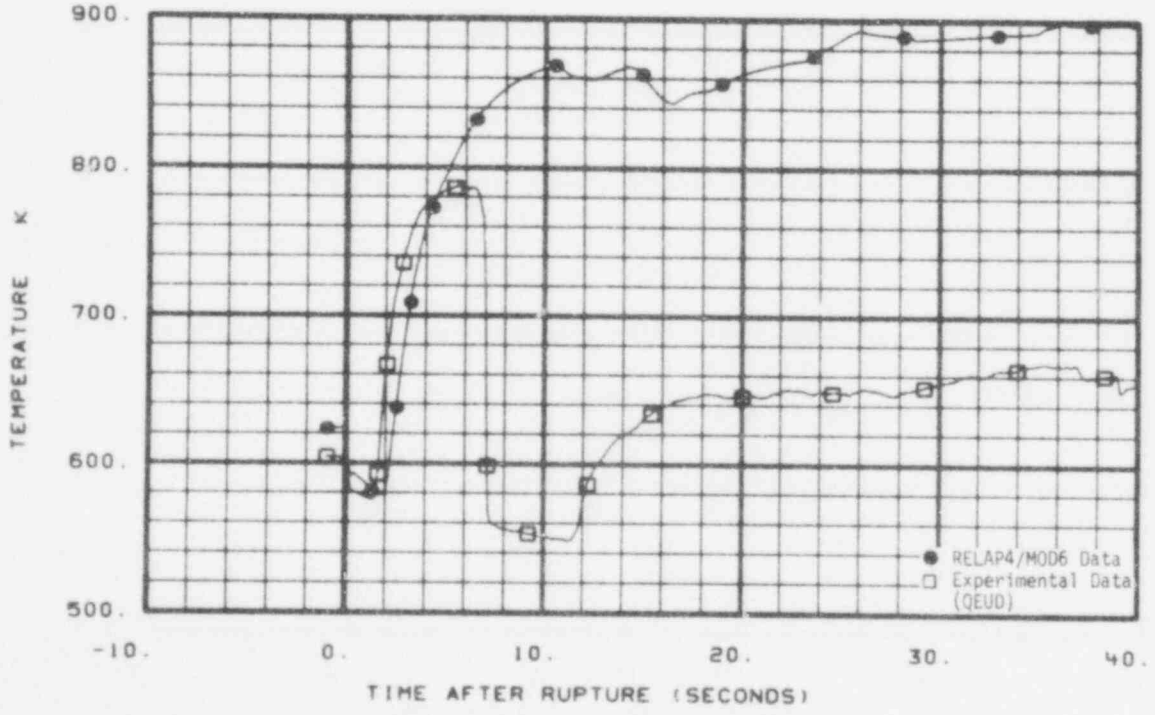

Fig. 88 Comparison of predicted and measured cladding temperature on FA5 pin J4 at 30 in. (TE-5J4-30).

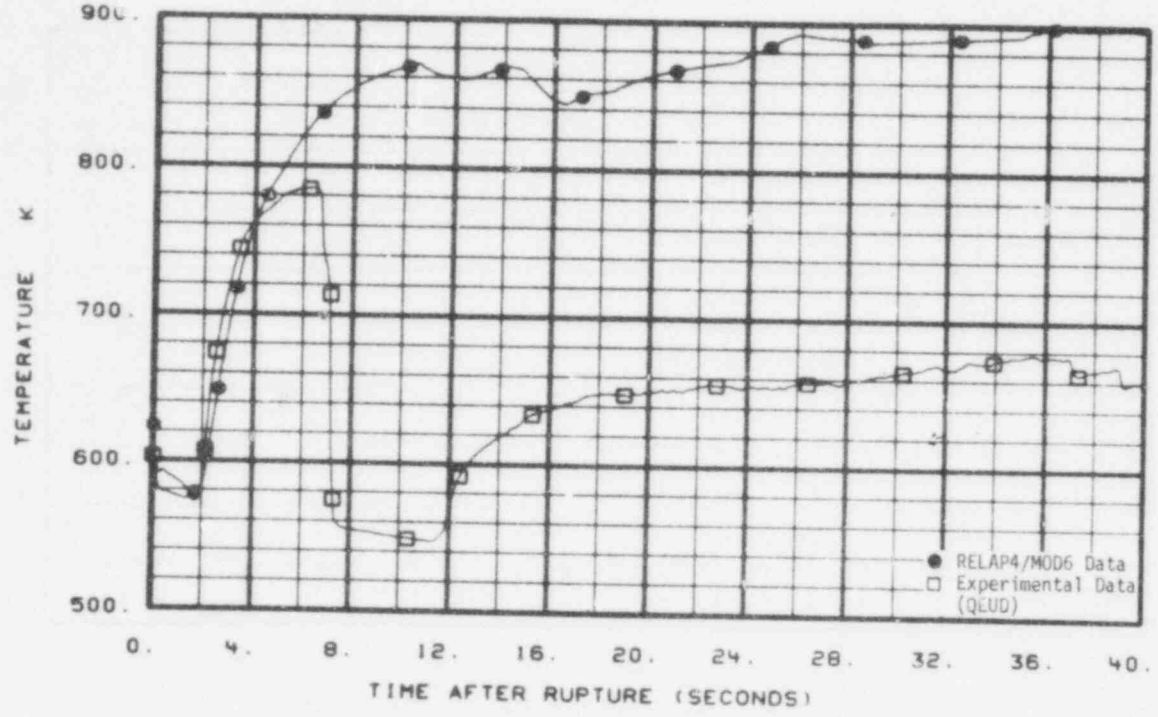

Fig. 89 Comparison of predicted and measured cladding temperature on FA5 pin F4 at 30 in. (TE-5F4-30).

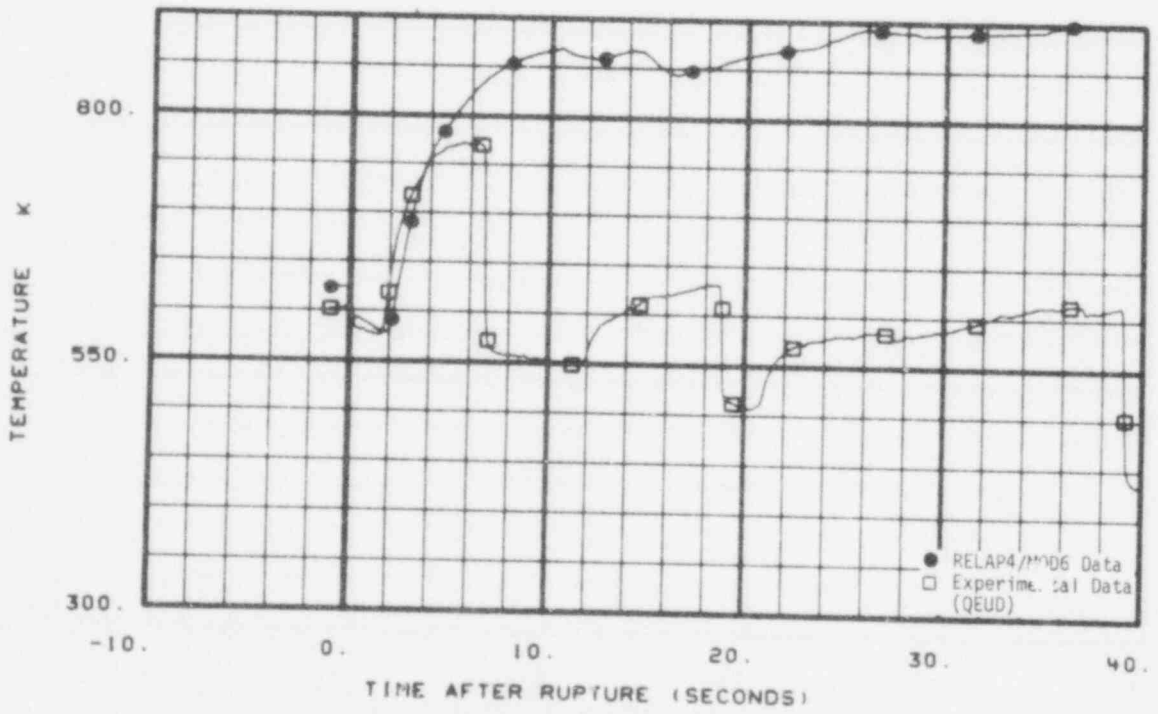

Fig. 90 Comparison of predicted and measured cladding temperature on FA5 pin L6 at 30 in. (TE-5L6-30).

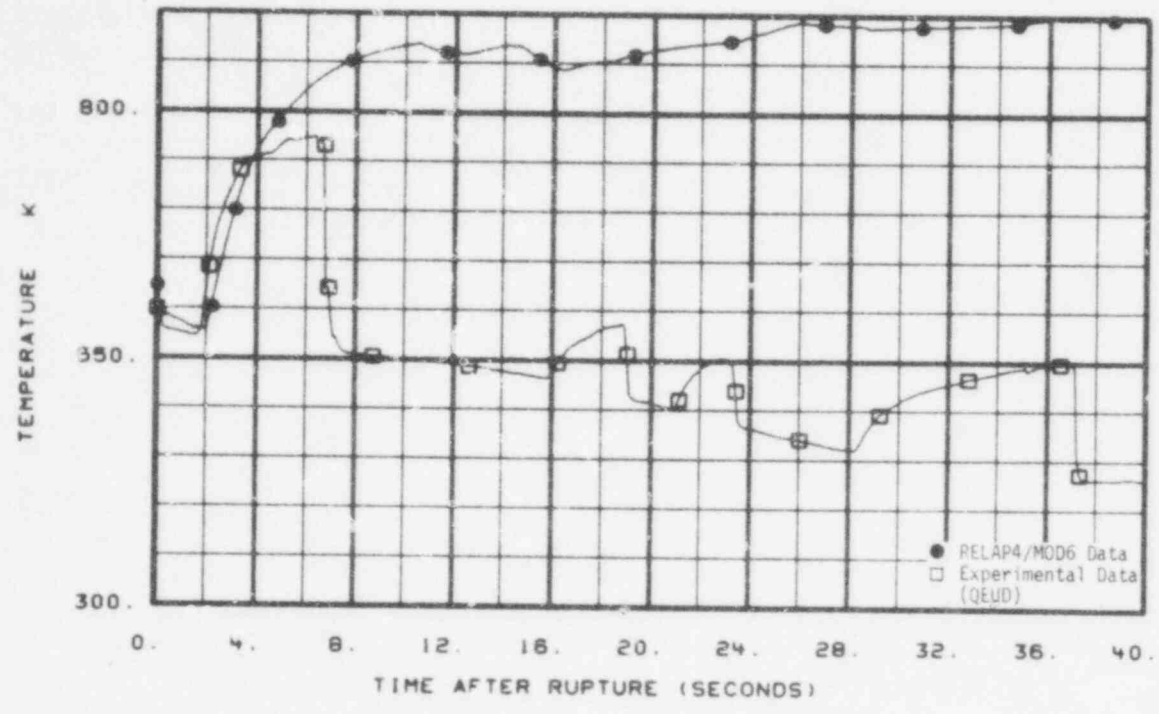

Fig. 91 Comparison of predicted and measured cladding temperature on FA5 pin D6 at 30 in. (TE-5D6-30).

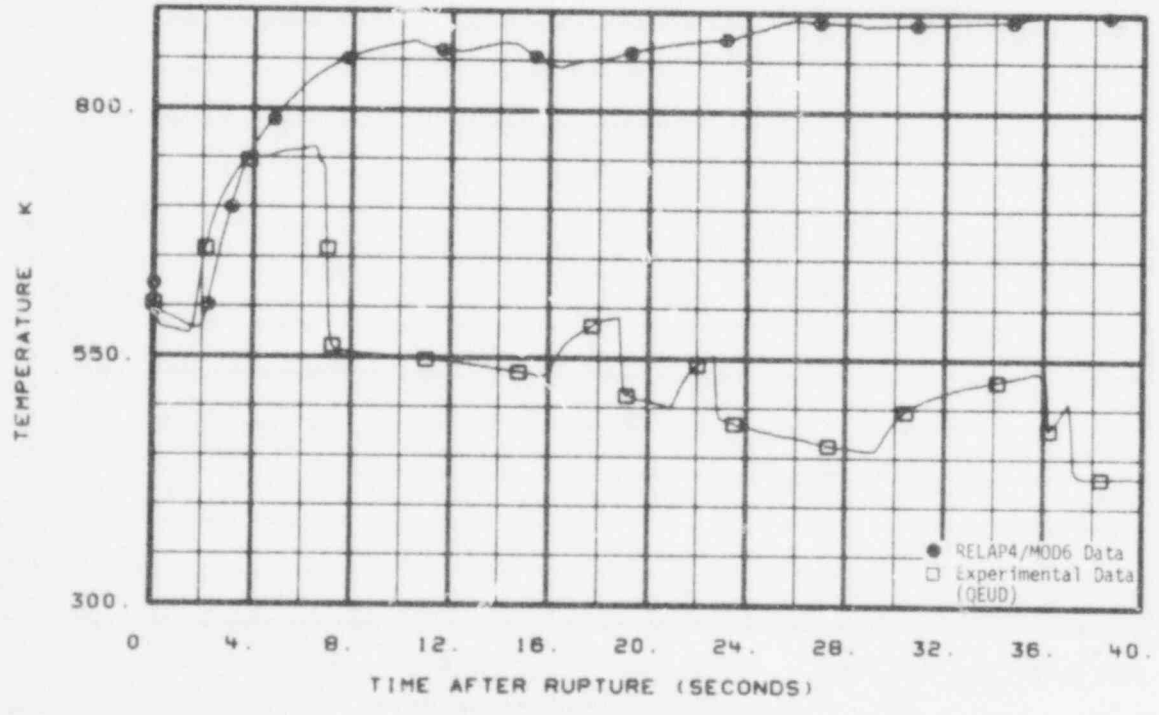

Fig. 92 Comparison of predicted and measured cladding temperature on FA5 pin D6 at 32 in. (TE-5D6-32).

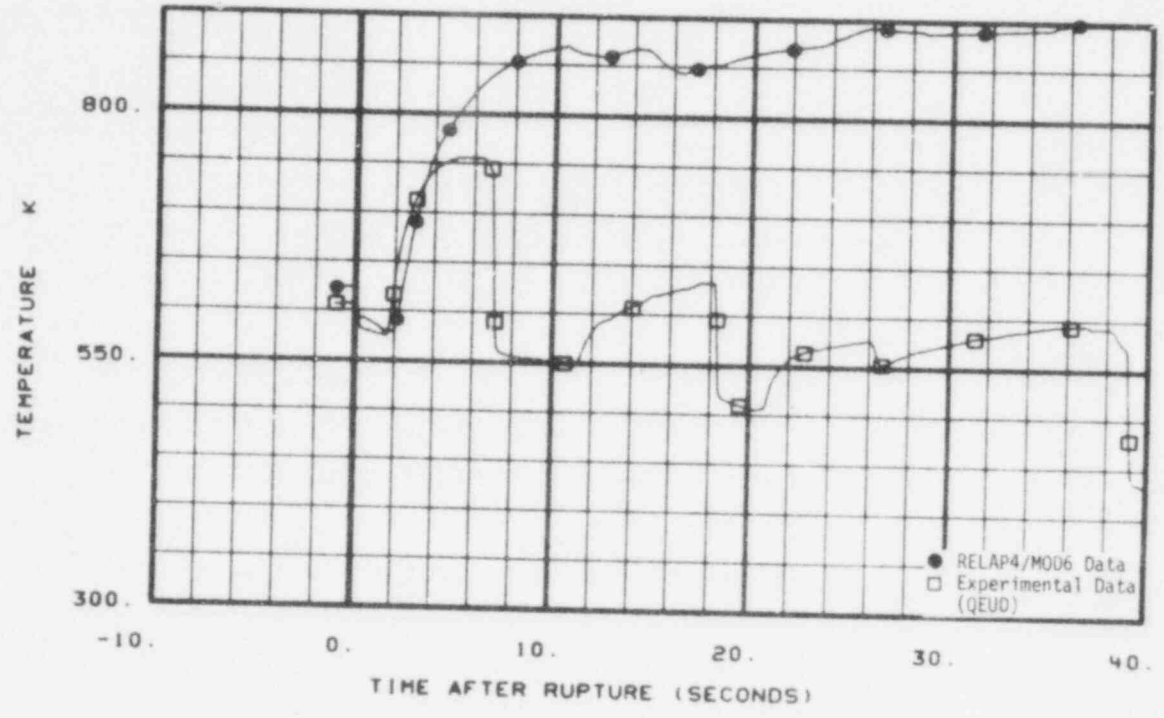

Fig. 93 Comparison of predicted and measured cladding temperature on FA5 pin L6 at 32 in. (TE-5L6-32).

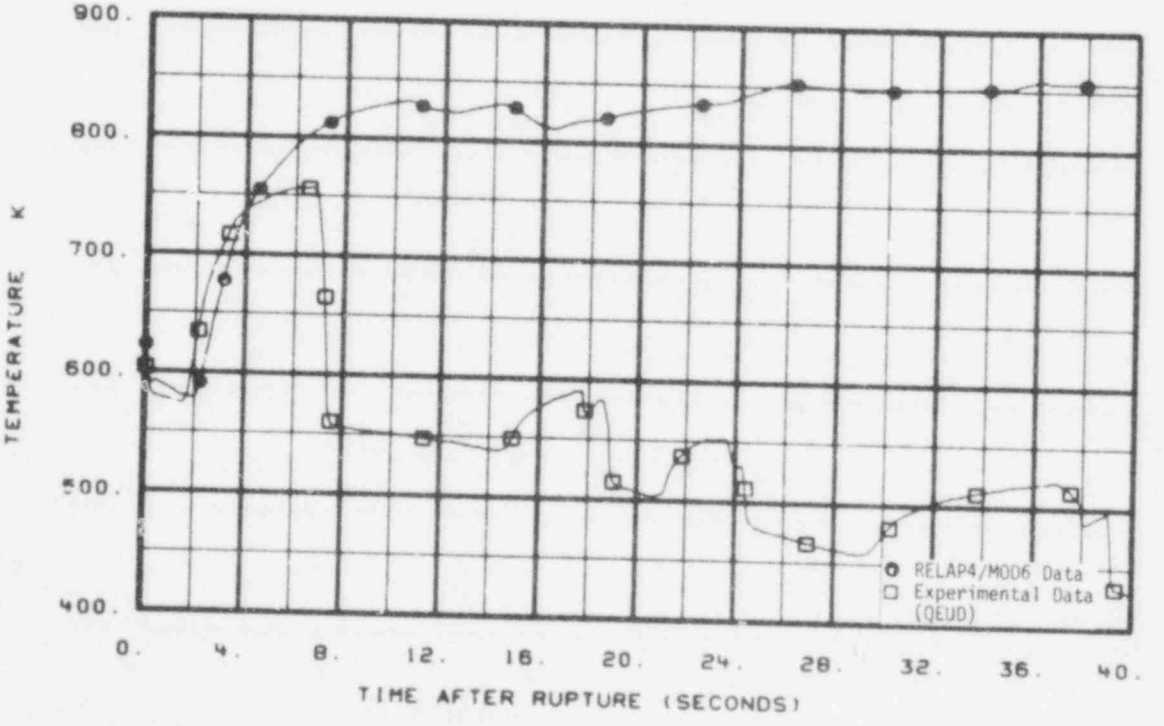

Fig. 94 Comparison of predicted and measured cladding temperature on FA5 pin D6 at 37 in. (TE-5D6-37).

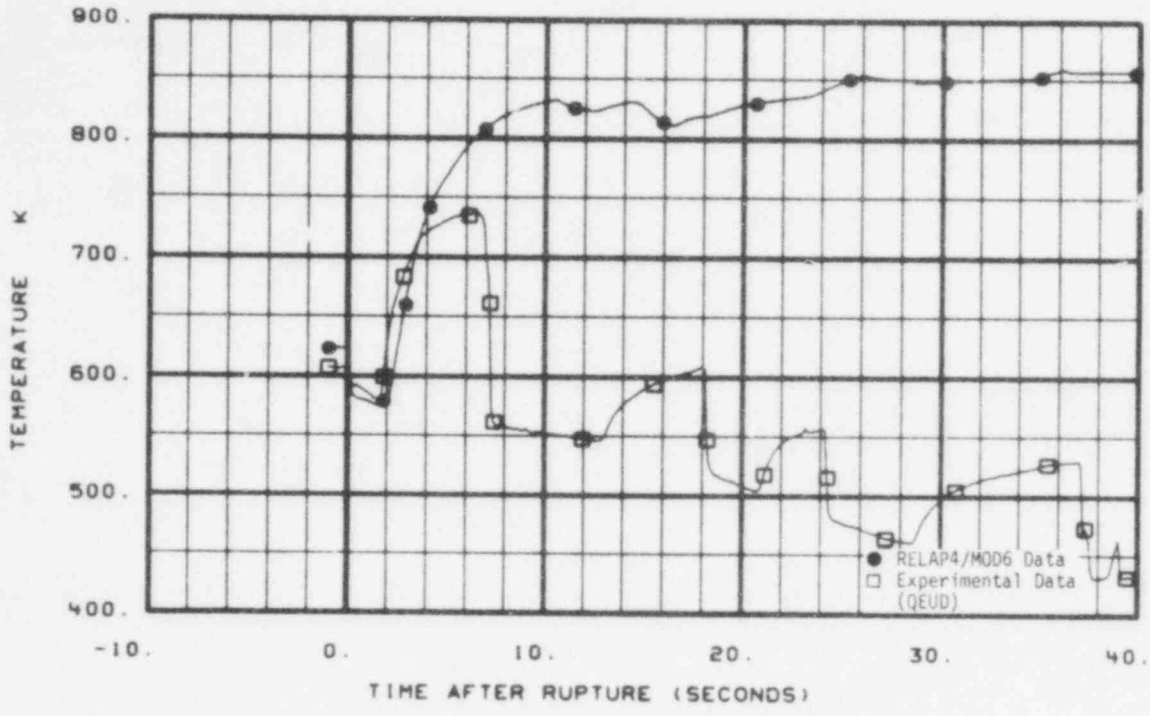

Fig. 95 Comparison of predicted and measured cladding temperature on FA5 pin L6 at 37 in. (TE-5L6-37).

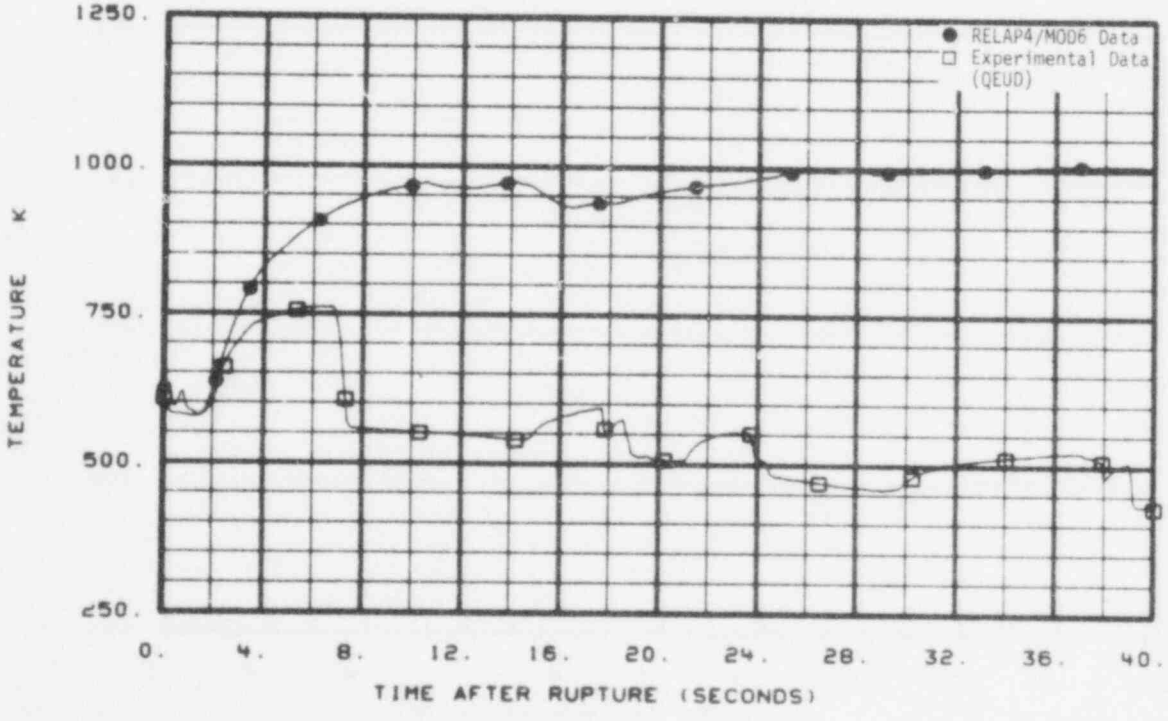

Fig. 96 Comparison of predicted and measured cladding temperature on FA5 pin D6 at 39 in. (TE-5D6-39).

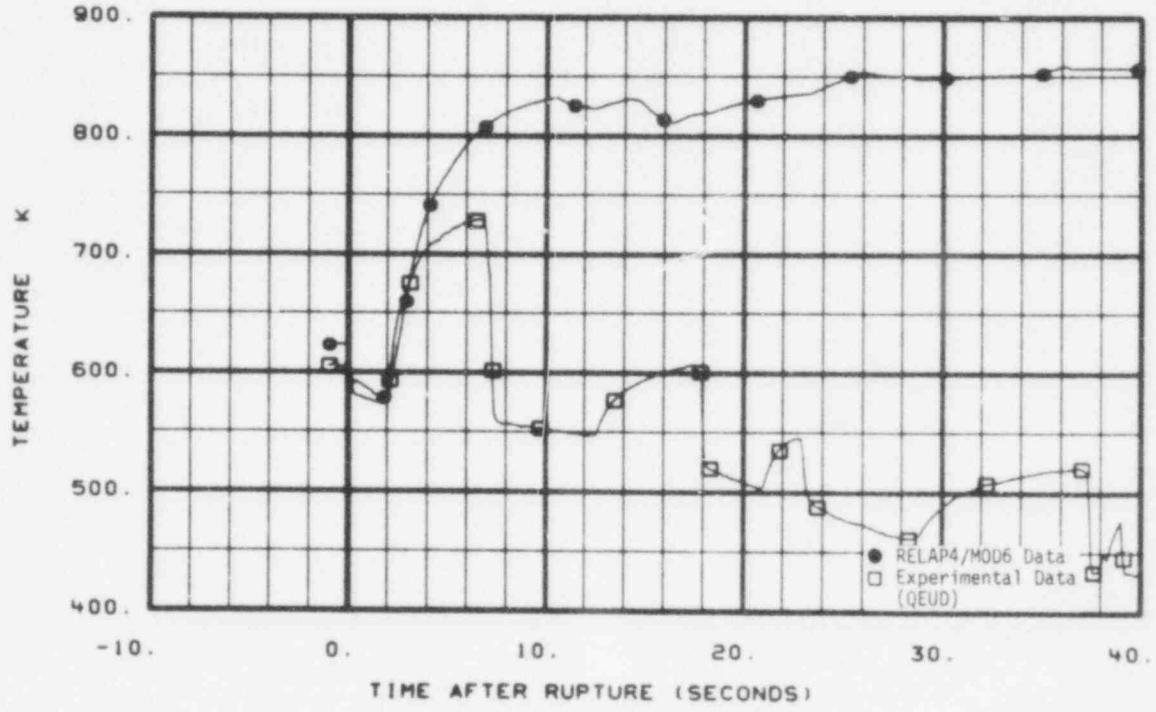

Fig. 97 Comparison of predicted and measured cladding temperature on FA5 pin L6 at 39 in. (TE-5L6-39).

3. CONCLUSIONS

In an integral type of experiment shown in these comparisons, an overall system response is difficult to attribute to any single or combination of parameters. On a qualitative comparison basis, one may infer where a calculation may be improved with respect to test data. To this end, the following is concluded from these comparisons.

(1) Break flow in both the hot and cold legs was calculated too high resulting in an early low system mass inventory and later in time, rapid depressurization.

(2) Mass flow in the intact loops was calculated too low. The combination of the disparity between intact and broken loop flow rates may result in the prediction of low core up-flow early in the transient.

(3) In general, the thermal-hydraulic behavior in the intact and broken hot legs did not compare well with the experimental data.

(4) The experimental initial conditions of pressure losses around the intact loop indicate that the LOFT RELAP4/MOD6 input model needs adjusting.

4. RECOMMENDATIONS

(1) The break flow model used in the calculations should be reviewed to ensure the actual break flow behavior is approximated closely.

(2) Transient calculations should be performed for a few seconds using the calculated steady state values obtained from the test boundary conditions (i.e., core power, hot leg temperature, steam generator mass flows, and primary coolant pump speed) without initiating blowdown to ensure the correct initial value boundary condition is satisfied. The broken hot leg temperature distribution function should be determined as well.

(3) The boundary conditions used during the calculations should be corrected including the steam generator feed and steaming rate and suppression tank pressure.

BLANK

APPENDIX A

UNCERTAINTY OF LOFT MEASUREMENTS

BLANK

APPENDIX A

UNCERTAINTY OF LOFT MEASUREMENTS

Table A-I is a listing of transducer uncertainties for the instruments used in this report. Generally, the measurements computed by COPERA do not have an uncertainty value available.

TABLE A-I

TRANSDUCER UNCERTAINTIES

Measurement	Range	Uncertainty
DE-BL-1	0 - 1 Mg/m^3	Not available
DE-BL-2	0 - 1 Mg/m^3	Not available
DE-PC-1	0 - 1 Mg/m^3	Not available
DE-PC-2	0 - 1 Mg/m^3	Not available
PDE-BL-1	0 - 0.35 MPa	±0.88 kPa RSS ±0.13% RD[a]
PDE-BL-5	0 - 10 MPa	±25 kPa RSS ±0.13% RD
PDE-BL-7	0 - 1.4 MPa	±3.3 kPa RSS ±0.11% RD
PDE-PC-1	0 - 0.7 MPa	±1.7 kPa RSS ±0.11% RD
PDE-PC-2	0 - 0.35 MPa	±0.88 kPa RSS ±0.13% RD
FT-P120-36-1	0 - 126 l/s	±0.73% RG
FT-P120-85	0 - 25 l/s	±0.73% RG
FT-P120-104	0 - 1.89 l/s	±0.73% RG
LIT-P120-44	0 - 3 m	±0.73% RG
LT-P004-8B	-3.7 - 1.46 m	±10% RG
LT-P139-6	-0 - 1.9 m	±0.73% RG
FR-BL-1	Not available	Not available

TABLE A-I (continued)

Measurement	Range	Uncertainty
FR-BL-2	Not available	Not available
FR-PC-1	Not available	Not available
FR-PC-2	Not available	Not available
ME-BL-1	3 - 74 $Mg/m \cdot s^2$	Not available
ME-BL-2	0.79 - 19 $Mg/m \cdot s^2$	Not available
ME-PC-1	3 - 74 $Mg/m \cdot s^2$	Not available
ME-PC-2	3 - 74 $Mg/m \cdot s^2$	Not available
ME-1ST-1	0.3 - 5 $Mg/m \cdot s^2$	19% RG
ME-1UP-1	0.3 - 5 $Mg/m \cdot s^2$	19% RG
ME-3UP-1	0.3 - 5 $Mg/m \cdot s^2$	19% RG
ME-2ST-1	0.3 - 5 $Mg/m \cdot s^2$	19% RG
PE-BL-1	0 - 21 MPa	±1.0% RD RSS ±0.2 MP
PE-BL-2	0 - 21 MPa	±1.0% RD RSS ±0.2 MP
PE-BL-6	0 - 21 MPa	±1.0% RD RSS ±0.2 MP
PE-PC-1	0 - 21 MPa	±1.0% RD RSS ±0.2 MP
PE-PC-2	0 - 21 MPa	±1.0% RD RSS ±0.2 MP
PE-1ST-1A	0 - 21 MPa	±1.0% RD RSS ±0.2 MP
PE-1ST-3A	0 - 21 MPa	±1.0% RD RSS ±0.2 MP
PE-1UP-1A	0 - 21 MPa	±1.0% RD RSS ±0.2 MP
PE-2ST-1A	0 - 21 MPa	±1.0% RD RSS ±0.2 MP
PE-SV-17	0 - 0.7 MPa	Not available
PT-P004-10A	0 - 8.27 MPa	1.0% RG
PT-P120-43	0 - 7.0 MPa	1.7% RG
RPE-PC-2	Not available	Not available

755 139

TABLE A-I (continued)

Measurement	Range	Uncertainty
FE-BL-1	2.0 - 45.0 m/s	Not available
FE-BL-2	0.6 - 15.0 m/s	Not available
FE-PC-1	0.6 - 15.0 m/s	Not available
FE-PC-2	0.6 - 15.0 m/s	Not available
TE-BL-1	270.0 - 1530.0 K	Not available
TE-BL-2	270.0 - 1530.0 K	Not available
TE-PC-1	270.0 - 1530.0 K	Not available
TE-PC-2	270.0 - 1530.0 K	Not available
TE-1ST-1	270.0 - 1530.0 K	±4.2% RD RSS ±0.13% RG
TE-1ST-2	270.0 - 1530.0 K	±4.2% RD RSS ±0.13% RG
TE-1ST-3	270.0 - 1530.0 K	±4.2% RD RSS ±0.13% RG
TE-1ST-4	270.0 - 1530.0 K	±4.2% RD RSS ±0.13% RG
TE-1ST-5	270.0 - 1530.0 K	±4.2% RD RSS ±0.13% RG
TE-1ST-6	270.0 - 1530.0 K	±4.2% RD RSS ±0.13% RG
TE-1ST-8	270.0 - 1530.0 K	±4.2% RD RSS ±0.13% RG
TE-1ST-9	270.0 - 1530.0 K	±4.2% RD RSS ±0.13% RG
TE-1ST-11	270.0 - 1530.0 K	±4.2% RD RSS ±0.13% RG
TE-1ST-12	270.0 - 1530.0 K	±4.2% RD RSS ±0.13% RG
TE-1ST-13	270.0 - 1530.0 K	±4.2% RD RSS ±0.13% RG
TE-1ST-14	270.0 - 1530.0 K	±4.2% RD RSS ±0.13% RG
TE-2ST-1	270.0 - 1530.0 K	±4.2% RD RSS ±0.13% RG
TE-2ST-2	270.0 - 1530.0 K	±4.2% RD RSS ±0.13% RG
TE-2ST-3	270.0 - 1530.0 K	±4.2% RD RSS ±0.13% RG
TE-2ST-5	270.0 - 1530.0 K	±4.2% RD RSS ±0.13% RG

TABLE A-I (continued)

Measurement	Range	Uncertainty
TE-2ST-7	270.0 - 1530.0 K	±4.2% RD RSS ±0.13% RG
TE-2ST-9	270.0 - 1530.0 K	±4.2% RD RSS ±0.13% RG
TE-2ST-10	270.0 - 1530.0 K	±4.2% RD RSS ±0.13% RG
TE-2ST-11	270.0 - 1530.0 K	±4.2% RD RSS ±0.13% RG
TE-2ST-14	270.0 - 1530.0 K	±4.2% RD RSS ±0.13% RG
TE-1LP-1	270.0 - 1530.0 K	±4.2% RD RSS ±0.13% RG
TE-6LP-1	270.0 - 1530.0 K	±4.2% RD RSS ±0.13% RG
TE-2UP-1	270.0 - 1530.0 K	±4.2% RD RSS ±0.13% RG
TE-3UP-4	270.0 - 1530.0 K	±4.2% RD RSS ±0.13% RG
TE-3UP-5	270.0 - 1530.0 K	±4.2% RD RSS ±0.13% RG
TE-3UP-8	270.0 - 1530.0 K	±4.2% RD RSS ±0.13% RG
TE-4UP-1	270.0 - 1530.0 K	±4.2% RD RSS ±0.13% RG
TE-5UP-9	270.0 - 1530.0 K	±4.2% RD RSS ±0.13% RG
TE-6UP-1	270.0 - 1530.0 K	±4.2% RD RSS ±0.13% RG
TE-3B12-26	270.0 - 1530.0 K	±4.2% RD RSS ±0.13% RG
TE-4H13-37	270.0 - 1530.0 K	±4.2% RD RSS ±0.13% RG
TE-5F4-15	270.0 - 1530.0 K	±4.2% RD RSS ±0.13% RG
TE-5F4-21	270.0 - 1530.0 K	±4.2% RD RSS ±0.13% RG
TE-5J4-21	270.0 - 1530.0 K	±4.2% RD RSS ±0.13% RG
TE-5J4-26	270.0 - 1530.0 K	±4.2% RD RSS ±0.13% RG
TE-5F4-26	270.0 - 1530.0 K	±4.2% RD RSS ±0.13% RG
TE-5J4-30	270.0 - 1530.0 K	±4.2% RD RSS ±0.13% RG
TE-5F4-30	270.0 - 1530.0 K	±4.2% RD RSS ±0.13% RG
TE-5L6-30	270.0 - 1530.0 K	±4.2% RD RSS ±0.13% RG

TABLE A-I (continued)

Measurement	Range	Uncertainty
TE-5D6-30	270.0 - 1530.0 K	±4.2% RD RSS ±0.13% RG
TE-5D6-32	270.0 - 1530.0 K	±4.2% RD RSS ±0.13% RG
TE-5L6-32	270.0 - 1530.0 K	±4.2% RD RSS ±0.13% RG
TE-5D6-37	270.0 - 1530.0 K	±4.2% RD RSS ±0.13% RG
TE-5L6-37	270.0 - 1530.0 K	±4.2% RD RSS ±0.13% RG
TE-5D6-39	270.0 - 1530.0 K	±4.2% RD RSS ±0.13% RG
TE-5L6-39	270.0 - 1530.0 K	±4.2% RD RSS ±0.13% RG

a. RSS - root sum square

e.g. $\sqrt{(0.042\ RD)^2 + (-0.042\ RD)^2}$ for TE-5L6-39

RG - range

RD - reading.

BLANK

APPENDIX B

LOFT SYSTEM WITH EXPERIMENTAL MEASUREMENT LOCATIONS

BLANK

APPENDIX B

LOFT SYSTEM WITH EXPERIMENTAL MEASUREMENT LOCATIONS

Figure B-1 shows the intact loop and external reactor vessel instrumentation. Figure B-2 shows the broken loop instrumentation and Figures B-3 and B-4 show the internal reactor vessel instrumentation. Figure B-5 shows a core map. The core thermocouple identification number can be used with this map to locate a transducer in the core. The identification number is broken down as shown

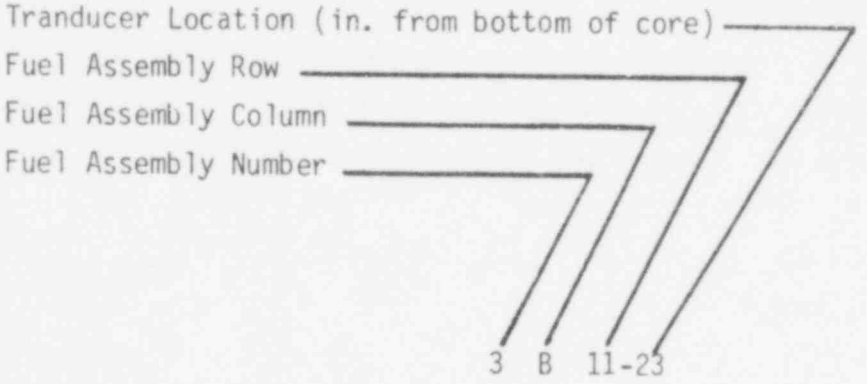

BLANK

LT-P139

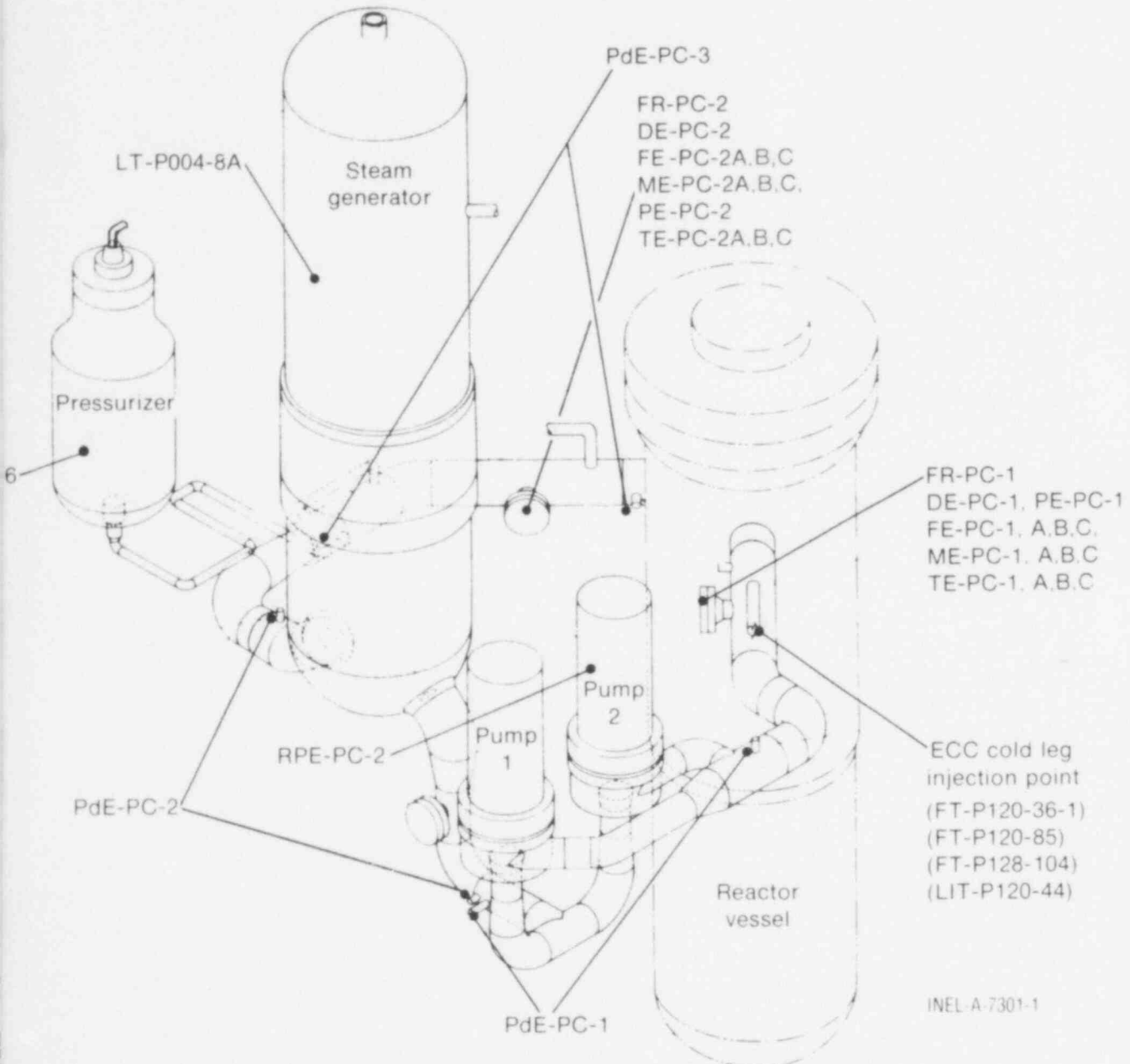

Fig. B-1 Intact loop measurement locations.

BLANK

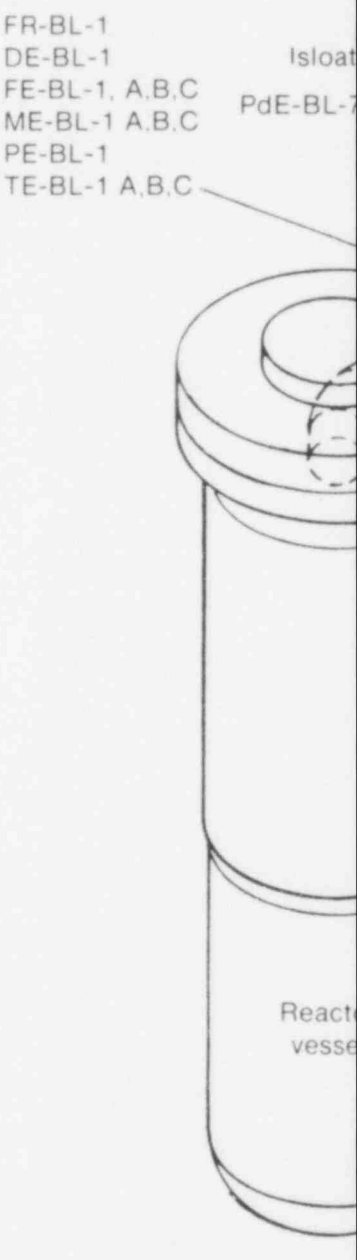
FR-BL-1
DE-BL-1
FE-BL-1, A,B,C
ME-BL-1 A,B,C
PE-BL-1
TE-BL-1 A,B,C
Isloat
PdE-BL-7
React
vesse

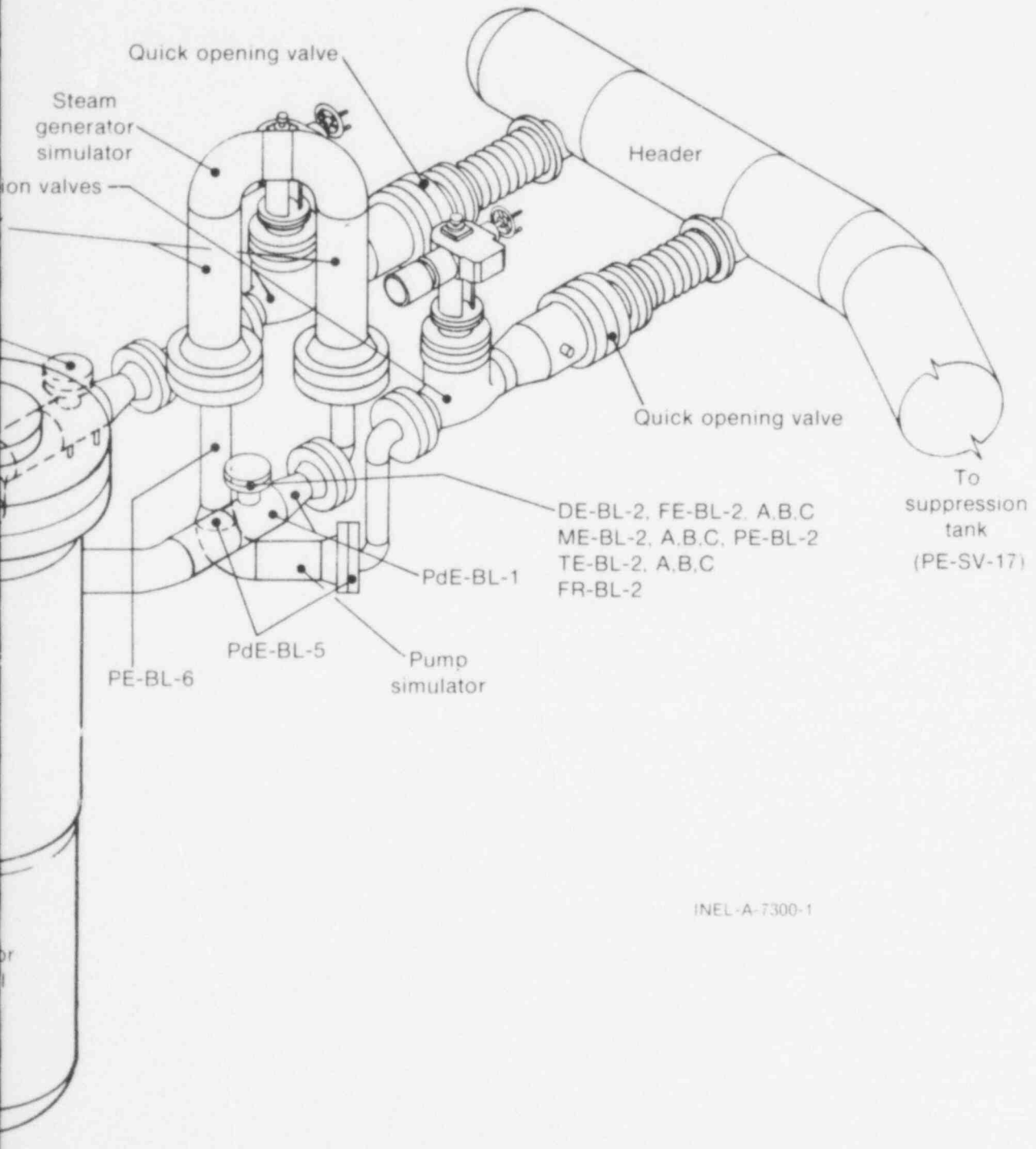

Fig. B-2 Broken loop measurement locations.

BLANK

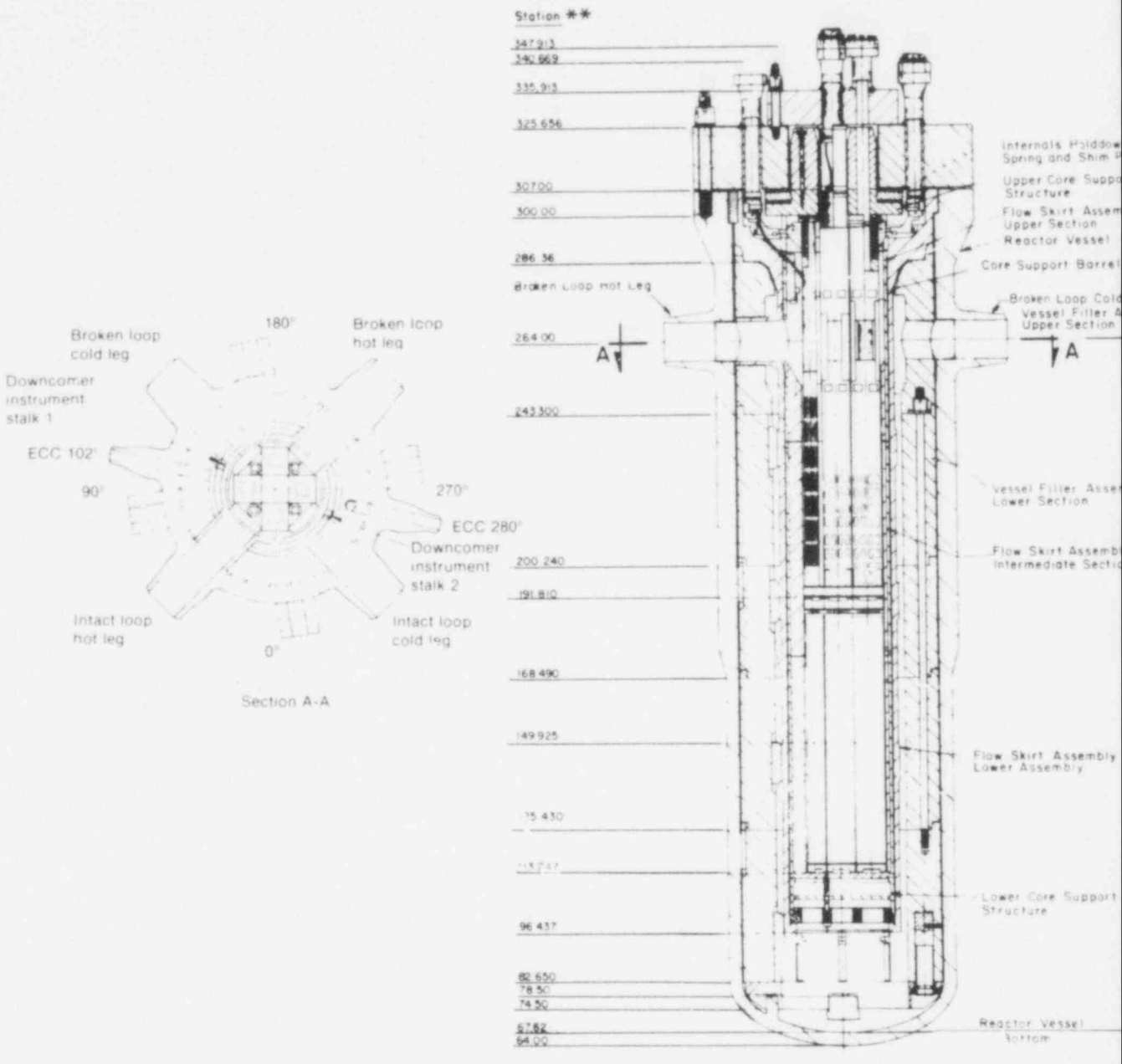

** Station numbers are a dimensionless measure of relative elevation within the reactor vessel. They are assigned in increments of 2.54 centimeters with station 500.00 defined at the core barrel support ledge inside the reactor vessel flange.

Fig. B-3 Reactor vessel

755

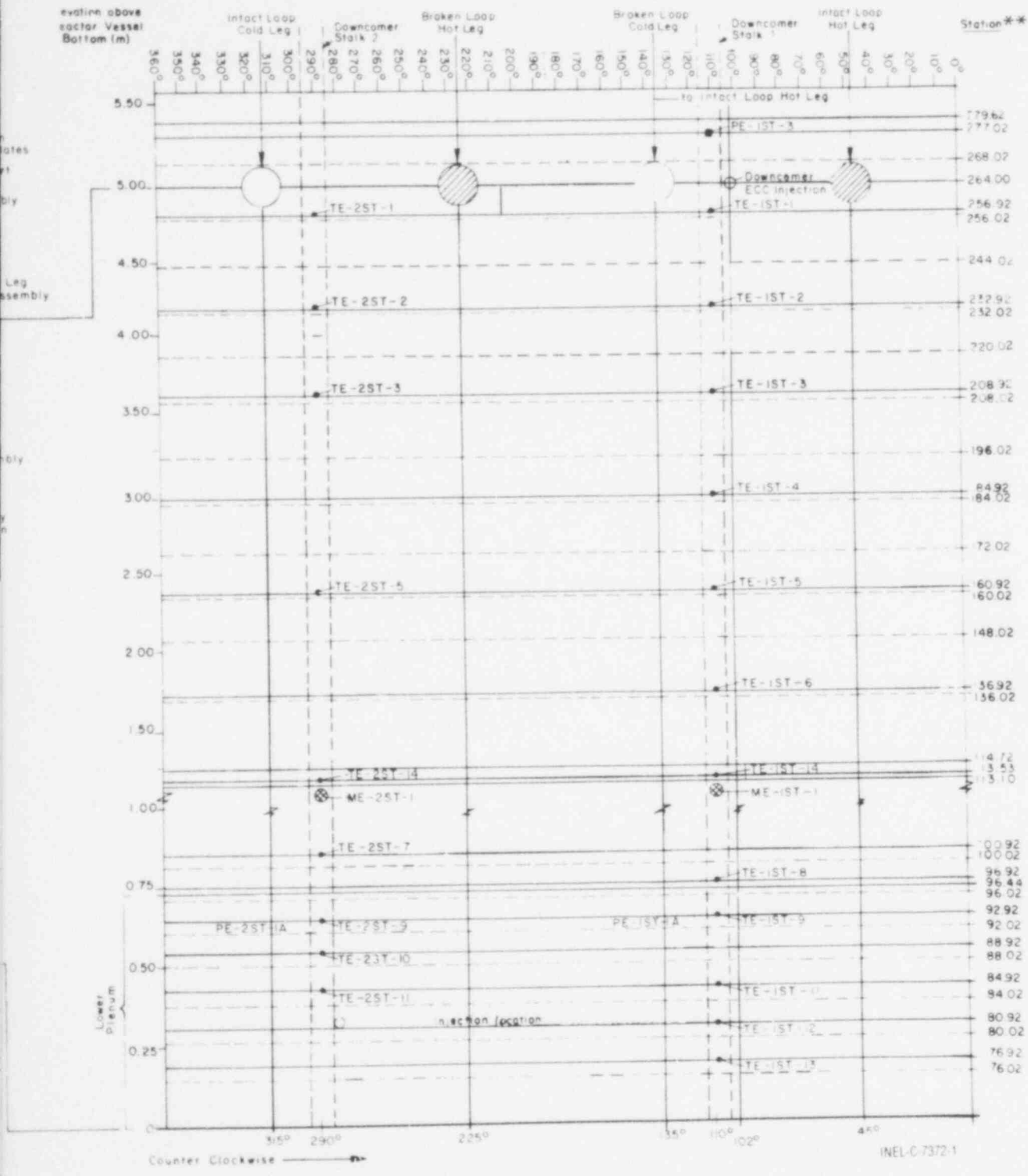

measurement locations.

BLANK

* Station numbers are a
relative elevation with
are assigned in incre
station 300.00 define
ledge inside the react

F

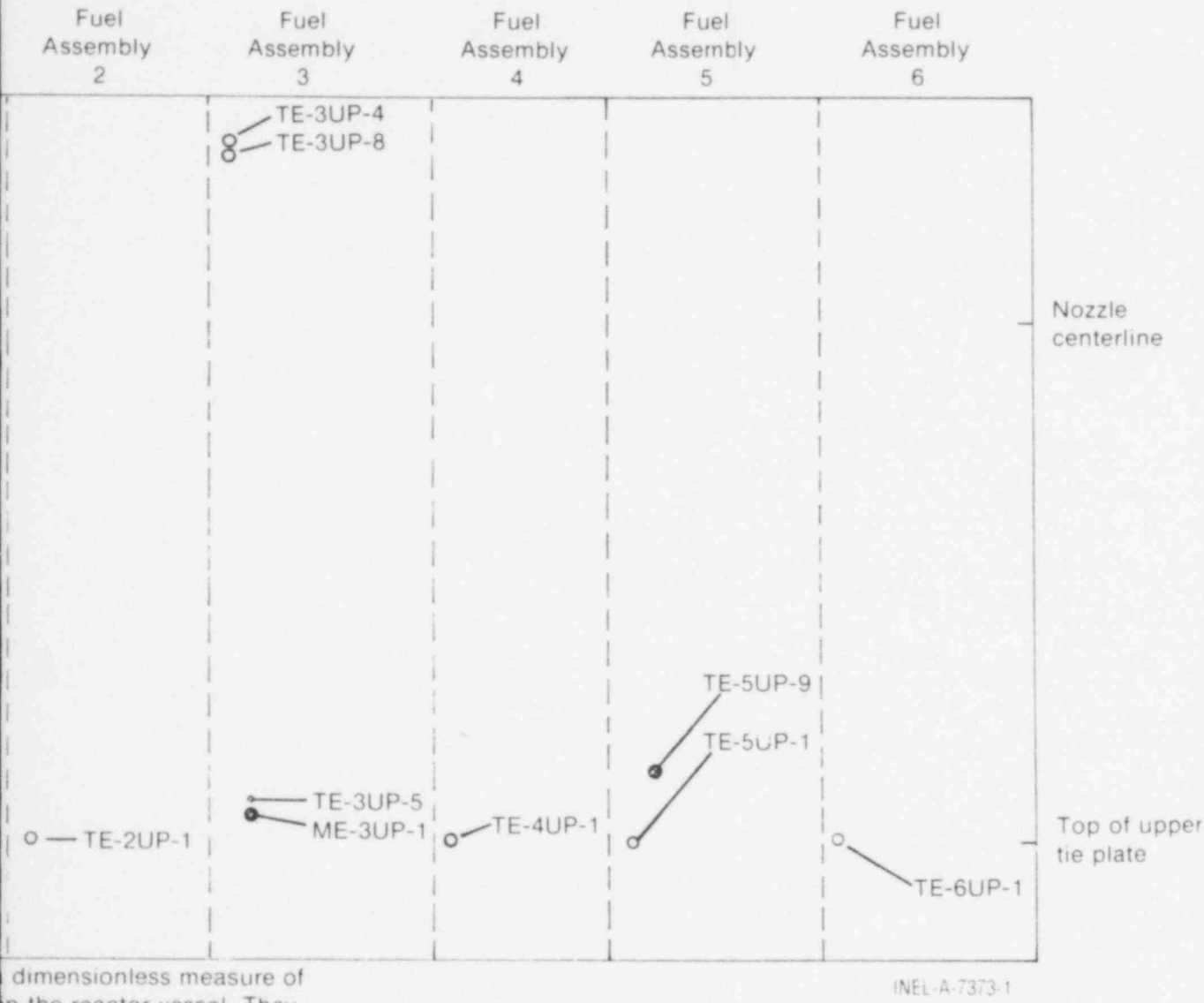

dimensionless measure of
in the reactor vessel. They
nents of 2.54 cm with
at the core barrel support
or vessel flange.

g. B-4 Reactor vessel upper plenum measurement locations.

BLANK

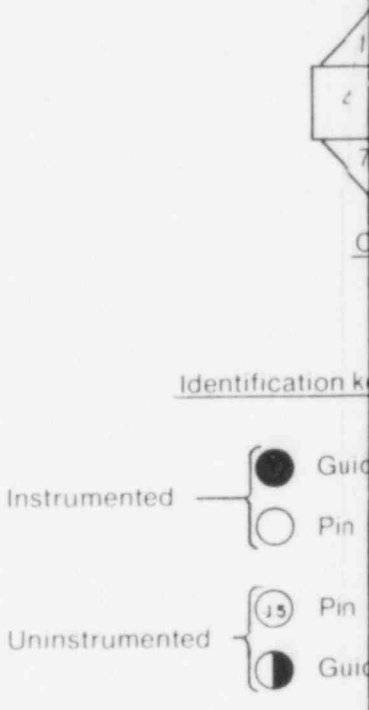

Identification k

Instrumented
- Guid
- Pin

Uninstrumented
- J5 Pin
- Guid

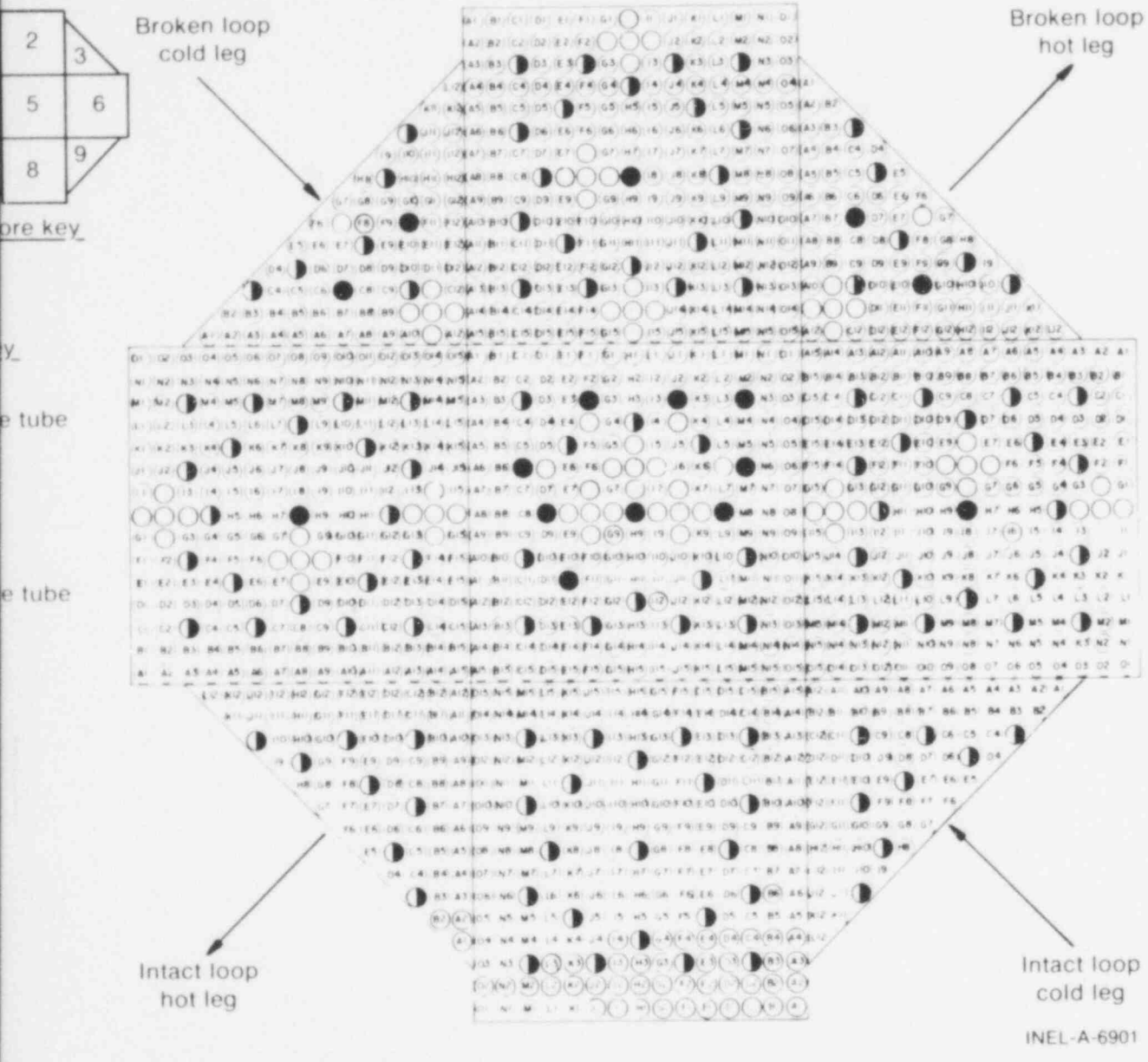

Fig. B-5 Core map showing position designations.